SISSA

Scuola
Internazionale
Superiore di
Studi Avanzati

Neuron-glia interactions and neuroinflammation: *in vitro* approaches to elucidate spinal cord disorders pathophysiology

Candidate
Giulia Panattoni

Supervisor
Prof. Laura Ballerini

A thesis submitted for the degree of *Philosophiae Doctor*
in Neurobiology for the Academic Year 2019-2020

Table of contents

List of abbreviations

CNS, Central Nervous System

TNF-α, tumor necrosis factor alpha

IL, interleukin

M-CSF, macrophage-colony stimulating factor

GM-CSF, granulocyte macrophage-colony stimulating factor

sEPSC, spontaneous excitatory post-synaptic current

sIPSC, spontaneous inhibitory post-synaptic currents

BBB, blood brain barrier

PNS, peripheral nervous system

GFAP, glial fibrillary acidic protein

SVZ, subventricular zone

NVU, neurovascular unit

NSC, neural stem cell

OPC, oligodendrocyte precursor cell

MBP, myelin basic protein

PLP, proteolipid protein

CSF, cerebral spinal fluid

TLR, toll-like receptor

AQP4, aquaporin 4

LPS, lipopolysaccharide

IFN-γ, interferon gamma

TGF-β, transforming growth factor

APP, amyloid β-protein precursor

Aβ, amyloid β

EAE, experimental autoimmune encephalomyelitis

DRG, dorsal root ganglia

CPG, central pattern generator

SCI, spinal cord injury

ALS, amyotrophic lateral sclerosis

SMA, spinal muscular atrophy

MS, multiple sclerosis

ECM, extracellular matrix

SOD1, superoxide dismutase 1

BDNF, brain-derived neurotrophic factor

NO, nitric oxide

CSF-1, colony stimulating factor 1

GJ, gap junction

DIV, day *in vitro*

WIV, week *in vitro*

GAD, glutamic acid decarboxylase

THA, threo-hydroxyaspartate

GPCR, G-protein-coupled receptors

ER, endoplasmic reticulum

Ryr, ryanodine receptor

mPTP, mitochondrial permeability transition pore

TRP, transient receptor potential

IP_3R, inositol triphosphate receptor

Cx, connexin

HC, hemichannel

CBX, carbenoxolone

Abstract

Neuroinflammation is a characterizing trait of various central nervous system (CNS) pathologies, from neurodegenerative diseases to neuropsychiatric disorders. In the effort of dissecting the impact of immune status alterations on neural circuit function, we focused our study on the effects of local inflammation in a controlled micro-environment where neurons and neuroglial cells maintain their appropriate organization: the organotypic spinal cord slices. These cultures, developed from the spinal cord of mouse embryos, represent a complex *in vitro* model where sensory-motor cytoarchitecture, synaptic properties and spinal cord resident cells, encompassing heterogeneous neuronal phenotypes and neuroglia, are retained in a 3D fashion. I have used this model to mainly investigate: 1) synaptic spinal changes induced by inflammation and mechanisms by which the inhibitory transmission is modulated; 2) resident microglia and astrocytes reactivity to inflammatory stress; 3) astrocytes calcium activity tuned by inflammation; 4) mechanisms which modulate calcium release and spreading in the inflamed tissues. Overall, my main aim was to understand the link between neuroinflammation and spinal pre-motor network. For the purpose, organotypic spinal cord slices are cultured for two weeks in vitro. Then, they are exposed for 4 and 6 hours to a cocktail of cytokines (CKs, 10 ng/mL), composed by tumor necrosis factor alpha (TNF alpha), interleukin-1 beta (IL-1 beta) and granulocyte macrophage-colony stimulating factor (GM-CSF), or to lipopolysaccharide (LPS, 1 µg/mL). I use single cell electrophysiology, live cell calcium imaging, immunocytochemistry, confocal

microscopy and immunoblotting analysis to investigate and compare the spinal tissue responses to neuroinflammation induced by CKs and LPS. I first focus on the synaptic level, describing a progressive increase in the frequency of spontaneous post-synaptic currents (sPSCs) and inhibitory post-synaptic currents (IPSCs) and the shortening of GABAergic current due to CKs incubations, absent in LPS treated ones. I further explore by immunofluorescence and confocal microscopy, resident neuroglia reactivity, describing the activation of different inflammatory status, given by the two different paradigms, confirmed by the presence of cytokines and chemokines released in the supernatants. By live calcium imaging, I document an increase in the occurrence of calcium oscillations displayed by the astrocytes located in the ventral horn, and by several pharmacological treatments, I dissect the behavior of the oscillations, trying to understand their origin and mechanism of spreading.

In conclusion, my work compared the effects of a cytokines cocktail and of LPS in altering the pre-motor circuits signaling, that may contribute to sustain spinal network increased excitability, eventually leading to neurodegeneration.

Introduction

1. Neuroinflammation and Neurodegeneration

The Central Nervous System (CNS) controls most functions of the body. This control emerges from the interplay between the brain and spinal cord functional units, the neurons, which communicate mainly by electrical or chemical synapses, and the neuroglia[1]. In several neuro-pathological conditions, including neurodegenerative diseases, neuroglia play a central role contributing to neuronal damage by developing inflammatory responses within the brain and spinal cord[2]. Neuroinflammation is mediated by microglia, astrocytes, neurons, T-cells, neutrophils and by cellular inflammatory mediators released by these cells[3] (Fig.1). The same cells control the canonical CNS homeostasis during physiological conditions[4]. The neuroinflammation is initially a protective response against the damage, but, although some inflammatory stimuli induce beneficial and repairing effects, uncontrolled inflammation may result in the production of neurotoxic mediators which amplify the injury state and eventually lead to cell death and neurodegeneration[5]. During prolonged and chronic neuroinflammation, the elevated levels of inflammatory mediators and the accumulation and proliferation of the inflammatory cells perform the opposite function of the physiological one, necessary for the resolution of the injury, by leading to the onset and the progression of ischemic conditions, neurodegenerative diseases and autoimmune diseases[2,6].

Neurodegeneration is characterized by the slow and progressive alteration of neuronal function and structure with reduced neuronal survival and enhanced neuronal death, in specific regions of the CNS[7].

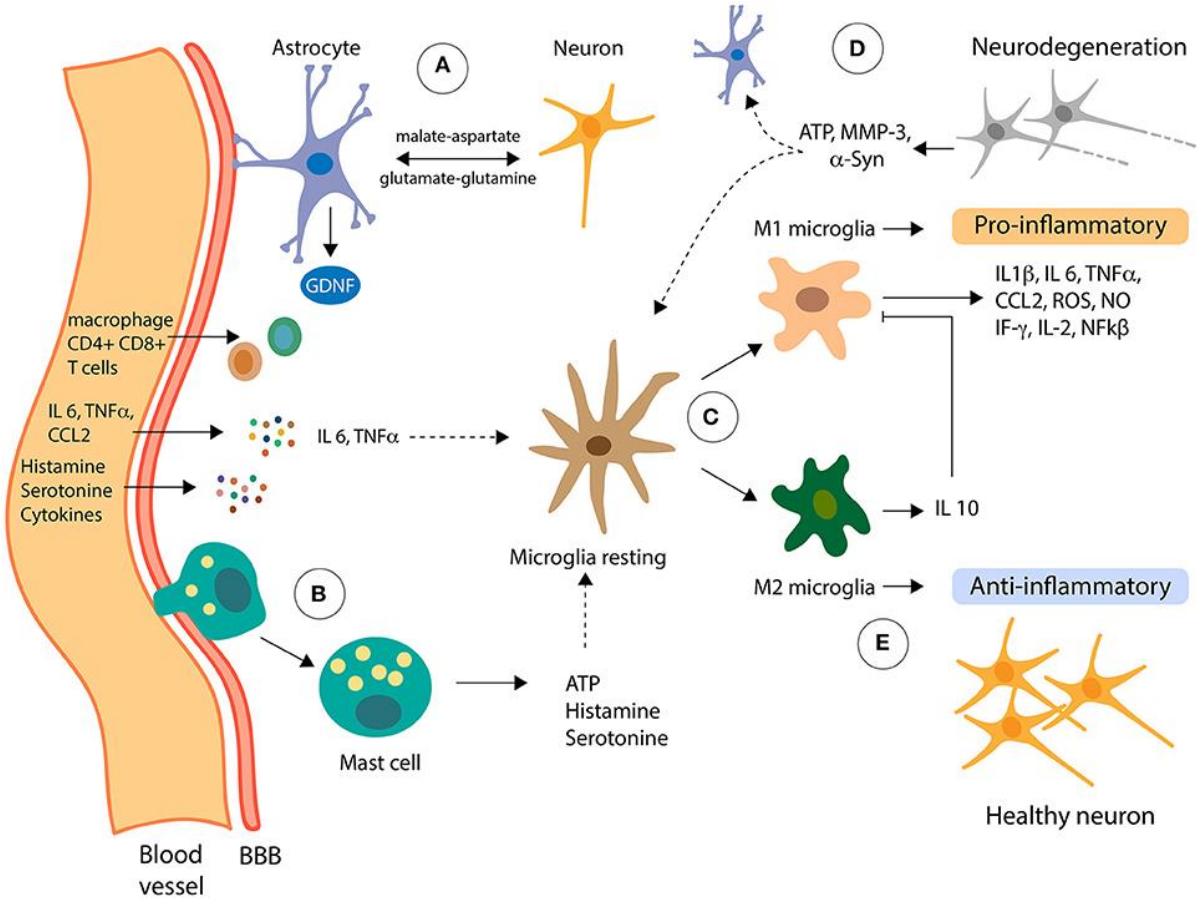

Figure 1 Inflammatory system activation

Pro-inflammatory molecules can reach the CNS from the periphery going across the blood-brain barrier (BBB). (A) Astrocytes, the most abundant cells in the CNS, are functionally connected with the BBB, receiving signals from the periphery and from inside the CNS. (B) Mast cells can infiltrate the CNS, inducing changes in the microglia by the delivery of proinflammatory effectors. (C) Resting microglia can be activated in two classical phenotypes, M1 and M2, depending on the effector signals from its microenvironment. Neurons in a cross-talk signaling with astrocytes and microglia, increasing the toxic-loop of neuroinflammation[Adapted from Ref.8].

1.1 Neuroglia

It is common to credit Rudolph Virchow, a German pathologist, with the discovery of glia. What Virchow described in 1856 does not exactly correspond to what we today consider to be glial tissue. He wrote: "this connective substance forms in the brain, in the spinal cord and in the higher sensory nerves a sort of putty, in which the nervous elements are embedded" (Fig. 2). For this reason, the term Neuroglia (or *Nervenkitt* in German), translated as "nerve-cement" or "nerve-glue" was born. The names survive, even if the original concept has radically changed[9].

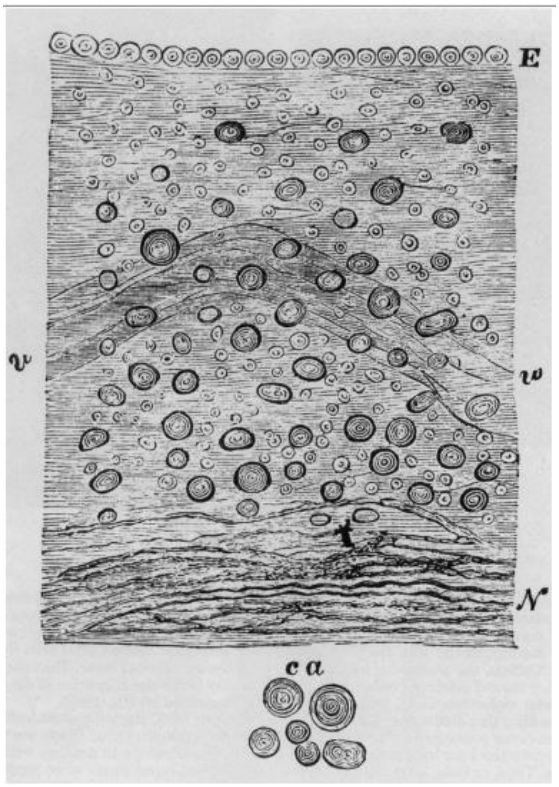

Figure 2 Virchow's illustration of subependymal neuroglia

E, ependymal epithelium; v-w, blood vessel in "connective tissue"; N, nerve fibers; ca, corpora amylacea[Adapted from Ref.9].

Today, the term neuroglia, or glial cells, indicates non-neuronal cells like astrocytes, microglia and oligodendrocytes in the CNS or Schwann cells in the peripheral nervous system (PNS), which play an essential and active role in development, signaling, synaptic plasticity and metabolic support for brain and spinal cord neurons.

Astrocytes

The term "astrocyte" was first used in 1893 by Michael von Lenhossek and refers to the typical stellate morphology of the cells[10]. They represent the most abundant fraction of glial cell types in the adult brain[11]. Glial fibrillary acidic protein (GFAP) is a class III intermediate filament protein, is a structural protein found only in the main branches of the astrocyte and it is widely used to identify astrocytic cells, even if it is estimated that *in vivo* it identifies around 15% of the cell[12]. Astrocytes can be very different between each other, but they share some common characteristics. Some criteria for defining this cell type have been defined: (i) non-excitability; (ii) a very negative membrane potential which is determined by the K^+ gradient; (iii) glutamate and GABA uptake by astrocyte-specific transporters; (iv) the presence of intermediate filament bundles; (v) the presence of glycogen granules; (vi) cell processes surrounding blood vessels and synapses; and (vii) the presence of gap junctions formed by connexin43 and connexin30. Each of these features is necessary but not sufficient in order to classify an astrocyte[13,14]. Astrocytes have been classified into two major morphologically differentiated and anatomically located groups: the fibrous astrocytes of the white matter and the protoplasmic astrocytes of the grey matter[15]. Protoplasmic astrocytes organize themselves into separate three-dimensional non overlapping territories known as distinct domains. On

the other hand, fibrous astrocytes are organized along white matter tracts and they do not organize themselves into domains[15].

There are three distinct pools of glial progenitors in the cerebral cortex, radial cells of the ventricular zone, postnatal glial progenitor cells of the subventricular zone (SVZ) and glial restricted precursors, which interface and communicate with the extracellular matrix components and molecules in order to define the different phenotypes[16]. Even if it is well established that astrocytes develop after neurons, in the CNS development, they are involved in driving axon migration and synaptic pruning[17]. They are also known to regulate the stability, dynamics and maturation of dendritic spines as well as the synaptic plasticity and synaptic transmission[18]. They are involved in neuronal metabolic support during development, maturation and injury. They are active components of the tripartite synapse, being responsible for the re-uptake of the glutamate in the synaptic cleft[19] and they are the main players in the interactions within the neurovascular unit (NVU), where they are essential for blood-brain barrier (BBB) maintenance and neurovascular coupling. Loss of normal astrocyte functions may contribute to reduced support for neurons and dysfunction of the NVU[20]. In particular, protoplasmic astrocytes form extensive contacts with blood vessels and the microvasculature and play a central role in regulating blood flow in the brain[10]. Astrocytes communicate with neighboring astrocytes via calcium signals, which pass through the gap junctions. These calcium signals are not just due to the synaptic activity, but they can occur spontaneously[21]. Astrocytes can remove glutamate released by neurons, in order to avoid the excitotoxicity by using specific transporters on peri synaptic astrocytic processes[22] (Fig. 3).

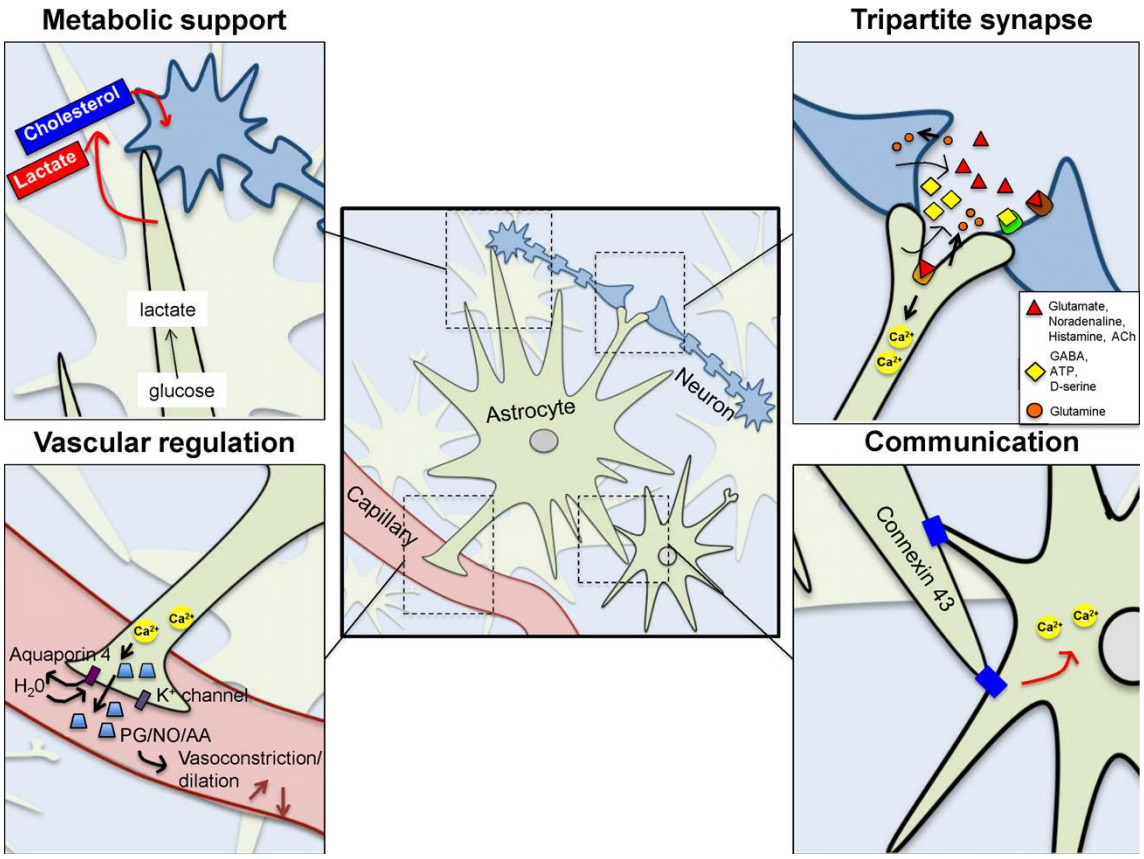

Figure 3 The many roles of the astrocyte

Astrocytes provide energy substrates for neurons, primarily in the form of lactate which is converted from glucose as well as providing cholesterol to support neuronal function. The intimate association of astrocytic processes with neuronal synapses enables the finely tuned regulation of synaptic transmission. Astrocytes couple together synaptic activity with local blood flow to ensure neurons have a sufficient energy supply. Gap junctions such as connexin 43 enable dialogue between neighboring astrocytes, which is mediated by intracellular changes in calcium levels[Adapted from Ref.10].

Microglia

In 1919, Pío Del Río-Hortega, who once worked with Cajal, phenotypically characterized the only immune cells in the brain parenchyma, previously observed by Cajal, which are now known as microglia. Microglia represent approximately the 10% of the total cells in the adult CNS in mammals, with a considerable heterogeneity in microglia density among the different CNS regions[23,24]. They are generally considered the immune cells of the CNS, because of their ability in phagocytosis, in releasing cytotoxic factors and inflammatory mediators and in priming the immune response to several kind of threating stimuli[25]. Lineage-tracing studies in mice have established that microglia are derived from yolk-sac progenitors, which migrate through the bloodstream to the developing CNS, starting at embryonic day 8.5 and continuing until the BBB is formed (Fig. 4)[26]. Microglia may be considered to be similar to tissue-resident macrophages in non-CNS tissues, with a hematopoietic origin, but it has recently been determined that microglia are the only myeloid cells that are derived solely from yolk sac precursors under normal conditions[27,28]. The transcriptional repertoire from the yolk sac to the adult in mice has revealed three major developmental states: early (less than E14), pre-microglia (E14 to a few weeks postnatal) and adult microglia (more than a few weeks)[27]. Microglia not only respond during threating conditions, but these cells are also necessary for the normal maintenance of the CNS homeostasis. It is well established that during early stages of CNS development microglia induce neuronal programmed cell death, promote neuronal fasciculation, limit axon outgrowth and trigger phagocytosis, a phenomenon that persists also after the CNS maturation.

Moreover, during the postnatal and adult CNS stages microglia interact with the mature neuronal synapses, in particular with those with the higher activity, and this interplay is necessary to attenuate the activity. It was indeed demonstrated that during CNS development, microglia are involved in synapse remodeling and maturation, and in supporting the oligodendrocytes progenitors during their maturation[28–31]. In these physiological conditions, the complement proteins mainly expressed by microglia are necessary for the synapse pruning, while in threating conditions they induce complement-mediated loss of neurons[30,31].

Microglia exist in three different conformations: the surveillant, the primed and the amoeboid one. In the first one they exhibit two modes of motility, indeed they constantly extend and retract their processes to survey the brain, but they also send out targeted processes to envelop sites of tissue damage[32]. The primed or "reactive" microglia are those cells involved in the release of pro-inflammatory cytokines and other inflammatory mediators[33]. The amoeboid conformation is necessary for the mechanism of phagocytosis.

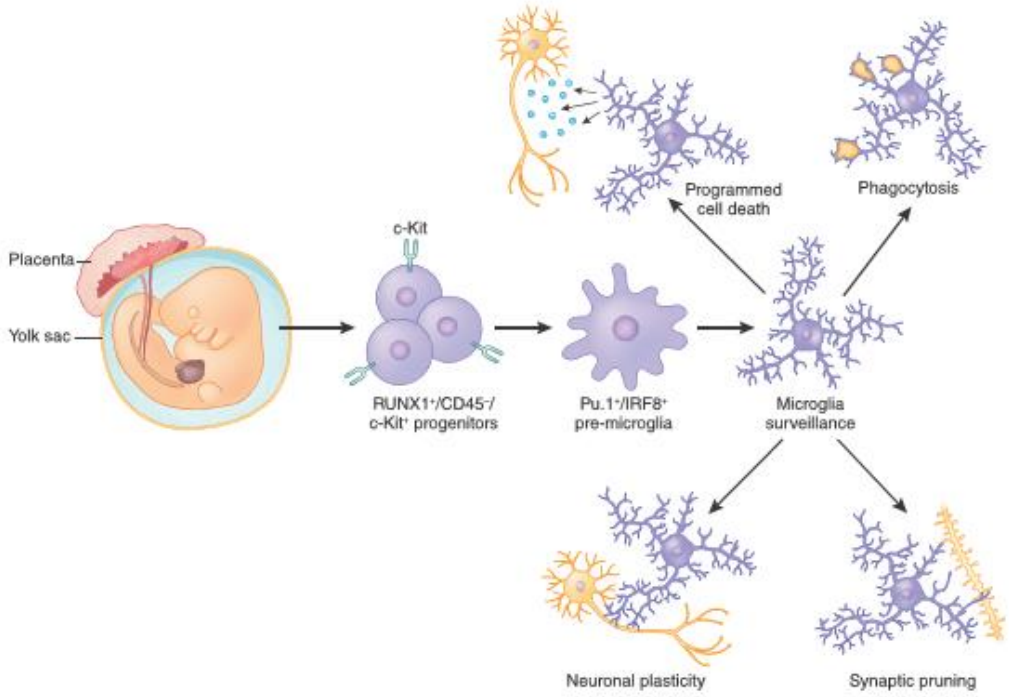

Figure 4 Ontogeny of microglia and physiological roles in CNS development, homeostasis and plasticity

Microglia develop from myeloid progenitors in the yolk sac that express the transcription factor RUNX1 and the receptor tyrosine kinase c-Kit, also known as CD117, but not CD45, and enter the CNS during early embryonic development (embryonic day 8.5 in mice). Microglia have crucial roles in brain development and CNS homeostasis, including programmed cell death and clearance of apoptotic new-born neurons, as well as pruning developing axons and synapses. Later in development and into adulthood, microglia processes are highly motile and continually survey their local environment, contacting neurons, axons and dendritic spines. Microglia have diverse physiological roles, including regulating neuronal and synaptic plasticity[Adapted from Ref.27].

Oligodendrocytes and Schwann cells

Oligodendrocytes are the cells producing myelin sheaths around the axons of several neurons and the myelination process is a largely postnatal process continuing into adulthood in humans[34]. Oligodendrocytes originate from neural stem cell (NSC)-derived oligodendrocyte precursor cells (OPCs) that differentiate into immature pre-myelinating oligodendrocytes (pre-OLs) and finally differentiate into mature oligodendrocytes that contact neuronal axons and start the production of myelin[35] (Fig. 5). Del Río-Hortega was able to recognize 4 different type of oligodendrocytes, from I to IV, according to their size, number, orientation of their processes and size of the axons they wrapped[36] (Fig. 6).

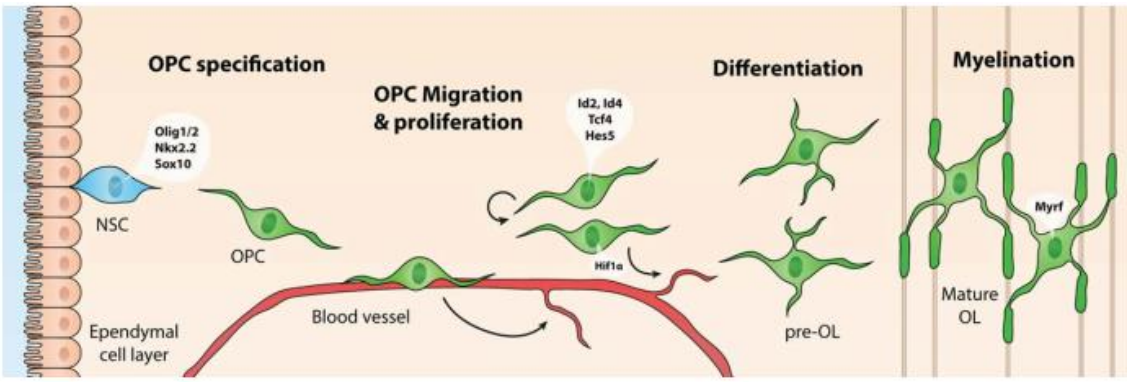

Figure 5 Schematic representation of oligodendrocyte (OL) development
Oligodendrocytes precursor cells (OPCs) originate from neuroepithelial zones surrounding the ventricles, where neural stem cells (NSCs) differentiate into (OPCs). OPCs migrate toward an appropriate site via blood vessels. At their final destination, OPCs proliferate to expand the pool of OPCs. When proliferation is inhibited, OLs differentiate into pre-myelinating oligodendrocytes (pre-oligodendrocytes), and finally into mature oligodendrocytes that enwrap neuronal axons with myelin sheaths[Adapted from Ref.35].

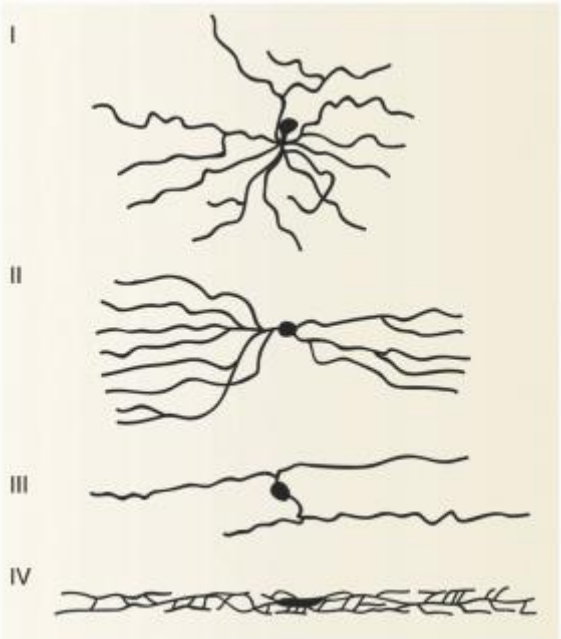

Figure 6 The four types of oligodendrocytes

The four type of oligodendrocytes recognized by del Rìo-Hortega[Adapted from Ref.36].

The major central nervous system myelin proteins are the myelin basic protein (MBP), and the proteolipid proteins (PLPs/DM20) which constitute the 80% of the total myelin proteins[37,38]. To form the myelin sheath, oligodendrocytes have to deliver large quantities of myelin along the axon, at the proper development stage. In the same way, neurons are responsible for the differentiation of the oligodendrocytes and for the transport of PLP[37]. The Schwann cells represents the major population of peripheral glial cells and they are responsible for the release of the myelin in the PNS. The Schwann cells precursors originate from the cells of the neural crest and they migrate along axons extending to their final target tissues[39]. It is possible to distinguish between two different types of Schwann cells: the non-myelinating one, also called Remark cells, which enwrap small

diameter axons; the myelinating one, responsible for myelinate the larger axons of sensory and motor neurons. Both of these cells are involved in the metabolic neuronal support, but just the myelinating accelerate the nerve fiber conduction[40]. On the contrary to oligodendrocytes, not reprogrammed to repair cells and for myelin regeneration, Schwann cells, in the PNS can convert to cells able to repair after injury[41].

1.2 Immune response in CNS

The CNS is firstly defended and protected against exogenous and endogenous threats by genuine physical barriers, such as the meninges, which surround the brain and the spinal cord and the cerebral spinal fluid (CSF). Pathogens, circulating immune cells and foreign factors within the blood are faced by a physical BBB, jointly maintained by tight junctions between brain endothelial cells, the basal lamina of these cells and astrocytes end feet processes[42,43] (Fig. 7). It is possible to have a leakage of blood material in the CSF and in the nervous tissues that triggers, at first, the activation of the innate immunity, in which the main functions are executed by those cells expressing the pattern recognition receptors (PRRs), e.g. the Toll-like receptor (TLR) expressed by microglial cells[44]. These receptors activate specific pathways which lead to the release of specific molecules involved in the progression or resolution of the inflammatory state, called cytokines and chemokines, e.g. tumor necrosis factor-α (TNF- α) or the interleukins 1 (IL-1).

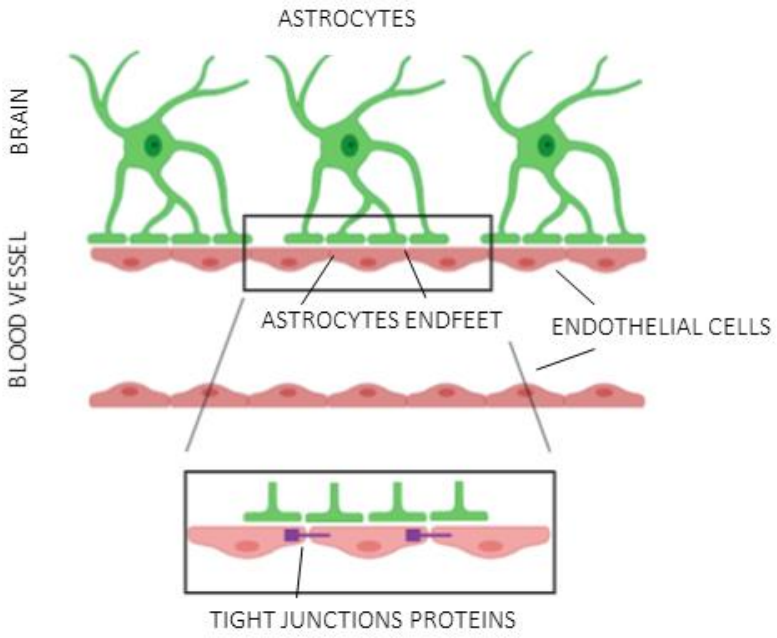

Figure 7 Blood brain barrier

The blood-brain barrier is made up of astrocytes end feet, endothelial cells that are tightly connected to each other by tight junction proteins (purple). These tight connections prevent the leakage of unwanted substances from the blood to the brain. [Sketch made with Biorender.com]

1.3 Neuroglia in inflammatory diseases

Microglia are primary mediators of inflammation. They trigger inflammatory responses similarly to peripheral macrophages, although these responses are less robust. This is partly due to the fact that their precursors enter the CNS during the early embryonic development and they are normally not replaced by infiltrating monocytes, during the other stages[45]. Thanks to the wide range of TLR on their membranes, they recognize specific ligands which start the inflammatory processes, activating signaling molecules

such as NF-κB and they promote the activation of the adaptive immune responses[46]. When insults like pathogens, tissue damage, abnormal stimulations, neurotoxins or infections occur, they firstly switch their surveillance phenotype toward the primed or reactive state, which is responsible for the release of the cytokines, within a few tens of minutes[33,47] and then toward the amoeboid one, which allows microglia to become phagocytic cells[48] (Fig. 8). The released cytokines can be pro- or anti-inflammatory, in response to different stimuli. According to this, microglia can adopt two different states, M1 and M2, respectively the pro-inflammatory and the anti-inflammatory and they can alternate between the two.

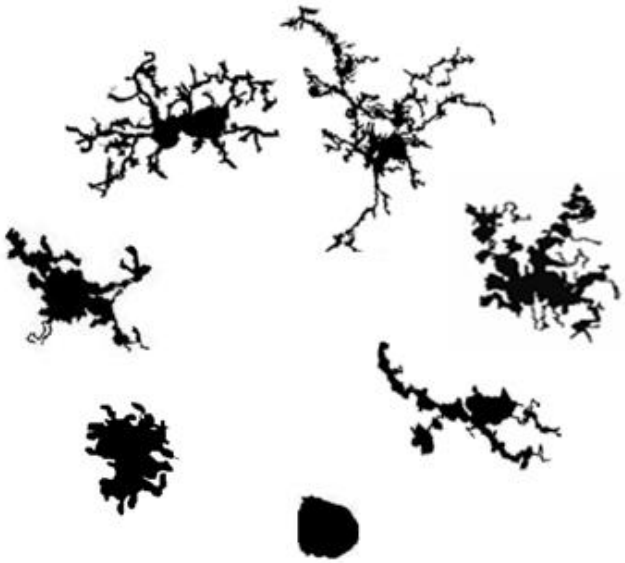

Figure 8 Different shapes of microglia

This picture shows the changes in morphology undergone microglial cells[Adapted from Ref.49].

In the first configuration, microglia show the expression of cytokines like TNF-α, IL-1β and IL-6 and of the respective receptors on the cell membrane surfaces. In the second one, they present anti-inflammatory cytokines, as IL-13 and IL-4[50]. The two different classes of cytokines induce several types of responses, that can be respectively detrimental or protective for the neurons and eventually for the tissue. In damaged tissues, microglia proliferate in response to specific cytokines such as macrophage-colony stimulating factors (M-CSF) and granulocyte macrophage-colony stimulating factors (GM-CSF)[51]. On the other hand, it has been shown that both microglia and astrocytes in response to pro-inflammatory cytokines stimulation release peculiar proteins called chemokines, that allow microglia expressing chemokines receptor, such as CCR2, CXCR10, to migrate toward the damage site, when they are in their reactive state[52].

Astrocytes are involved in several homeostatic functions, such as neurotransmitter, pH, water and ion homeostasis, they are part of the BBB and they are normally maintained in a resting state. They are not immune cells *per se*, but, following an insult to the brain, together with microglia, astrocytes undergo a process known as ‘‘reactive astrogliosis’’, which is characterized by finely gradual and progressive changes in genes expression and cellular morphology[53]. Moderate reactive astrogliosis develops if the triggering mechanism is transient and there is the potential for resolution. On the opposite, extreme levels of reactive astrogliosis occur in response to overt tissue damage and inflammation and the phenomenon involves scar formation that incorporates newly proliferated cells[54] (Fig. 9).

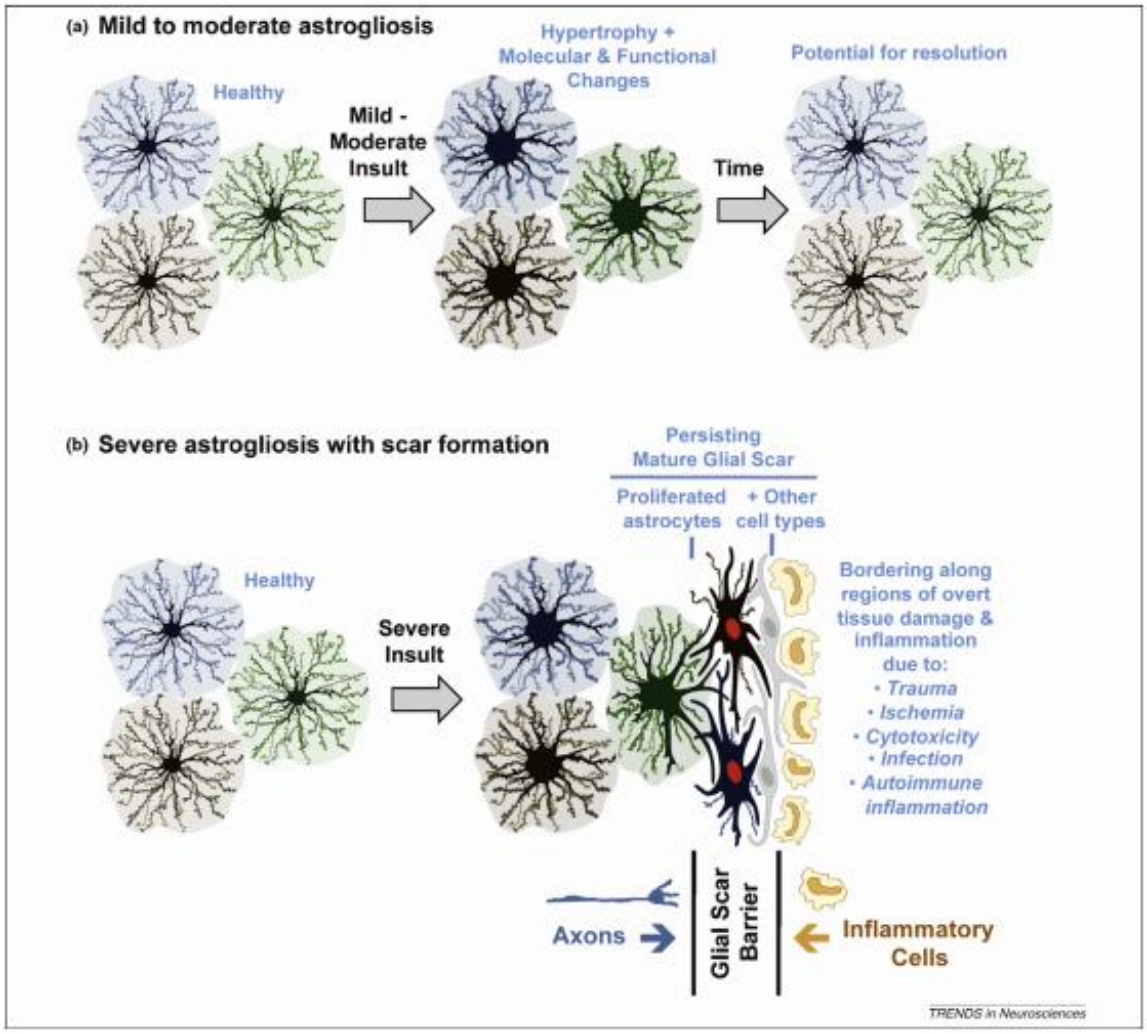

Figure 9 Schematic representations of different gradations of reactive astrogliosis a) Variable changes in molecular expression and functional activity together with variable degrees of cellular hypertrophy. Such changes occur after mild trauma or at sites distant from a more severe injury, or after moderate metabolic or molecular insults or milder infections or inflammatory activation; b) this reactive astrogliosis with persisting scar formation generally occurs along borders to areas of overt cell and tissue damage and inflammation. Glial scar formation includes newly proliferated astrocytes (with red nuclei in figure) and other cell types. Mature glial scars tend to persist for long periods and act as barriers not only to axon regeneration but also to inflammatory cells in a manner that protects healthy tissue from nearby areas of intense inflammation[Adapted from Ref.54].

According to the macrophage nomenclature, reactive astrocytes can be divided in two different groups based on their phenotype. We refer to A1 astrocytes when they highly upregulate many classical complement cascade genes known to be destructive for the synapses and detrimental to neuronal functions. They are induced by reactive microglia via pro-inflammatory cytokines such as TNF-α and the ones of the IL family. They may be harmful. On the other hand, we refer to A2 astrocytes, when they upregulate neurotrophic factors and for this reason they are protective[55]. Well-known hallmarks of astrocytes reactivity are the increase in GFAP expression and the altered expression of AQP4 (aquaporin 4), a water channel widely expressed in the astrocytes end-feet, which controls brain water homeostasis[56]. Together with astrocytes and microglia, oligodendrocytes as well are directly involved in neuroinflammation and immune modulation in CNS diseases like multiple sclerosis due to the expression of tumor necrosis factor-α (TNF-α) receptor, TNFR2[57].

In conclusion, the exact molecular triggers of astrocyte and microglia reactivity during inflammation and initial stages of neurodegenerative diseases, before significant neuronal loss, are unknown, it is suggested that they sense altered neurotransmission, release of stress signals such as cytokines and chemokines, presence of mediators of the innate immunity like lipopolysaccharide (LPS), glucose deprivation, hypoxia, presence of reactive oxygen species and abnormally folded proteins, like amyloid-β for the Alzheimer disease. It is also evident that astrocytes and microglia cooperate both during development and adult life in regulating synaptic functions and providing trophic support, and most importantly, in triggering neurorepair following injury[58].

1.4 Cytokines pathways in neuroinflammation

With the term cytokines we refer to small proteins synthetized by the cells of the immune system such as microglia, but also by astrocytes and involved not only in mediating the intensity and duration of the immune and inflammatory responses, but also in neurogenesis, cell growth and differentiation and in tissue homeostasis in CNS[59,60]. They are a large and diverse group of pro- or anti- inflammatory factors that are assimilated into families based on their structural homology or on that one of their receptors. Chemokines are a group of secreted proteins within the cytokine family which induce macrophages migration. These "chemotactic cytokines" are involved in leukocyte chemoattraction and trafficking of immune cells. As well as cytokines, chemokines belong to two categories according to their biological activity: the maintenance of homeostasis and the induction of inflammation. The binding of a cytokine or chemokine ligand to its receptor results in the activation of the receptor itself, which induces a signaling cascade in order to regulate various cellular functions such as cell adhesion, phagocytosis, other cytokines secretion, cell activation, cell proliferation, cell survival and cell death, apoptosis, angiogenesis and proliferation. The main cytokines include the interleukins family, TNF-α, interferon- γ (IFN-γ), GM-CSF and transforming growth factor-β (TGF-β). On the other hand, the principal chemokines produced in the CNS are CCL2, CXCL8, CXCL10, CCL5 and CCL3[61]. For instance, increased circulating pro-inflammatory cytokines have been associated with the neurodegenerative conditions of Alzheimer's disease and Parkinson's disease and moreover some cytokines have been associated with specific symptoms[62,63].

IL-1 family is primarily associated with innate immunity. The pro-inflammatory IL-1 was described to regulate the amyloid β-protein precursor (APP) processing and amyloid β (Aβ) synthesis, in particular increasing it and this may contribute to plaque formation and progression, dystrophic neurite proliferation and to neuronal loss[64,65]. IL-6 overexpression induces extensive gliosis and suppresses Aβ deposition in in *vivo* APP mice model[66]. TNF-α is another mediator, actively produced by microglia during inflammation. Its expression is low in healthy conditions, for this reason it is difficult to determine TNF-α physiological function when released at basal levels. TNF-α plays a key role in neuroinflammation-mediated cell death, thanks to the presence on target cells of the so called "death receptors", which, after ligand engagement, induce caspase activation and cell death. TNF-α stimulates BACE1 expression and enhances amyloidogenic processing from APP expressing astrocytes and cortical neurons. TNF-α increases the frequency of spontaneous miniature post-synaptic currents (minis)[67]. IFN-γ is another cytokine, only produced by lymphocytes, up-regulated in AD brains with pleiotropic effects, exhibiting both deleterious and protective functions[68]. It was demonstrated that in experimental autoimmune encephalomyelitis (EAE) animal model, administering IFNγ during the early stages of the pathology exacerbates clinical disease, although the administration during the late phases leads to amelioration. IFNγ can also inhibit TH cell production of IL-17, known to facilitates the development of neuroinflammatory lesions[69]. Moreover, astrocytes produce chemokines in response to IFNγ, and silencing IFNγ signaling specifically in astrocytes ameliorated EAE[70]. IFNγ may promote BBB integrity by enhancing expression of tight junction proteins in endothelial cells.

TGF-β1 plays a central role in the brain response to injury, and elevated TGF-β1 levels have been found in CSF and serum of AD patients[71]. Even if the clinical association between cytokines and disease hallmarks have been elsewhere understood, the pathophysiological mechanisms behind several classes of cytokines are still unknown.

2. Spinal Cord: a brief overview

2. 1 Anatomy and functions of the Spinal Cord

As part of the CNS, the spinal cord is considered the focus of information transfer between body and brain and a center for neuronal circuits that integrate and coordinate complex sensory, motor and autonomic functions[72]. It is contained and preserved by the spinal column and surrounded by the meninges. Along its length the spinal cord is divided in three segments, each associated with groups of sensory neurons, whose cell bodies form the dorsal root ganglia (DRG), while the axons centrifugally innervate the periphery. In humans, depending on the position of the segments, they can be cervical, thoracic, lumbar and sacral, in a rostro-caudal orientation. Internally, the spinal cord is also divided into grey and white matter. This latter surrounds the cord and comprises the myelinated motor and sensory axon tracts that relay signals to and from the brain. The grey matter shows a peculiar butterfly shape with two ventral horns and two dorsal horns, which comprise the termination of primary afferent neurons, neurons ascending from the brain, interneurons and ascending tract cells projecting to higher CNS levels[72]. It further includes microglia, astrocytes, oligodendrocytes and unmyelinated axons, as well[72]. The neurons contained in the grey matter are ordered in different layers called laminae, from I to X (Fig. 10). Spinal neurons are involved in two main functions: i) they relay sensory information to spinal and supra-spinal centers located in the brain stem ii) and they integrate sensory inputs and motor outputs. These two functions are also anatomically differentiated.

Indeed, the sensory neurons are concentrated in the dorsal spinal cord, whereas circuits involved in proprioception and motor control are located in the ventral spinal cord[73].

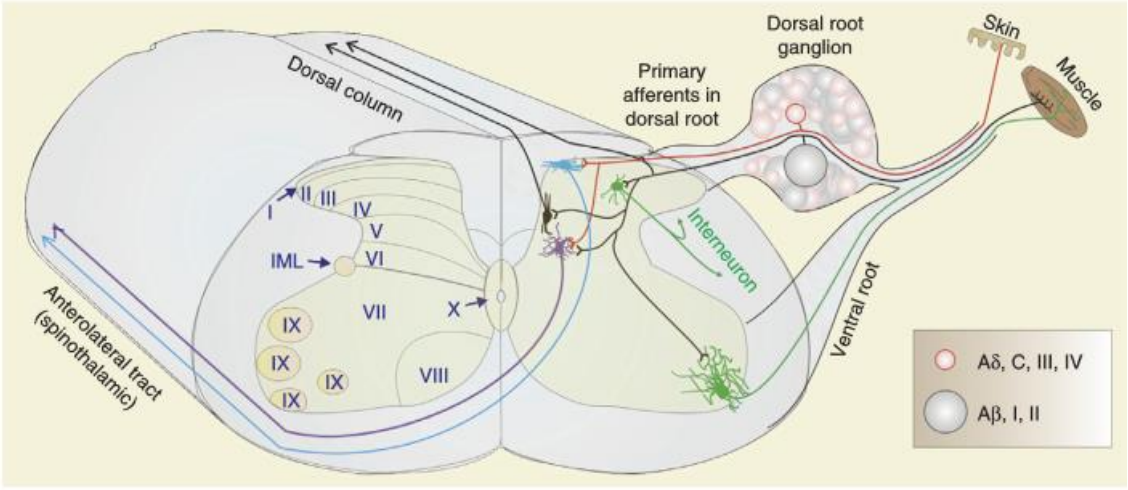

Figure 8 The segmental organization of the spinal cord

The spinal cord is divided in sensory dorsal horn (laminae I-VI), intermediate layer (lamina VII) and ventral horn (VII-IX). Motor neurons nuclei are located in lamina IX and their axons, along with sympathetic preganglionic neurons located in intermediolateral nucleus (IML), exit via ventral roots. Sensory information is transmitted to brain through two principal axon tracts, the dorsal column and anterolateral system[Adapted from Ref.72].

The somatosensory system

The somatosensory system is a complex circuit which allows to perceive a wide net of heterogeneous signals coming from the periphery, thanks to the presence of a range of receptors distributed all over the body. According to the type of signal, receptors are classified as: chemoreceptors, thermoreceptors, mechanoreceptors and nociceptors and translate physical stimuli into electrical signals. Primary afferent axons, whose cell bodies

are inside DRG, located alongside the spinal cord, can be divided into thickly myelinated fast-conducting Aβ fibers, thinly myelinated fast-conducting Aδ fibers and unmyelinated slow-conducting C fibers. The dorsal horn receives several inputs from these fibers, in multiple sensory modalities. Information are then processed by local interneurons, whose axons remain in the spinal cord and modulated by descending axons before being transmitted to the brain. Interneurons in the external laminae are both inhibitory (GABA/glycine) and excitatory (glutamate/substance P)[74]. Primary afferents release glutamate as a neurotransmitter to evoke fast postsynaptic responses composed of early AMPA/kainate and late NMDA receptor-mediated components. The continuous signals coming from the periphery are strictly regulated by depolarization of their terminals thanks to the direct synaptic actions of interneurons[75,76], in order to avoid conditions such as neuropathic pain, due to imbalances between central excitatory and inhibitory signaling such that inhibitory interneurons and descending control systems are impaired[77]. Indeed, one of the main functions of the dorsal horn is to integrate and relay pain information to higher area of the brain.

The motor system

The ventral horn is involved in motor functions. The laminae are occupied by glutamatergic excitatory and GABA/glycinergic inhibitory interneurons. In the lamina IX cholinergic motorneurons are located, which send their long axons out of the ventral horn to innervate the skeletal muscle fibers at the neuromuscular junction. Motorneurons are the ultimate actors in the contraction process. They are divided into α-motoneurons, which supply skeletal (extrafusal) muscle fibers and are responsible for

movement and γ-motoneurons, smaller than the others, which innervate intrafusal muscle fibers in order to control muscle tone by regulating the sensitivity of muscle spindles to stretch[72]. In order to control the correct functioning of the motor behavior and to protect body from harm, spinal cord needs reflexes. Spinal reflexes are involuntary and stereotyped responses to sensory stimuli arising from receptors in muscles, joints, and skin, either directly or indirectly via one or more interposed interneurons, and the neural circuitry responsible for the motor response is entirely contained within the spinal cord. Even the simplest reflex is a fine and regulated mechanism, in which the interplay between motorneurons and interneurons results in the correct excitation and inhibition ratio, in order to generate flexors and extensors muscles contract/release[72]. Central pattern generators (CPGs) are intrinsic neuronal networks generally defined as networks of neurons capable of enabling the production of central commands, specifically controlling stereotyped and rhythmic motor behaviors, as for example deglutition, mastication, respiration, defecation, micturition and ejaculation[78]. More specifically, the CPG controlling locomotion-like activities in absence of sensory and descending inputs from the brain cortex, which carry timing information, resides along the ventromedial portion of the lower thoracic and lumbar spinal cord of limbed vertebrates[79]. CPGs studies have been also conducted in invertebrate species, such as lampreys, where the presence of neuronal networks capable in inducing swimming behavior was demonstrated[80].

2. 2 Neurodegenerative diseases and inflammation in the spinal cord: some example

The standpoint regarding the pivotal role of neurons in CNS in health and disease has changed, microglia and astrocytes are known to play an essential and active role in development, synaptic plasticity and support for spinal cord neurons. On the other hand, the key homeostatic functions of neuroglia may be compromised, turning them into the major drivers of neuronal cell death. Neurorepair begins with the elimination of damaged tissues when the pro-inflammatory response of microglia and astrocytes decrease and an anti-inflammatory response, such as the secretion of the anti-inflammatory cytokines IL-4 and IL-10 starts to predominate. However, the extensive and/or prolonged damage can prevent efficient repair, resulting in chronic neuroinflammation, as is the case of spinal cord injury (SCI), motor diseases like amyotrophic later sclerosis (ALS), spinal muscular atrophy (SMA) and multiple sclerosis (MS).

Spinal cord injury

Traumatic or non-traumatic SCI is a devastating condition with high incidence, causing mortality or severe neurological deficits and permanent disability[81]. When SCI occurs, synaptic connections are lost, demyelination and axon damage disrupt signal propagation, and neurons undergo mechanically induced cell death. Currently, there are not therapies able to restore neuronal connections and re-establish neuronal circuits responsible for complex functions such as standing or walking. Since the primary injury activates non neuronal cells, such as glia and pericytes, potential therapies can target these cells, their mutual interaction or their interaction with neurons. Non neuronal cells

activation induces cascades of vascular and inflammatory events, further leading to cell death, but also known to facilitate repair. In detail, following SCI, glial cells secrete toxins and cytokines in response to the mechanical damage. SCI activates resident astrocytes, which migrate to the lesion epicenter and seclude inflammatory cells, leading to tissue repair. However, active astrocytes gradually transform into scar-forming astrocytes, thanks also to type I collagen in the extracellular matrix (ECM) that form astrocytic scars[82]. Scars formation is irreversible and it permanently inhibit axonal regrowth in both rodents and humans[83]. On the other hand, the fibrotic scars have a beneficial, tissue-preserving role, confining inflammation to the lesion epicenter and restricting tissue damage and neural loss after SCI[84].

Due to the astrocyte's impairment, the BBB is disrupted during SCI, and this facilitates the entrance of immune cells, such as microglia, which have been shown to modify the microenvironment, causing an upregulation of factors that promote oligodendrocyte progenitor cell proliferation[85].

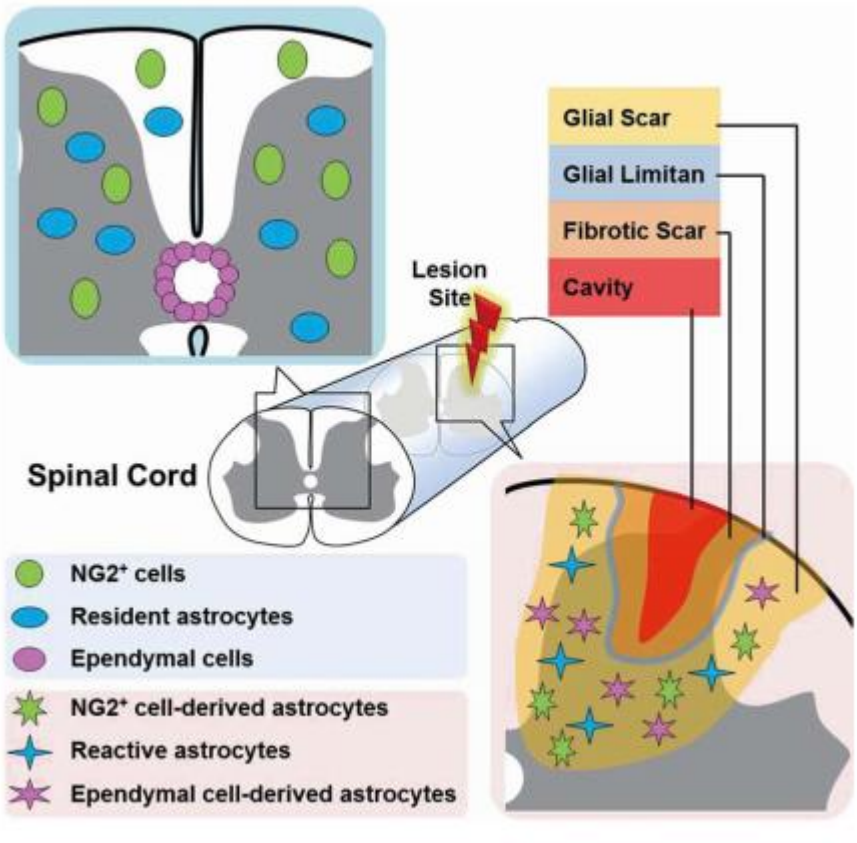

Figure 9 Scar formation scheme

Astrocytes, $NG2^+$ cells and ependymal cells are involved in the scar-formation after SCI[Adapted from Ref.86].

Motor diseases

ALS is a relentless, adult-onset, fatal paralytic disorder confined to the voluntary motor system[87]. Between the neurodegenerative motor diseases, it is the most known, commonly arising as a sporadic condition, but ~ 10 % of the disease is inherited and due to superoxide dismutase 1 (SOD1) mutation. These rare familial occurrences are clinically and pathologically indistinguishable from the sporadic cases of ALS. It is characterized by

the loss of motorneurons and by the massive activation of astrocytes and microglia. SMA is the second most common autosomal-recessive disorder of infancy, often leading to death[88]. It is characterized by a selective loss of motorneurons within the anterior horns. Other pathological hallmarks of SMA are glial bundle formation, predominantly in the spinal cord anterior roots and in the lumbar region and reactive gliosis, even if, on the contrary to ALS, there is any model of the disease in which gliosis has been demonstrated[89]. These kinds of pathologies are part of the neurodegenerative diseases, whose prominent feature is neuroinflammation, characterized by active gliosis. This means that microglia can became primed, triggered by cytokines and chemokines, such IFN-γ, TNFα, GM-CSF originating from neurons and astrocytes. They can, then, became surveillant, exhibiting thicker cell bodies and proximal processes and eventually lead to motorneurons death[90]. In the same way, astrocytes show a typical reactive morphology with hypertrophic nuclei and with the increased expression of GFAP protein in their processes. In this scenario, they can have a protective or detrimental behavior, helping or preventing motorneurons survival, respectively thanks to the release of neurotrophic factors or to the synthesis of nitric oxide[91].

Multiple sclerosis

Differently from the above-mentioned diseases, MS is an autoimmune and not hereditary pathology characterized by inflammatory cascade in the CNS, which is mainly caused by inappropriately activated T cells, that trigger an immune response against myelin and oligodendrocytes. Astrocytes are recognized as cells that critically contribute to the early development of MS lesions, since they are involved in the myelin phagocytosis, which

induces the MS lesions[92]. Myelin uptake induces NF-kB signaling activation, which leads to chemokines production, such as CCL3, CCL5 and CXCL9 and to the resulting activation of microglia[92].

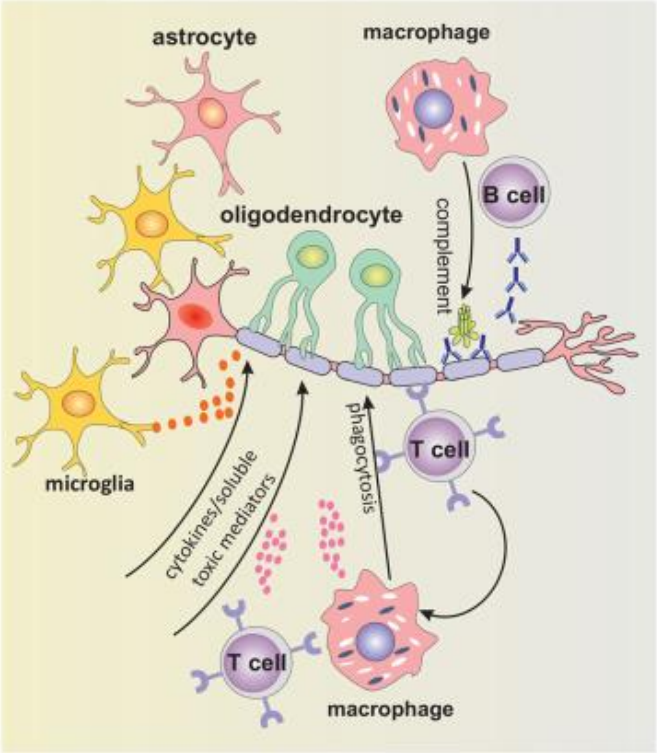

Figure 10 Involvement of immune cells in MS pathogenesis

T cells recognize myelin and activate macrophages and microglia to damage myelin by phagocytosis. Cytokines and toxic mediators such as NO released by immune cells cause myelin damage[Adapted from Ref.93].

Indeed, reactive astrocytes are present in the active margins of demyelinating lesions. During these events, astrocytes become hypertrophic, they increase the volume of the cell bodies and they induce disruption of astrocyte-oligodendrocyte networks. *In vivo* experiments reveal that reactive astrocytes likely contribute to tissue damage in MS also

through impaired glutamate re-uptake[94]. On the other hand, astrocytes and microglia are known to drive neuroprotective effects thanks to brain-derived neurotrophic factor (BDNF) expression in those inflammatory cells detected around the lesioned regions[95]. Microglial cells as astrocytes contribute to myelin lesion formation and to oligodendrocytes degeneration, thanks to nitric oxide (NO) and TNF-α production, which activate mechanisms of apoptosis and the resulting activation of astrocytes[96,97]. Consequently, astrogliosis elicits BBB impairment.

3. Synaptic activity and inflammatory milieu

3.1 Microcircuit synapses and soluble signaling in inflammation

Cytokines are the main actors during the inflammatory events but regardless this role, they are also involved in crucial activities in the CNS, related to its growth and development. Moreover, it is now well established that cytokines are powerful neuromodulatory molecules capable of influencing synaptic transmission and neuronal excitability, either directly by activating their neuronal receptors in the spinal cord, or indirectly by promoting the release of such molecules from glia or the endothelium, like nitric oxide[98]. Synaptopathy is the recent term used to indicate pathological synaptic alterations, dysfunction and loss and it has been implicated in many CNS disorders, which involve features as neuroinflammation, such as MS[99]. Indeed, the inflammatory microenvironment seems to directly influence the structural modifications and loss of the presynaptic and postsynaptic elements, as observed in post-mortem brain of MS patients, where decreased levels of proteins crucial for synaptic maintenance and functions, have been found[100]. Moreover, in MS a permanent increase in pro-inflammatory cytokines levels and increased availability of glutamate can upregulate neuronal GluR expression and induce synaptic dysfunction, thereby reinforcing the local glutamate excitotoxicity[99]. Research on this subject has led to a deep understanding of the role of pro-inflammatory cytokines in driving synaptic function and plasticity. Especially, TNF-α, IL-1β and IL-6 are attracting considerable interest due to their implication in a wide spectrum of synaptic dysfunctions typically concerning neurological and spinal disorders[101,102]. TNF-α modulates glutamate and $GABA_A$ receptors at the

neuronal membrane, resulting in increased excitotoxicity stress and neuronal death. In particular, TNF-α can exhibit its function affecting the expression of AMPARs on the cell membrane by TNF-R1[103]. In addition, TNF-α can also modify extracellular glutamate levels by inducing glutamate release from microglia and as well as blocking the astrocytic glutamate re-uptake[104,105]. TNF-α further induces a rapid decrease of GABAergic synaptic strength associated with a down-regulation of cell surface $GABA_Ar$[106]. Similarly, IL-1β plays a crucial role in synaptic modulation by binding its receptor and up-regulating the surface expression of NMDA receptors, which leads to a marked Ca^{2+} efflux with the subsequent neuronal hyperexcitability in spinal slices[107]. Spinal cord slices acutely incubated with TNF-α enhanced the frequency of spontaneous excitatory post-synaptic currents (sEPSCs), while the incubation with IL-6 reduced the frequency of spontaneous inhibitory post-synaptic currents (sIPSCs). Notably, IL-1β both enhanced the frequency and amplitude of sEPSCs and reduced the frequency and amplitude of sIPSCs. Consistently, TNF-α and IL-1β enhanced AMPA- or NMDA-induced currents, and IL-1β and IL-6 suppressed GABA- and glycine-induced currents[101]. IL-1β also acted to increase mEPSC amplitudes and frequencies, through presynaptic glutamate release and postsynaptic AMPA receptor activity, in the spinal dorsal horn[108]. Concerning the family of the M-CSFs, some of them are involved in the changes induced at the synaptic level. For instance, the colony stimulating factor 1 (CSF-1) increases the amplitude and frequency of sEPSCs of the dorsal spinal neurons[109]. Although great effort has been applied in the studies of the dorsal horns undergone pro-inflammatory cytokines exposure, less is known about the behavior of the ventral one, which is the focus of the motor networks, impaired during diseases like MS, and it is also known that

coordination between neurons is largely controlled by glycinergic and glutamatergic interactions[110]. Regarding this, recently in our group, it has been shown that in spinal cultured tissues exposed to a cocktail of pro-inflammatory cytokines composed by TNF-α, IL-1β and GM-CSF, all known to be released in experimental autoimmune encephalomyelitis (EAE) models, ventral interneurons displayed a significant increase in spontaneous synaptic activity, also characterized by a speeding up of the GABAergic decay time constant[111].

In conclusion, during pathological conditions, the final downstream effects of cytokines on synaptic transmission and neuronal survival depends on the synaptic cytokine concentrations and on the subcellular expression of their receptors in specific neuronal compartments. Likewise, the balance between pro-inflammatory and anti-inflammatory cytokines is important for the final effects and for the resolution of the inflammatory events[112]. This approach on the synaptopathies could represent a novel and promising target for future therapies. Overall, these results indicate that the above-mentioned cytokines are involved in the spinal neurons synaptic activity impairment, disrupting the excitatory/inhibitory ratio and probably leading to excitotoxicity or eventually to neuron death. This provides the necessity to investigate the cross-talk between the immune system, the main source of cytokines, and neurons exploiting synaptic activity, but also the entire network activity as primary evaluation tools.

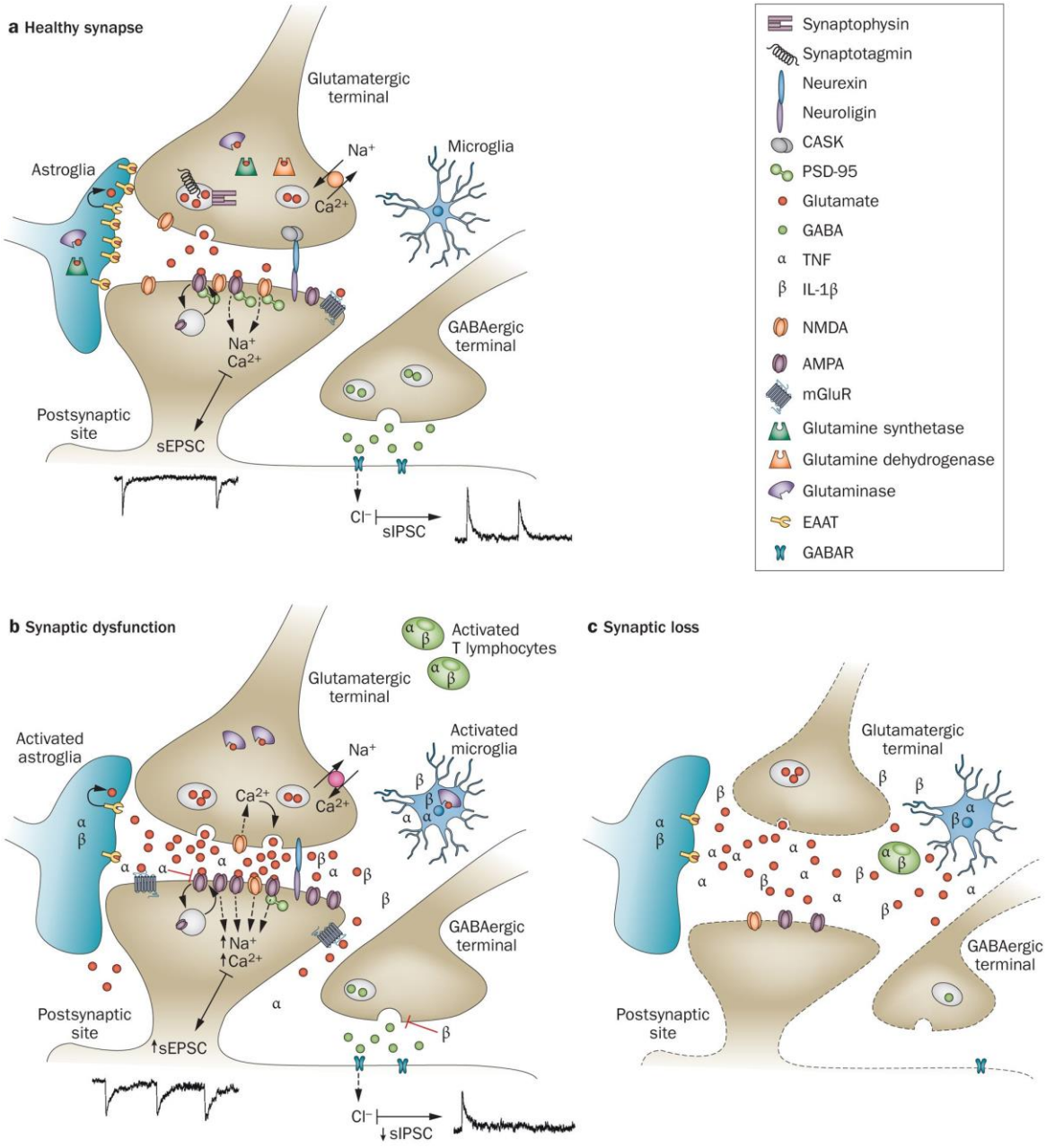

Figure 11 Inflammatory synaptic dysfunction

a The concentrations of excitatory (glutamate) and inhibitory (GABA) neurotransmitters at the synaptic cleft are modulated by strict control of transmitter release, degradation or reuptake. **b** Proinflammatory cytokines released by autoreactive lymphocytes and activated microglia induce synaptic dysfunction in both glutamatergic and GABAergic systems[Adapted from Ref.99].

3.2 Cross-talk among neuroglia and neurons in physiology and inflammation

A single astrocyte can contact tens of thousands of individual synapses and has highly dynamic processes capable of altering the extracellular space[113,114]. Likewise, activated astrocytes release gliotransmitters and are sensitive to neurotransmitters suggesting that astrocytic processes interact with pre- and post-synaptic neuronal elements[115]. The interaction between neurons and astrocytes is known to occur in physiological conditions, in diverse fashions like the tripartite synapse, the exosomes communication and the gap junctions (GJs) coupling[116,117,118] and astrocytes exert several homeostatic functions that collectively contribute to maintain the microenvironment in such conditions in order to ensure the optimal neuronal functions. For example, thanks to the presence of a high number of inward rectifier channels on astrocytes, the extracellular potassium concentration is always preserved within the correct range[119]. This latter mechanism, together with the glutamate uptake by astrocytes from the extracellular milieu[19], contributes to avoid neuronal depolarization, hyperexcitability and excitotoxicity. Some studies speculated that alterations in K^+ buffering in astrocytes from glial scars and altered expression, localization and function of astrocytic Kir4.1 channels in brain tissue from epileptic patients and in the ventral horn of spinal cord could be plausible mechanisms involving abnormal K^+ buffering activity[120,121]. Likewise, under physiological conditions, glial-derived exosomes mediate important functions participating in neural circuit development and maintenance, promoting neurite outgrowth, synaptic activity and neuronal survival. On the contrary, after a neural insult, astrocytes and microglia became activated and release exosomes containing mutated

and inflammatory proteins, such as superoxide dismutase 1 (SOD1) and pro-inflammatory cytokines, leading to neurodegeneration[122,123]. Exosomes crucially contribute to intercellular communication, representing key vectorized systems able to spread and actively transfer signaling molecules from neuroglia to neurons, ultimately modulating target cell functions. Exosomes are also able to cross the blood brain barrier propagating the neuroinflammatory response to the periphery. Similarly, microglia are involved in the regulation of neuronal activity contributing to the development, plasticity and maintenance of neuronal circuits. Furthermore, the surveillant microglia are able to sense and monitor the functional state of synapses, as observed *in vivo* by Wake and colleagues[124]. Under pathological conditions or after stimulation, microglia undergo a conformational and functional change and they become active or "primed" and this process is followed by the release of neurotransmitters, small molecules as nitric oxide, trophic factors and cytokines, known to control neuronal function and synaptic transmission[125]. An example is given by the microglia stimulation performed with LPS, which induced both ATP release with the subsequent release of glutamate from the neighbor astrocytes and increase in the spontaneous AMPA PSCs frequency in hippocampal neurons. This did not occur in pure astrocytes cultures[126].

In conclusion, this tight collaboration among neurons and neuroglia and the neuroglial support could be even more important during pathological events such as inflammation, but microglia and astrocytes, once stimulated, release pro-inflammatory mediators such as TNF-α and IL-1β, known to impair glutamate uptake/release and to increase excitatory transmission, which are detrimental for the neurons[127].

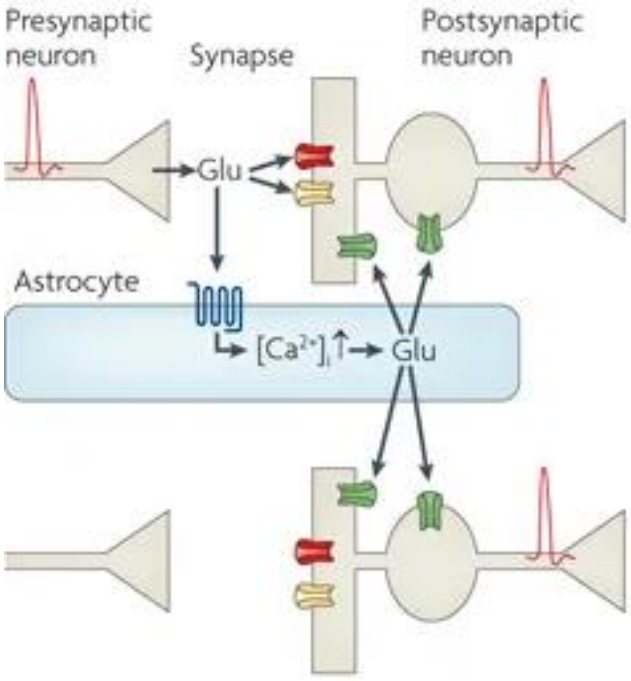

Figure 12 Glutamate released from astrocytes

Stimulating the left neuron evokes glutamate release that triggers fast synaptic currents in the right cell, as well as an increase in intracellular Ca^{2+} ($[Ca^{2+}]_i$) in astrocytes mediated by mGluRs (blue). This releases glutamate from the astrocytes, which activates extra synaptic NMDARs (green) in nearby cells, generating slow inward currents that enhance excitability and synchronize firing of these neurons (the two neurons on the right) [Adapted from Ref.115].

3.3 Diverse treatments mimic diverse neuroinflammatory insult: cytokines and LPS effects on spinal cord cells

Dissecting the impact of immune status alterations on spinal circuit function is important to better understand the progress of several diseases, among them MS and ALS, and to develop therapeutic strategies in order to deal with these pathologies. We have mentioned how soluble mediators, such as cytokines, mainly released by neuroglia, mediate the synaptic transmission and how relevant is the coupling between neuroglia and neurons, both in health and disease, in the CNS. What about the specific effects on spinal cord tissues due to LPS, known to be a potent trigger of cytokine induction and the most common stimulus used to investigate microglial reactivity in brain inflammation and to pro-inflammatory cytokines, well-known determinant in the etiology of different immune disease[5,128]? The innate immunity of $SOD1^{G37R}$ transgenic mice was triggered with systemic administration of LPS, which exacerbates the disease progression[129]. This suggest that inflammation is a key event in the pathogenesis of ALS and may mediate motor neuron injury. In rat neonatal spinal slices, LPS-mediated inflammation induces both the increase in the mRNA level of IL-1β and severe degeneration of motor neurons but relatively slight damage to interneurons, which is similar to the pathological change in ALS[130]. Moreover, treatment of spinal cord slice cultures with LPS disrupts axonal integrity, induced by the phagocytic activity of microglia[131]. As already assessed, microglial activation and synaptic dysfunction are both early features of many CNS diseases. LPS stimulation, both through intrathecal injection and through bath application, induces at first microglia activation, which secondly leads to a decrease in Glyr and $GABA_Ar$ expression and this modulation correlates with a differential modulation

of GABAergic and glycinergic neurotransmission[132]. It is also important to underlie that the activation of microglia, triggers the subsequent activation of astrocytes, mediated by Il-1α, TNF and the complement protein C1q[55]. It is well established that LPS induces the immune response thanks to the presence mainly on microglia of TLR4, even if it was more recently demonstrated that LPS-induced TLR4 signaling in neurons rapidly enhances calcium-permeable AMPAr currents[44,133,134]. Once activated, microglia release cytokines, known to produce profound changes, some of them briefly mentioned in the previous paragraphs. Among these cytokines, IL-1β, one of the first expressed during the induced signal cascade, enhances glutamate release in the spinal dorsal horn[107,108]. Moreover, TNF-α increases sEPSC frequency in dorsal horn neurons in a rat model of pain[135]. Spinal slices, obtained from $SOD1^{G93A}$ mice and co-cultured with motoneurons, show elevated levels of IL-1, IL-6, and IL-12p70, which were responsible for the toxicity induced on cocultured motorneurons, resulting in shortened neurite lengths[136]. Spinal cultured tissue exposed to a cocktail of pro-inflammatory cytokines, composed by TNF- α, IL-1β and GM-CSF display significant changes at the synaptic level (see paragraph 3.1), that were accompanied by significant production of cytokines and chemokines, astrogliosis and microglia activation[111].

4. Organotypic spinal cord and dorsal root ganglia co-cultures

Although the etiology of diverse neuroinflammatory and neurodegenerative diseases is likely distinct, they display shared common features: first, neurodegeneration results in clinical neurological disability and second, the occurrence of chronic microglial cell and astrocytes activation. Identifying novel therapeutics remains challenging due to undetermined etiology, the variable disease course marked by a prolonged subclinical phase and the paucity of validated targets. These factors make difficult to model neurodegenerative diseases in univocal way and they underlie the strong need to develop relevant model systems able to recapitulate as close as possible the *in vivo* brain structure and, at the same time, allowing manipulations and an easy access to individual cells. Furthermore, due to the essential role of synaptic activity during all the phases of brain development and how its impairment could be responsible also of late-onset disorders, a possible strategy is to focus more on the properties on immature neuronal circuits. An *in vitro* cell culture assay obviously fails to account for the complex interplay between cell types in the CNS, while animal based studies, even if demonstrate disease phenotypes, may not adequately recapitulate the pathophysiology of the disease in its completeness and they are difficult to manipulate experimentally in a high through-put manner[137,138]. The use of an *ex vivo* spinal cord slice culture system offers an alternative to these assays. Slice cultures maintain the basic tissue architecture and neuronal connections at the synaptic level. This allows us to account for the complexity of cellular interactions and several modifications of variables and manipulations of the system are permitted.

Ex vivo CNS slice culture system partly models the *in vivo* environment and it allows the development of specific disease models[131]. CNS slice preparations include acute or fresh slices and organotypic cultured slices. The first type of slices can only be maintained *ex vivo* for limited amount of hours, while in the second type the slices are maintained in culture for several weeks enabling to design studies *in vitro* over a period of days to weeks or months in a context that reflects organ features[139]. Organotypic slice cultures can be prepared from both late embryonic and early postnatal animals, because the essentials of the cytoarchitecture (such as dorsoventral organization) are already established in most CNS areas and they do not suffer of necrotic events as often happens with more aged animals[140].

4.1 *Ex-vivo* explants from mouse embryos spinal cords: cellular component and development

In order to develop organotypic spinal cord cultures, it is possible to take advantage of two major techniques: i) roller-tube cultures (dynamic)[140] and ii) interface cultures (static)[141]. In both these techniques cultures, the basic characteristic cytoarchitecture of the tissue of origin is retained with excellent cellular differentiation. The major difference between these techniques is the final slice thickness. Roller-tube cultures become thinner (100-200 µm), compared to the interface ones[140]. In the roller-tube culture, the tissue is embedded in a plasma clot on glass coverslips, it undergoes slow rotation that ensures oxygenation thanks to the continuous changing of the liquid-gas interface and finally it survives for several weeks or even months *in vitro*, like in the case of interface cultures.

Longevity and tissue flattening are the main features which make roller-tubes cultures the most suitable for electrophysiological and live cell imaging experiments, to investigate the dynamics of maturation processes that rely on neuronal-glia network activity. Many studies conducted in our laboratory report that spinal cord organotypic slice cultures preserve the basic spinal tissue cytoarchitecture, synaptic connections and the dorsal-ventral orientation of the spinal segment from which they are derived[142,143,144]. They are obtained from the spinal cords of mouse embryo and this represent an advantage, since during the culturing the cells undergo proliferation, migration and differentiation in the spinal cord, like in the *in vivo* spinal cord. As shown by our group and other groups, these cultures have peculiar characteristic. For example, mechanisms as synaptogenesis and myelin formation take place.

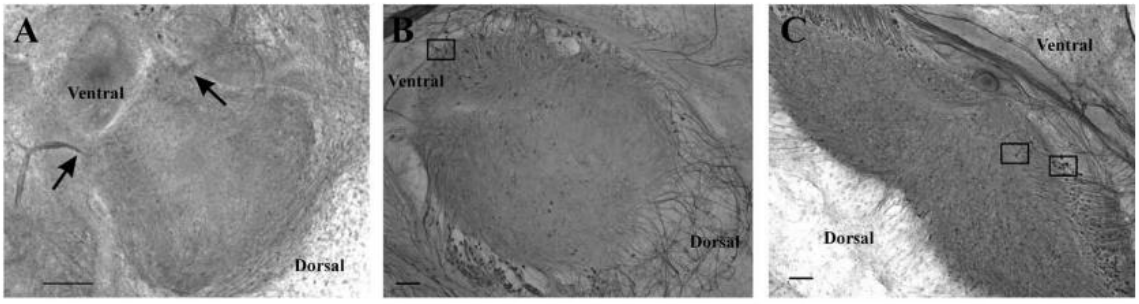

Figure 13 Immunocytochemistry of organotypic cultures with the anti-NF-H antibody SMI32

A) The culture at 8 days *in vitro* (DIV) labelled with SMI32 show processes exiting bilaterally from the ventral part of the slice (arrows). DRG cells present in the top part of the picture. B) The culture at 14 DIV show motoneurons located in the ventral region, bilaterally to the ventral fissure. C) Slice at 21 DIV notes motor neurons and DRG neurons in the ventral horn. All the images show the correct ventral-dorsal orientation typical of the spinal cord[Adapted from Ref.143].

In addition, they display heterogeneous neuronal phenotypes and neuroglial cells are preserved in a three-dimensional fashion and maintain the presence of DRG and their incoming output[111,143,145]. During spinal network maturation, two fundamental developmental steps regarding GABA and glycine neurotransmitters occur: the switch of GABA function from depolarizing to hyperpolarizing and the following shift in the spinal cord from GABA receptor-mediated to glycine receptor-mediated synaptic transmission[146,147]. These functional steps have also been described in spinal slices. During spinal network development progressive changes in network properties are required to generate mature motor behavior and some of these changes occur also during the *in vitro* development of organotypic spinal cord explants. For example, at early stage of development *in vitro* (1 week of *in vitro* growth, 1WIV), that corresponds to the late embryonic stage, ventral interneurons display a synchronous bursting activity which drives the muscle contractions and which is mediated by excitatory synaptic transmission via GABA/glycine receptors[148]. In fact, in this developmental stage, GABAergic and glycinergic synapses act as depolarizing endings, able to elevate intracellular Ca^{2+} concentration, necessary to guide growth and differentiation. At later stages (2 and 3 WIV), representing the early postnatal phase, when GABA and glycine receptor activities have an inhibitory role, bursting activity is drastically reduced as well as its correlation with motor responses[148]. Moreover, these developmental changes are associated with a progressive decrease in glutamic acid decarboxylase (GAD) immunoreactivity in the ventral area, which is the enzyme responsible of GABA synthesis in the period between 1 and 2-3 WIV. In this latter range, GAD-labeled neurons are localized principally in the dorsal horn regions[143].

These considerations identify organotypic spinal slices from mouse embryos as an eligible *in vitro* model to study the mechanisms of neurogenesis, glial differentiation, myelination, muscle formation and synaptogenesis. In fact, they represent an ideal experimental tool to design and perform several experiments, including the study at a single cell level of the dynamics of spinal network activity under stress conditions, such as inflammation.

4.2 Electrophysiology of spinal slices

Electrophysiological experiments such as patch-clamp recordings have been widely exploited by our group with the purpose to detect changes in neural mechanisms and activity, also relevant when the organotypic spinal cord slices are interfaced to different pathological environments. In particular, previous studies focused on the neural mechanisms responsible for the generation of rhythmic behavior, essential for clarifying the basis of locomotion, which resides in the ventral horn of the spinal cord. They took advantage of several features of these tissues, among which the possibility to easily identify interneurons based on their shape and localization, allowing to conduct electrophysiological patch-clamp experiments useful to observe the spinal network activity[152,153]; the fact that the slices maintain the correct dorsal-ventral orientation, providing the possibility to focus on a specific spinal area, and the correct structure of the pre-motor circuits, encompassing the complex interplay between interneurons and motor neurons, supported by the DRG and their incoming output[143]; the ability to reproduce suitable inflammatory responses mediated by the *in vitro* activation of microglia, astrocytes and oligodendrocytes[114,154]; the possibility of isolating a specific

mediated-receptor current using pharmacological blockers[151]. Patch-clamped ventral interneurons, identified thanks to their small diameter, their localization and their firing properties, revealed spontaneous rhythmic activity, following the co-application of pharmacological blocker of the inhibitory transmission and the same activity was inducible by rising the extracellular K^+ concentration[149,150]. Furthermore, during the development of spinal circuits, GABAergic synapses are modulated by glutamatergic transmission and display a developmental switch in spontaneous activity from stable bursting to random patterns, after the first week in culture. During this first week spontaneous bursts of interneurons correlate with muscular contractions due to the activation of motoneurons via AMPA-receptors. Conversely, bursting recorded in the presence of strychnine and bicuculline became increasingly regular with time *in vitro*[142,148]. Together, these results, are useful for studying the developmental changes in spinal circuits. More recently, in our group, organotypic cultures interfaced with carbon nanotube scaffolds were exploited to investigate whether and how the interactions at the monolayer level were translated to multilayered nerve tissues and they showed not only that slices neurite outgrowth was enforced, but also that the ventral interneurons spontaneous activity was improved[152]. Finally, Medelin and colleagues further exploited organotypic cultures from $SOD1^{G93A}$ mice to investigate on glycine-receptor mediated postsynaptic currents, demonstrating that the speeding up of the decay phase of glycine-PSCs was higher in SOD^{1G93A} interneurons compared to the wild type ones and this is an important feature in the regulation of the excitatory transmission[153].

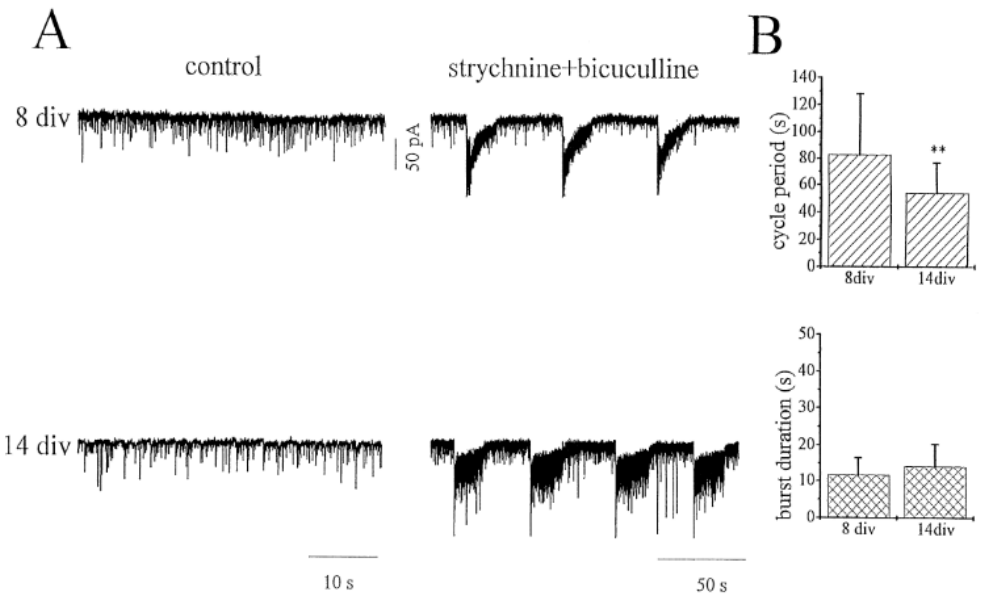

Figure 14 Spontaneous activity of ventral interneurons

Spontaneous synaptic activity in control solution (A, left) is shown at both one (8 DIV, top tracings) and two weeks in culture (14 DIV, bottom tracings). Co-application of strychnine and bicuculline (A, right) induces the appearance of rhythmic bursts of inward current. At 14 DIV frequency of bursting is higher than at 8 DIV[Adapted from Ref.149].

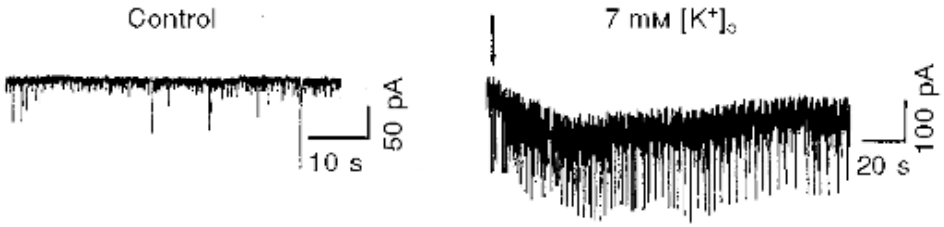

Figure 15 Increased extracellular [K¤] induces patterned activity in ventral interneurons

Left, spontaneous synaptic activity in control solution. Right, increased extracellular K^+ (7 mM; arrow indicates the start of application) induced a slow inward current which reached a peak value of −65 pA 40 s later[Adapted from Ref.150].

4.3 Organotypic slices in disease

The organotypic spinal cord system represent an excellent setting to perform several kinds of experiments and assays, in order to study its circuitry and the behavior of its resident cell types, that replicate the ones of the spinal cord region by which the slices are obtained. Moreover, since these slices can be kept in culture for weeks, it is possible to administer them drugs, toxic agents and neuroprotective substances in order to perform long-term experiments. For this reason, the system can be used to dissect the mechanisms underlying diverse pathological conditions, such as SCI or inflammation and neurodegeneration and they can offer a link between *in vitro* experiments and animal models[154].

A variety of models reproducing SCI *in vitro* have been developed, as for example the one in which the mechanical disruption of the slice is useful for studying the pathophysiological mechanisms associated with neurotrauma[155]. Chemically induced models of SCI are able to mimic metabolic perturbations occurring during the damage, such as hypoxia. Organotypic spinal cord slices cultured in glucose-free medium and anaerobic incubator could replicate hypoxia-ischemia of the spinal cord reliably[156]. The organotypic spinal slice system is also a platform to study pathologies such as ALS. Administering IgG to organotypic spinal slices offers a model to evaluate the role of IgG in the pathogenesis of ALS. Organotypic cultures contribute to study of the impact of IgG on motor neurons by mimicking physiological conditions[157]. Threo-hydroxyaspartate (THA), a glutamate uptake inhibitor, has been used as model of ALS as it causes loss of motoneurons[158].

Since glutamate-induced excitotoxicity is one of the major contributor to motorneurons degeneration in ALS, it has been developed a model in which the neuroprotective effect of glutamate receptor antagonists was evaluated, when they were administered to slices obtained from different spinal cord regions (i.e. cervical, thoracic and lumbar)[159]. Altogether, these studies provide a new way of addressing at mechanisms involved in glutamate-induced excitotoxicity, or in hypoxia and they may therefore be important for the development of treatment strategies to protect the spinal tissue in neurodegenerative disease and traumatic injury.

5. Calcium waves and oscillations

Ca^{2+} plays crucial physiological roles in the CNS and intracellular Ca^{2+} is a well-known second messenger. In the CNS a neuronal depolarization triggered at the membrane level, such as an action potential, induces a huge and fast increase in the intracellular Ca^{2+} concentration, from the nanomolar range to the millimolar one[160], comparable to the extracellular concentration. There is, indeed, a considerable gradient between intra- and extracellular Ca^{2+} concentrations that could promote a huge influx of the ion in the cell if there were not multiple strategies for controlling Ca^{2+} homeostasis via alternative mechanisms necessary to maintain low intracellular Ca^{2+} concentration and to avoid the excitotoxicity and eventually the neuronal death[161,162]. Ca^{2+} is equally involved in several and different events, such as cellular differentiation, proliferation and activation of transcriptional factors. Indeed, all the activity-dependent developmental events that involve gene expression and the large majority of the developmental instructions brought by spontaneous activity are triggered initially by Ca^{2+} influx and the resulting transient increases in Ca^{2+}. Overall, all these activities are induced by the intracellular Ca^{2+} concentration increase.

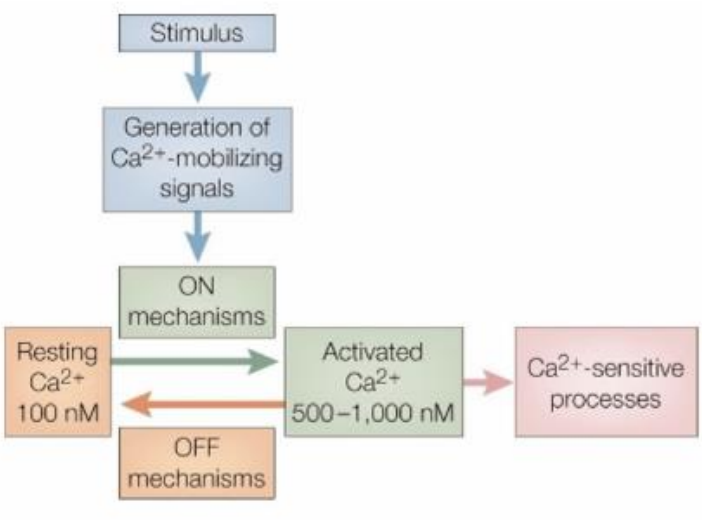

Figure 16 Calcium signaling network

Stimuli act by generating Ca^{2+}-mobilizing signals that act on various ON mechanisms to trigger an increase in the intracellular concentration of Ca^{2+}. The increased level of Ca^{2+} stimulates various Ca^{2+}-sensitive processes to trigger many different cellular pathways. The response is terminated by OFF mechanisms that restore Ca^{2+} to its resting level[Adapted from Ref.161].

5.1 Calcium signaling in the spinal networks

Spontaneous activity is thought to be crucial for the CNS expression of distinct neuronal phenotypes, axon growth, axonal path finding, neurotransmitter phenotypes selection, initial set of synapses connections and signaling processes[163]. In the spinal cord, immature activity during embryonic stages is slow and synchronous and usually comprises spontaneously recurring episodes emerging more as a population behavior, due to the concomitant firing of large amounts of neurons, rather than the outcome of specific and localized rhythm generating networks[164]. The immature firing usually

requires synaptic activity, comprising excitatory synapses, as well as inhibitory ones, mediated by GABA or glycine generating depolarizing signals in the embryonic and early post-natal neurons displaying high intracellular Cl^- concentrations. These depolarizations are able to elevate intracellular Ca^{2+} concentration[165]. Intracellular Ca^{2+} signaling is of paramount importance for spinal network development because transient elevations of intracellular Ca^{2+} direct the emergence of cell phenotypes and the formation of neuronal connectivity. Live calcium imaging experiments reveals that embryonic amphibian spinal neurons exhibit spontaneous elevations of intracellular Ca^{2+} concentration both in culture and *in vivo* during the early differentiation[166]. With Ca^{2+} transients or Ca^{2+} waves it is possible defining a localized increase in cytosolic Ca^{2+} that is followed by a succession of similar events in a wave-like fashion. Neuronal cell bodies and growth cones can exhibit multiple spontaneous elevations in Ca^{2+} concentration, necessary during the development and Ca^{2+} transients are able to stimulate or drive neuronal differentiation[167,168,169]. Neuronal activity raises Ca^{2+} concentration in developing oligodendrocytes in *in vivo* zebrafish spinal cord and myelin sheath elongation is promoted by a high frequency of Ca^{2+} transients[170]. Ca^{2+} increase in the mature spinal cord neurons can drive output signals such as contraction in muscular cells, neurotransmitter release at the presynaptic terminals of chemical synapses or exocytosis in secretory cells and the spontaneous motor neuron activity may function at earlier stages to enable correct matching of pre- and postsynaptic partners[171]. The responses of cells to elevations in intracellular Ca^{2+} concentration are determined by their amplitude, frequency, pathway of entry, sources and spatial location[163]. Several processes, related to activity-dependent development, rely on Ca^{2+}-induced Ca^{2+} release from internal

stores, which requires a threshold amount of Ca^{2+} entry to occur[172]. Some studies reveal the existence of two different types of intracellular Ca^{2+} transients, Ca^{2+} spikes and Ca^{2+} waves: (i) spikes depend on Ca^{2+} influx through voltage-gated channels and Ca^{2+} release from intracellular stores; they last approximately 10-20 seconds, and since they involve Na^{+}-dependent bursts of action potentials they propagate throughout neurons; (ii) waves are kinetically slower (mean duration 30 seconds in growth cones) and do not involve action potentials for their generation. They occur locally and decay with distance from their site of initiation. They appear to be produced by a different Ca^{2+} entry pathway, which depends on Ca^{2+} influx and is active at resting potentials, since voltage-gated calcium channels and several classes of ionotropic receptors are not involved and calcium entry triggers calcium release from the intracellular stores, which amplifies the waves. Spikes and waves are both required for specific aspects of differentiation. Their elimination by removal of extracellular Ca^{2+} or suppression with intracellular BAPTA prevents normal development[168,173].

Ca^{2+} activity-independent signaling is of paramount importance for spinal network development since, at embryonic stages, neuronal populations expressing synchronous Ca^{2+} transients, which propagate through the gap-junctions and regenerate thanks to Ca^{2+}-induced Ca^{2+} release from intracellular stores, represents a global signal to drive (mostly via transient Ca^{2+} elevations) network refinement and synaptic consolidation[164,174].

5.2 Mechanisms of calcium elevation and recruitment in astrocytes and role of calcium signaling in pathophysiology

Several *in vivo* brain studies demonstrate that astrocytes exhibit both spontaneous Ca^{2+} increases and Ca^{2+} responses to neuronal activity and that the first kind of activity has been detected in the soma of astrocytes under basal conditions, suggesting that Ca^{2+} elevations initiating in astrocyte processes can propagate to the soma without the need of neuronal activity. The study revealed also that Ca^{2+} activity was much more frequent and dynamic in astrocyte processes or vascular endfeet[175]. Several mechanisms trigger the elevation of astrocyte intracellular Ca^{2+} levels. For example, the activation of G-protein-coupled receptors (GPCR) triggers the IP_3 signaling cascade and results in robust intracellular Ca^{2+} elevations, mainly via the IP_3 receptor type 2 activation (IP_3R2). Ca^{2+} release from the endoplasmic reticulum (ER) via ryanodine receptor (RyR) also contributes to astrocytic Ca^{2+} signals[176,177]. Mitochondria, which are abundant in astrocytic processes, are the main active source of Ca^{2+} for localized events in far distant microdomains and it has been reported that Ca^{2+} release from mitochondria via the mitochondrial permeability transition pore (mPTP) mediates Ca^{2+} transients[178]. Moreover, astrocytes express several types of transient receptor potential (TRP) channels and their blockade contributes to a slight decrease in resting Ca^{2+} levels[178]. In addition, synaptic activity induces an increase in astrocytes Ca^{2+} concentration, through the stimulation of the Ca^{2+}-permeant ionotropic receptors or via reversal of Na^{+}/Ca^{2+} exchangers following neurotransmitter uptake or pumping activities[179].

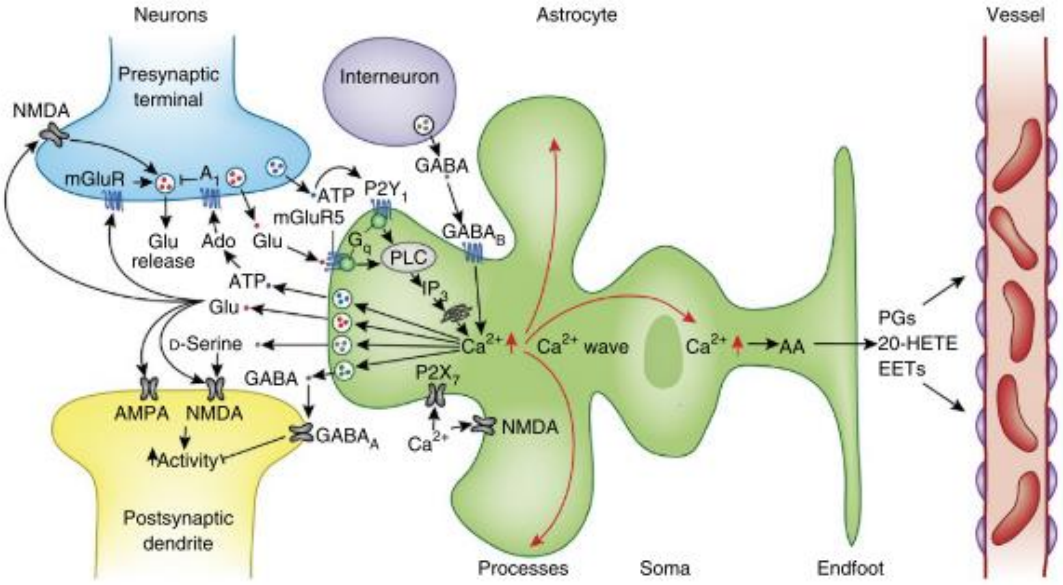

Figure 17 Sketch of the Ca^{2+} elevation functions

Elevation of astrocytes intracellular Ca^{2+} evoked by GPCRs induces the release of gliotransmitters ATP, glutamate and GABA. These can modulate neuronal activity pre- or post-synaptically. Ca^{2+} waves can spread through the astrocyte's processes to the soma and to its vascular endfeet, where vasoactive messengers are released[Adapted from Ref.180].

In the past, astrocytes were considered electrically silent, chemical and physical insulators, necessary for the neuronal activities. The finding that astrocytes express GPCRs, linked to a series of intracellular signaling cascades, among which the elevation of intracellular Ca^{2+} levels, changed the view on these cells. Moreover, the discovery that these calcium elevations could propagate along other astrocytes and neurons, through the GJs, raised the possibility that astrocytes might have a signaling network, like neurons. The specific consequence of Ca^{2+} increase, occurring in response to sensory or motor

stimuli in living animals, is the release of gliotransmitters, among them, ATP, one of the predominant extracellular messengers that mediates Ca^{2+} waves in astrocytes, which are themselves involved in modulating neuronal activity. Gliotransmitters are able to modulate other glial cells, neuronal and vascular activity[179]. For instance, the gliotransmitter substance P induces an elevation in the intracellular Ca^{2+}, which is responsible of processing sensory information in the spinal dorsal horn[181]. The direct imaging of living astrocytes in spinal cord reveals that astrocytes actively participate to sensory processing, shown by the increase in intracellular Ca^{2+} levels during the stimulation[182]. Again, in spinal dorsal horn, ATP and UTP, which induce a raise in the level of intracellular Ca^{2+} concentration, through thapsigargin-sensitive stores, play a role in neuronal-glial signaling[183,184]. Experiments conducted in mice and rats brain slices reveal that IP_3R2-mediated Ca^{2+} signaling in astrocytes is essential for plasticity and learning. On the contrary brain tissue damage in ischemic brain injury and neurodegenerative disease were ameliorated in IP_3R2-KO mice[177]. Moreover, several evidences indicate that astrocytic Ca^{2+} elevations, preceding the release of gliotransmitters, lead to an increase in the GABAergic currents frequency, which means that astrocytes can modulate synaptic transmission and that they are required to modulate synapses in the human brain[185,186]. In the brain, during strokes or ischemia, the damaged areas are associated with an increased in ATP concentration from dying cells, and this facilitates astrocytes Ca^{2+} waves, which may further assist the release of glutamate. Significant alterations in astroglial Ca^{2+} homeostasis and signaling, e.g. elevation in resting Ca^{2+} concentration levels and enhanced spontaneous Ca^{2+} oscillations are common in neurodegenerative disease like ALS[187]. All these examples strength the notion that astrocyte functions are intimately

regulated by cellular Ca^{2+} signaling. Ca^{2+} signaling acts as an important part of glial excitability and the signals are initiated by neurotransmitters released by neurons, by gliotransmitters and by a wide variety of other chemical factors. Finally, these Ca^{2+} waves control vital and physiological functions of glial cells, as gliotransmitter release, homeostasis and neuronal-glial-vascular syncytium and critical and pathological functions, as the reactive gliosis.

5.3 Calcium activity in organotypic slices

As described in the paragraph 4, organotypic slices from embryo spinal cords are an excellent *in vitro* system able to reproduce the different spinal segments growth and circuitries[143,148]. Exploiting this culture model at early developmental stages, in our group, we observed a novel type of neuronal Ca^{2+} signal arising spontaneously as repeated oscillations independent of action potential or synaptic activity, from the ventral interneurons, as already shown in other neuronal cell types[188,189]. These signals may represent an additional type of activity-independent calcium transients that contributes to specific developmental processes during spinal circuit formation. Moreover, we observed that such oscillations were mainly due to the mitochondrial Ca^{2+} buffering. More recently, still in our group, we demonstrated that neuronal and synaptic growth shifted the generation of spontaneous Ca^{2+} signals from early waves driven by synaptic activity invading the entire spinal region to late, activity-independent asynchronous oscillations generated by few neurons (15%) in restricted ventral areas[190]. Organotypic spinal cord cultures, developed from chick embryos have also been used to

examine excitotoxicity in motorneurons. It has been shown that the slices retain their rhythmic activity with spontaneous Ca^{2+} transients in motorneurons, but when the slices were undergone excitotoxic treatments, increase in the frequency of Ca^{2+} transients was observed, followed by a sustained deregulation of intracellular Ca^{2+} from the stores, in particular from the thapsigargin-sensitive ones[191].

In conclusion, neurons and astrocytes have access to an extensive Ca^{2+} signaling toolkit, given by the several number of receptors, from which they can assemble different kind of signals. How these signals occur and work during developmental stages is quite clear. The challenge is to better understand the significance of Ca^{2+} signaling during pathological conditions, not only in neurons but also in neuroglia, since, as above-described and anticipated in the paragraph 4, the organotypic spinal cord system is an excellent setting which reproduces the spinal cord tissue architecture, encompassing different cell types, eligible for live cell Ca^{2+} imaging experiments and helpful for dissecting the mechanisms underlying diverse pathological conditions, related to the Ca^{2+} oscillations.

Moreover, since neuroglia as well as neurons are involved in the onset of several pathological conditions, it is reasonable to focus also on the glial Ca^{2+} oscillations role and on their impact on the interplay between neurons and glial cells in spinal organ slices, a topic not yet addressed by the literature.

6. Gap junctions (GJs) and hemichannels (HCs) communications in the spinal cord astrocytes

6.1 GJs and HCs components in astrocytes: connexin 43

A typical feature of astrocytes is to express a high level of connexins (Cxs), whose specific role is the formation of GJs and HCs, mediating the direct glial intercellular communication[192]. Cxs represent a family of ~ 20 isoforms identified in mice and humans, forming hexamers (or connexons) on plasma membranes. Cx43 is the major astroglial Cx detected in cultured astrocytes, even if more recently, it was demonstrated that the presence of cortical neurons co-cultured with mature astrocytes, induced in these latter the expression of Cx30, as well[13,193]. The connexons can align and dock with other hexamers provided by neighboring cells to form GJs channels. GJs channels provide a unique direct cytoplasm-to-cytoplasm pathway, allowing ionic and biochemical coupling between adjacent cells. They allow direct exchange of a variety of small molecules including ions (Ca^{2+}), energy metabolites, neurotransmitters and signaling molecules (cAMP and IP_3), with a cut-off around 1-1.2 kDa, coordinating electrical and metabolic activities of connected cells[194]. Besides the classical formation of GJs, Cxs hexamers exist as single membrane channels, as well, known as HCs, which directly connect the cell cytoplasm to the extracellular milieu. Since HCs are thought to be poorly selective large pores, permeable to numerous low molecular weight molecules, they are generally closed under normal conditions in order to maintain cell integrity, but they are opened by various factors such as low external calcium concentration, depolarization, pro-inflammatory agents and a moderate rise in intracellular calcium concentration.

Once opened, HCs allow the release of gliotransmitters, such as ATP and glutamate or other neuroactive substances such as K^+, known to modulate neuronal activity[195]. Cxs, like other membrane proteins, have a high turnover and exhibit half-lives of only 1.5-5.0 hours both in cultured cells and *in vivo*[196]. Once synthetized, on their transit from the ER through the trans-Golgi network, Cxs are oligomerized into hexamers. Then, connexon-containing vesicles are transported from the Golgi to the cell surface via the secretory pathway[197]. Cxs do not only exhibit GJs and HCs functions, they also mediate cell morphology and growth, the regulation of cell polarity and they influence cell motility and the adhesion between radial glial cells and neuroblasts[198,199].

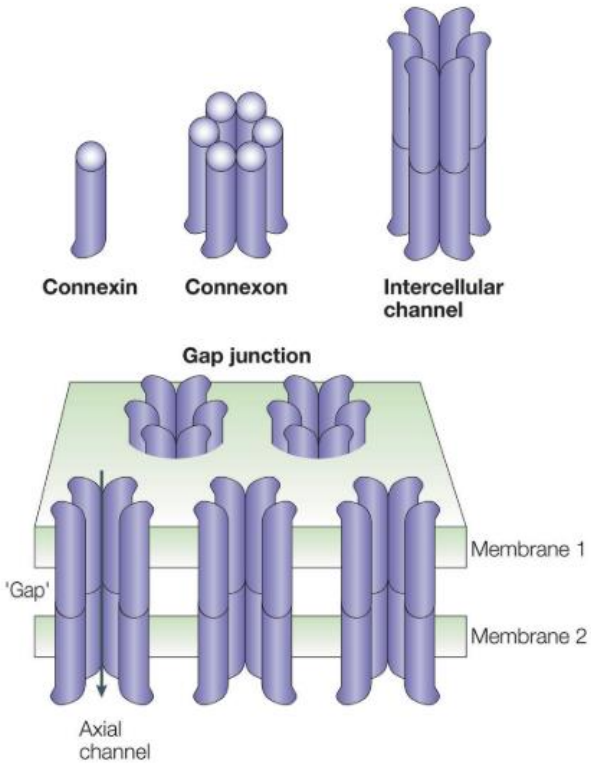

Figure 18 Sketch of connexin (Cx), connexon/hemichannel (HC) and intercellular channel and gap junction (GJ)

The schematic picture shows the relationships between the Cx monomer, the hexameric assembly of Cxs into an HC and the two HCs forming an intercellular channel[Adapted from Ref.197].

Specifically regarding Cx43, the key functions are homeostatic buffering, synchronization of astrocyte networks, metabolic support for neurons, regulation of vascular components and modulation of synaptic activity and plasticity[200]. Concerning the Cx43 expression, contrasting results among different pathological CNS conditions have been reported. For example, in Alzheimer's disease, Cx43 was found to be up-regulated in amyloid plaques[201]. In contrast, Cx43 is down-regulated after treatment of human fetal cultured astrocytes with the proinflammatory cytokine IL-1β[202],

or after treatment of microglia and astrocytes co-cultures with TNF-α and IL-1β[203], and after brain mechanical lesions[204] or ischemia[205]. Furthermore, the inflammatory molecule, LPS, reduces Cx43 expression in cultured rat astrocytes via the ubiquitin-proteasome pathway[206]. More specifically concerning the protein expression in spinal cord, in an animal model of MS, the expression of Cx43 in astrocytes is significantly reduced and in inflamed regions it is not compensated for by the other major astrocytic gap junction protein Cx30[207]. More recently, Zhang et al. reported that 3 hours treatment of spinal primary astrocytes with a mixture of TNF- α and IFN-γ induced a reduction in the Cx43 levels[208]. On the contrary, a progressive increase in Cx43 expression in astrocytes in the $SOD1^{G93A}$ mouse model of ALS was observed and this impacts on motoneuron survival[209].

6.2 GJs and HCs in calcium signaling and synchronization

As already mentioned, astrocytes participate in brain function as an integrated and a coordinated syncytium thanks to the presence of intercellular GJs, that can provide a pathway through which signaling molecules, such as cAMP, Ca^{2+} and IP_3 spread between cells. Beside these functions, the dissipation of Ca^{2+} waves between adjacent astrocytes is attributable to GJs and HCs[210,211]. Cornell-Bell and collaborators firstly reported the occurrence of intercellular Ca^{2+} waves in astrocytes and proposed that GJs communication in astrocytes may constitute a long-range signaling system within the brain, with the important feature that astrocytes were not only able to respond to external stimulation with increases in intracellular Ca^{2+} concentration, but they were able to transmit these Ca^{2+} signals to adjacent non-stimulated astrocytes[212]. The propagation

of intercellular Ca^{2+} waves mediated by GJs was, instead, first observed between neurons and astrocytes in co-culture[213]. In this way, astrocytes are able to constitute an extra-neuronal pathway for rapid long-distance signal transmission within the CNS. The same authors proposed that ''if Ca^{2+} activity in the network of astrocytes constituted another form of intercellular communication, such signaling should have a physiological relevance, influencing neuronal activity and thus being bi-directional''[212]. Electrotonic coupling through GJs is thought to be essential for synchronizing neuronal responses[214]. Fabbro and colleagues have more recently demonstrated that GJs also contribute to the periodicity and synchronization of the Ca^{2+} oscillation of spinal organotypic interneurons, thanks to the observation that using the GJs blocker carbenoxolone (CBX) the oscillations period was prolonged but not blocked[189].

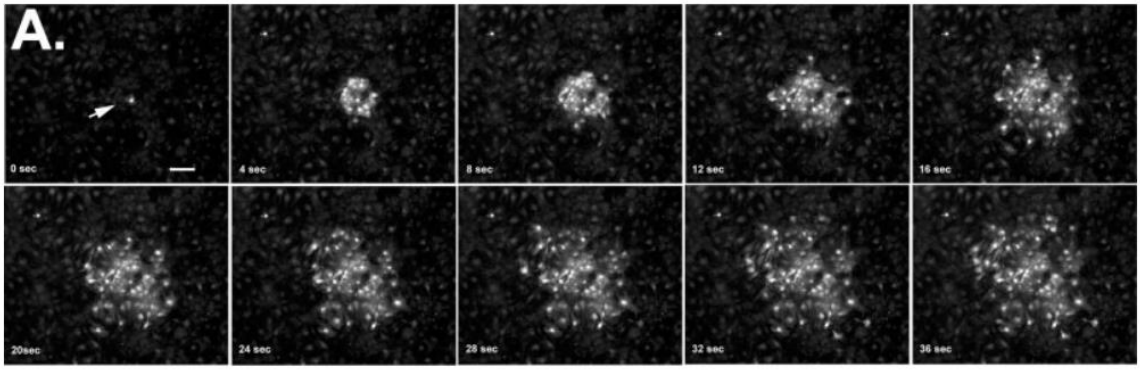

Figure 19 Intercellular Ca^{2+} waves

The transmission of intercellular Ca^{2+} signals between astrocytes is illustrated in the sequential images obtained from Fluo-3-AM loaded spinal cord astrocytes. Mechanical stimulation (arrow) of a single astrocyte in culture induces intracellular Ca^{2+} elevation (displayed as an increase in fluorescence intensity) in the stimulated cells, which is then followed by Ca^{2+} increases in neighboring astrocytes[Adapted from Ref.215].

6.3 Pathophysiological implication of GJs and HCs

For a long-time it was believed that GJs and HCs would remain closed under physiological conditions, in order to maintain cell integrity and homeostasis. On the contrary, they are involved in neurogenesis and development, in neuronal excitability, in synaptic transmission and in synaptic plasticity, thanks to their permeability to different signaling molecules, such as ATP or glutamate[194,216]. Most of the evidence implicates HCs as pathological rather than physiological entities, contributing to cell swelling and cell death. In brain cells, excessive hemichannel opening allows the entry of Na^+ and Ca^{2+} and the outflow of K^+, ATP and other small metabolites, leading to osmotic shifts, energy depletion, Ca^{2+} overload and eventually cell death[202,217,218,219]. HCs also propagate secondary damage signals following spinal cord injury and O'Carroll and colleagues demonstrated that Cx mimetic peptides treatment on an *in vivo* model of spinal cord injury prevented swelling, reduced astrogliosis and cytokines release and increased neuronal survival after spinal cord injury, in a concentration- and time-dependent manner[220,221]. In a rat spinal cord compression model, Cx43 downregulation by local application of antisense oligodeoxynucleotides immediately after injury reduced inflammation and improved the locomotion score after injury. Like in the above-mentioned model, it decreased spinal tissue swelling and disruption, it attenuated astrogliosis and the infiltration of neutrophils[222]. Animals with astrocyte specific Cx43 knockout displayed reduced areas of post-traumatic ATP release, suppression of reactive gliosis, less tissue loss following spinal cord injuries and a strongly improved locomotor score[223].

In a similar fashion, other experiments revealed that partial deletion of astrocytic Cx43 reduced pro-inflammatory cytokines levels induced by systemic LPS injections, and blocked microglial activation[224]. Moreover, the reduction of glutamate-mediated excitotoxicity via administration of the GJs and HCs blocker, INI-0602, in the injured spinal cord elicited, the attenuation of pro-inflammatory cytokines and the subsequent release of anti-inflammatory cytokines, followed by neurobehavioral improvement and extensive suppression of glial scar formation[225]. Altogether these results may suggest that the GJs and HCs made of Cx43 are involved in the regulation of neuroinflammation, since they can enhance spinal cord synaptic transmission and maintain neuropathic pain in the late-phase via releasing chemokines, as demonstrated in one case by the block of Cx43-HCs and the consequent block in the release of ATP, after the application of a Cx43 mimetic[226], or in another case, after spinal injection of CBX and Cx43 mimetics[227]. It remains unclear whether GJs and HCs play a protective or detrimental role for the entire system. It is therefore important implementing all these *in vitro* systems, in which we observe the block or the reduction in GJs and HCs activity, in order to better understand which are the concentration and time ranges that make the used compounds more efficient. It is then important to probe the compounds in *in vivo* system, in order to assay the animal behavior, with the aim of producing drugs useful for human patients with neuroinflammatory disease, such as ALS, SCI or MS.

Aim of the thesis

The main aim of my thesis was to investigate the neuroinflammation mechanisms, which interfere with the synaptic transmission, and to understand the impact of the immune status alterations on the neural and glial circuit function and on the interplay between neurons and glial cells. Since several neurodegenerative disorders, involving spinal microcircuits and synapses, are frequently accompanied by an inflammatory feature, which eventually leads to neuronal cell death, I combined electrophysiological techniques and immunofluorescence analysis to characterize the ventral interneurons located in spinal circuits. For that purpose, I used a combination of two distinct elements:

1. The organotypic spinal cultures obtained from mice embryos, which represent an excellent model well characterized in our laboratory;

2. two different inflammatory paradigms: 1) a specific cytokines cocktail composed by TNF-α, IL-1β, and GM-CSF, reported to be highly concentrated in blood and CSF from MS patients and EAE model; 2) a more general inflammation inductor, LPS.

In the first part of my work, by using patch clamp voltage-mode techniques, I recorded the synaptic activity from visually identified ventral interneurons and I focused on understanding the effects of the different inflammatory threats on $GABA_A$ receptor-mediated currents. In doing this, I also monitored the astrocytes and microglia reactivity by immunofluorescence techniques.

In the second part of my project, I exploited the same experimental settings, to insult the organ slices and induce inflammation, but focusing for the first time on the activity of the main characters of the neuroinflammatory process: the glial cells. For the purpose, I exploited live Ca^{2+} imaging techniques and pharmacology to characterize the astrocytes Ca^{2+} oscillations in an inflamed environment, and to understand their mechanistic backgrounds.

Methods and results

1. Cytokine inflammatory threat, but not LPS one, shortens GABAergic synaptic currents in the mouse spinal cord organotypic cultures

Giacco et al. Journal of Neuroinflammation (2019) 16:127
https://doi.org/10.1186/s12974-019-1519-z

Journal of Neuroinflammation

RESEARCH Open Access

Cytokine inflammatory threat, but not LPS one, shortens GABAergic synaptic currents in the mouse spinal cord organotypic cultures

Vincenzo Giacco[1,5], Giulia Panattoni[1], Manuela Medelin[2], Elena Bonechi[3], Alessandra Aldinucci[3], Clara Ballerini[4*] and Laura Ballerini[1*]

Abstract

Background: Synaptic dysfunction, named synaptopathy, due to inflammatory status of the central nervous system (CNS) is a recognized factor potentially underlying both motor and cognitive dysfunctions in neurodegenerative diseases. To gain knowledge on the mechanistic interplay between local inflammation and synapse changes, we compared two diverse inflammatory paradigms, a cytokine cocktail (CKs; IL-1β, TNF-α, and GM-CSF) and LPS, and their ability to tune GABAergic current duration in spinal cord cultured circuits.

Methods: We exploit spinal organotypic cultures, single-cell electrophysiology, immunocytochemistry, and confocal microscopy to explore synaptic currents and resident neuroglia reactivity upon CK or LPS incubation.

Results: Local inflammation in slice cultures induced by CK or LPS stimulations boosts network activity; however, only CKs specifically reduced GABAergic current duration. We pharmacologically investigated the contribution of $GABA_AR$ α-subunits and suggested that a switch of $GABA_AR$ α1-subunit might have induced faster $GABA_AR$ decay time, weakening the inhibitory transmission.

Conclusions: Lower GABAergic current duration could contribute to providing an aberrant excitatory transmission critical for pre-motor circuit tasks and represent a specific feature of a CK cocktail able to mimic an inflammatory reaction that spreads in the CNS. Our results describe a selective mechanism that could be triggered during specific inflammatory stress.

Keywords: Organotypic spinal slices, Patch-clamp, Synaptic currents, Neuroinflammation, GABAergic inhibition, GABAergic receptors, Spinal circuits, NKCC1, Resident neuroglia

Background

Neuroinflammation is a characterizing trait of various central nervous system (CNS) pathologies, from neurodegenerative diseases to neuropsychiatric disorders [1]. Currently, intense research efforts are dedicated to the understanding of how the different signaling pathways, activated in neurons and neuroglia by the inflammatory milieus, may ultimately promote synaptic dysfunction [2–4]. For example, several studies documented, in the interplay between the immune system and neuronal function, the involvement of pro-inflammatory cytokines (CKs), such as TNF-α, IL-1β, and IL-6 [5–7]. Similarly, lipopolysaccharide (LPS, an endotoxin derived from gram-negative bacteria)-induced neuroinflammation may lead to synaptic dysfunctional signaling contributing significantly to cognitive disturbances [8]. In contrast to the general agreement on the emergence of synaptopathy due to inflammation [2], the rules governing the specific neurotransmission systems involved, and their tuning, are unclear. Conflicting evidence indicate that exogenous CK applications may increase [9] or decrease [10] glutamatergic

* Correspondence: clara.ballerini@unifi.it; laura.ballerini@sissa.it
[4]Dipartimento di Medicina Sperimentale e Clinica, University of Florence, 50139 Florence, Italy
[1]International School for Advanced Studies (SISSA/ISAS), 34136 Trieste, Italy
Full list of author information is available at the end of the article

synaptic transmission, as well as for GABAergic transmission, where both decreases [11, 12] and increases [13, 14] are reported.

With the aim of dissecting the impact of immune status alterations on neural circuit function, we focused our study on the effects of local inflammation in a controlled micro-environment where neurons and neuroglial cells maintain appropriate organization: the organotypic slice cultures developed from the embryonic mouse spinal cord. In this complex in vitro model, the sensory-motor cytoarchitecture, synaptic properties, and spinal cord resident cells are retained in a 3D-fashion [15–17]. By the use of this model, we preliminarily reported the emergence of synaptopathy in pre-motor circuits following CK transient exposure, characterized by a speeding up of the decay phase of GABAergic inhibitory currents [17]. A broader question is to what extent the tuning of GABAergic current duration may occur as a response to any local alteration in the inflammatory status of the spinal cord, disrupting physiological excitability levels, being GABAergic neurotransmission an important determinant of spinal circuit coordination [18].

In the present study, we compare the effects on synaptic transmission of different experimental inflammatory models, LPS, a potent trigger of cytokine induction [19, 20] and the most common stimulus used to investigate microglial reactivity in brain inflammation, and a pro-inflammatory cocktail containing interleukin-1β (IL-1β), well-known determinant of neuropathy [1, 2], tumor necrosis factor α (TNF-α), present during Th1/Th17-mediated inflammatory reactions, and granulocyte macrophage-colony stimulating factor (GM-CSF), targeting resident microglial cells. These cytokines are key factors known to affect neuronal functions and responsible for pro-inflammatory effects in the CNS of multiple sclerosis animal models [21]. We adopted relatively acute treatments (hours), known to trigger inflammatory responses, without inducing direct neurotoxicity, yet still able to alter synaptic transmission [17]. Thus, organotypic spinal cord cultures were transiently exposed to pro-inflammatory CK cocktail (TNF-α, IL-1β, and GM-CSF, 4 and 6 h; [17]) or to LPS (4, 6, and 24 h).

To compare CKs and LPS impact on synaptic activity, in particular on GABAergic currents, we used single-cell patch-clamp recordings. We further explore by immunofluorescence and confocal microscopy resident neuroglia reactivity, and we measure the local production of cytokines and chemokines in response to the two inflammatory stresses. CKs and LPS significantly increase the generation of these signaling proteins, and both danger signals boost basal synaptic activity, inducing a distinct transformation of resident neuroglia morphology. To note, only CKs promote changes in inhibitory transmission time course. Finally, we investigated the mechanisms responsible for the shortening of GABAergic current duration upon CK treatment, since these may emerge as potential targets for novel therapeutics.

Methods

Organotypic spinal cord cultures, pro-inflammatory treatments, and pharmacology

All experiments were performed in accordance with the EU guidelines (2010/63/UE) and Italian law (Decree 26/14) and were approved by the local authority veterinary service and by our institution (SISSA) ethical committee. All efforts were made to minimize animal suffering and to reduce the number of animals used. Animal use was approved by the Italian Ministry of Health, in agreement with the EU Recommendation 2007/526/CE.

Organotypic spinal cord and dorsal root ganglia (DRG) slices were obtained from mouse embryos (C57BL/6 J) at E12-13 of gestation as previously described [15–17, 22]. Briefly, pregnant mice were sacrificed by CO_2 overdose and fetuses delivered by cesarean section. Isolated fetuses were decapitated, and their backs were isolated from low thoracic and high lumbar regions and transversely sliced (275 μm) with a tissue chopper. After dissecting the spinal cord slices and the DRG from the surrounding tissue, slices were embedded into a thick matrix obtained by chicken plasma (Rockland) and thrombin (Sigma) clot. Slices were cultured in plastic tubes with 1 mL medium. The tubes were kept in a roller drum rotating 120 times per hour in an incubator at 37 °C in the presence of humidified atmosphere, with 5% CO_2. Experiments were performed on spinal cultures at 14–21 days in vitro (DIV). The day of the experiment, organotypic slices were incubated with standard medium (control) or, for 4 or 6 h (4H and 6H), with two different inflammatory paradigms: (i) a cocktail of the mouse recombinant cytokines (10 ng/mL each) TNF-α (R&D Systems, #210-TA/CF), IL-1β (R&D Systems, #M15330), and granulocyte-macrophage colony-stimulating factor (GM-CSF; R&D Systems, #P04141; [17, 23]); (ii) lipopolysaccharide (LPS; 1 μg/mL, Sigma, O55:B5). For LPS, we also tested a longer incubation time point (24H). CKs or LPS were removed after the incubation times, prior to electrophysiological recordings.

Bumetanide (Sigma) was diluted in phosphate buffer solution (PBS 1×, Sigma) and used to block the $Na^+/K^+/Cl^-$ co-transporter (NKCC1; [24]). To decrease the cytoplasmic chloride concentration, slices were incubated for 24 h at 37 °C with 10 μM bumetanide (BUM24H), after 24H, the CK cocktail was added for additional 4 h (BUM24H + CKs4H).

Immunofluorescence, imaging, and analysis

Organotypic cultures were fixed with 4% formaldehyde (prepared from fresh paraformaldehyde; Sigma) in PBS (1×) for 1 h at room temperature (RT; 20 to 22 °C) and washed in PBS. Free aldehyde groups were quenched in 0.1 M glycine in PBS for 10 min. Slices were permeabilized and blocked in PBS 1×, 5% FBS (Sigma), 1% BSA (Sigma), and 0.3% Triton X-100 (Sigma) at RT for 1 h and then incubated overnight at 4 °C with anti-GFAP (mouse monoclonal, 1:400, Sigma), anti-Iba1 (rabbit polyclonal, 1:200, Wako), anti-SMI32 (mouse monoclonal, 1:200, EMD-Millipore), and anti-MAP 2 (mouse monoclonal, 1:200, Sigma) primary antibodies.

For β-tubulin III and GAD65/67 co-immuno-labeling, fixed samples were quenched with Na-(meta) periodate 2.3% in deionized water for 5 min and Na-borohydride 1% in TRIS 0.1 M for 10 min. Slices were blocked in free-floating with PBS 1×, 10% FBS (Sigma), 1% BSA (Sigma), 1% fish gelatin (Sigma), and 0.3% Triton X-100 (Sigma) at RT for 1 h and then incubated overnight at 4 °C with anti-β-tubulin III primary antibody (mouse monoclonal; 1:500, Sigma) and anti-GAD65/67 (rabbit polyclonal; 1:500, ABCAM).

Subsequently, the slices were PBS-washed and incubated with secondary antibodies diluted in blocking solution for 2 h at RT in the dark. The secondary antibodies were Alexa 488 goat anti-mouse (1:500, Invitrogen), Alexa 488 goat anti-rabbit (1:500, Invitrogen), Alexa 594 goat anti-mouse (1:500, Invitrogen), Alexa 594 goat anti-rabbit (1:500, Invitrogen), and DAPI (Thermo Fisher Scientific). Samples were mounted on glass coverslips using Vectashield mounting medium (Vector Laboratories).

Images were acquired using Nikon C2 confocal microscopes with Ar/Kr, He/NE, and UV laser with × 20, × 40, or × 63 oil objectives (1.4 N.A.) using oil mounting medium (1.515 refractive index). Confocal sections were acquired every 0.5 μm up to a total *Z*-stack thickness of 5 μm. For each condition, we performed > 3 and < 6 independent cultures; from each culture series, we used 4 slices, and from each slice, ≥ 5 fields were randomly acquired. Offline analysis of the image *Z*-stack was performed using the open source image-processing package FIJI (http://fiji.sc/Fiji).

For the quantitative analysis of microglia morphology, we used the particle measurement feature in *ImageJ*, to automatically measure the area and the perimeter, necessary to calculate the transformation index [25], as $\frac{[\text{perimeter of cell } (\mu m)]^2}{4\pi \cdot [\text{area of cell } (\mu m^2)]}$, which defines microglia ramification status. Indeed, cells with long processes and small soma show a large index that depends on cell shape, regardless of the cell size.

Quantification of GAD65/67 immunoreactivity was performed measuring the intensity of fluorescence and the number of GAD65/67 clusters using the Volocity3D Image Analysis Software. Clusters were determined after thresholding of images. Thresholds were determined using the "voxel spy" facility of the software and chosen such that all recognizable punctuate structures were included into the analysis (size > 0.03 μm^3 and separate touching objects of 0.5 μm^3).

Electrophysiological recordings and data analysis

For patch-clamp recordings (whole-cell, voltage clamp mode), a coverslip with the spinal culture was positioned in a recording chamber, mounted on an inverted microscope (Nikon Eclipse TE200) and superfused with a standard saline solution containing (mM) 152 NaCl, 4 KCl, 1 MgCl2, 2 CaCl2, 10 HEPES, and 10 glucose; the pH was adjusted to 7.4 by NaOH (305 mOsm). Patch pipettes were pulled from borosilicate glass capillaries (4 to 7 MΩ) and filled with intracellular solution containing (mM) 120 K gluconate, 20 KCl, 10 HEPES, 10 EGTA, 2 $MgCl_2$, and 2 Na_2ATP. The pH was adjusted to 7.3 with KOH (295 mOsm). All electrophysiological recordings were performed at RT. The reported voltage values are corrected for the liquid junction potential (− 14 mV) [26]. Electrophysiological responses were amplified (EPC-7, HEKA), sampled, and digitized at 10 kHz with the pCLAMP software (Axon Instruments) for offline analysis. The value of series resistance was < 10 MΩ enabling recordings of synaptic currents without significant distortion and thus was not compensated for [16, 26]. Recordings were performed from ventrally located spinal interneurons visually identified based on previously reported criteria [27]. Spontaneous post-synaptic currents (PSCs) were recorded at − 70 mV holding potential by the Clampfit 10 software (pClamp suite, Axon Instruments). On average, ≥ 400 events were analyzed from each cell in order to obtain mean kinetic and amplitude parameters. From the average of these events, we measured the rise time defined as the 10–90% time needed to reach the peak of the synaptic current, the peak amplitude, and the decay time constant (τ) that was obtained by fitting a mono-exponential function [27].

We compared the passive membrane properties among control and CK- and LPS-treated spinal interneurons. We detected no differences in cell capacitance (51 ± 31 pF control; 43 ± 23 pF CKs 4H; 43 ± 21 pF CKs 6H; $n = 62$, 47, 54 respectively; 55 ± 23 pF control; 44 ± 18 pF LPS 4H; 48 ± 22 pF LPS 6H; $n = 35$, 38, 34, respectively) and input resistance (470 ± 195 MΩ control; 587 ± 137 MΩ CKs 4H; 481 ± 114 MΩ CKs 6H; 430 ± 123 MΩ control; 399 ± 121 MΩ LPS 4H; 439 ± 146 MΩ LPS 6H).

Inhibitory GABAergic post-synaptic currents (IPSCs) were recorded at − 84 mV holding potential in the presence of CNQX (10 μM; Sigma), strychnine (1 μM; Sigma), and APV (25 μM; Sigma). Tetrodotoxin (TTX; 1 μM,

Latoxan) was used to isolate $GABA_A$-receptor-mediated miniature events (mIPSCs).

Recordings of the IPSCs at different holding potentials were used to measure the chloride equilibrium potential (E_{Cl}), which was determined as the *x*-axis intercept point of the resulting I/V curve extrapolated by linear regression.

The imidazopyridine zolpidem (zolpidem, Sigma), a benzodiazepine ligand with high selectivity for $GABA_A$Rs containing the α1-subunit and moderate affinity to α2- or α3-subunit, [28], was dissolved in water stock solution (1 mM) and diluted to the concentration of 100 nM [29] in extracellular solution for bath application (15–20 min).

Cytokine and chemokine measurement

TNF-α, IL-4, IL-6, IL-10, INF-γ, CXCL1, and CXCL2 concentrations were measured in organotypic culture supernatants by Milliplex assay (Merck Millipore, #MCYTOMAG-70 k), using the Bio-Plex apparatus (Biorad), according to the manufacturer's recommendations.

Statistical analysis

All values from samples subjected to the same experimental protocols were pooled together, and results are presented as mean ± S.D., if not stated otherwise, with n = number of neurons. A statistically significant difference between two data sets was assessed by Student's t test (after checking variances homogeneity by Levene's test) for parametric data and by Mann-Whitney's test for non-parametric ones. Two-way analysis of variance (two-way ANOVA) and one-way ANOVA were used for parametric data or Kruskal-Wallis test for non-parametric ones, to determine significance when multiple groups were compared. Statistical significance was determined at $P < 0.05$.

In box plots, the thick horizontal bar indicates the median value, the cross indicates the mean value, the boxed area extends from the 25th to 75th percentiles while whiskers from the 5th to the 95th percentiles.

Results

CKs but not LPS regulate $GABA_A$ receptor-mediated synaptic currents in spinal organotypic cultures

We used organotypic spinal cord and DRG co-cultures (Fig. 1a) to study the impact of neuroinflammation on the GABAergic synaptic transmission within ventral horn premotor circuits [16]. Two different danger signals were used to trigger neuroinflammation in cultured slices: a pro-inflammatory cocktail of CKs [17] and LPS [19]. In both conditions, after 4H and 6H treatments (see the "Methods" section), patched clamped ventral interneurons displayed a significant increase in the frequency of spontaneous PSCs (represented by heterogeneous inward currents of variable amplitudes, see Additional file 2: Figure S1 A–D) in accordance with previous reports [5, 17, 30, 31].

Since fast Cl^--mediated neurotransmission is a potential pro-inflammatory cytokine target in spinal circuits [5, 17, 32], we recorded $GABA_A$ receptor-mediated synaptic events (IPSCs; Fig. 1b) pharmacologically isolated in the presence of CNQX (10 μM), APV (25 μM), and strychnine (1 μM), to block AMPA, NMDA, and glycine receptor-mediated synaptic currents [17]. CK and LPS treatments increased IPSC frequency, without altering IPSC amplitudes (sample tracings in Fig. 1b and box plots in Additional file 3: Figure S2 A and B), when compared to control.

We next explored the kinetic properties of the IPSCs. Consistent with our preliminary findings [17], CK treatments (4H and 6H, $n = 33$ and 37, respectively) significantly accelerated the IPSC decay time constant (τ) (23.7 ± 6.5 ms CKs 4H; 25.7 ± 6.6 ms CKs 6H; Fig. 1c, top, box plot and scaled averaged IPSCs are superimposed in the inset) when compared to control (31.5 ± 9.6 ms control, $n = 40$; $^{***}P < 0.001$ control vs CKs 4H, $^{**}P = 0.004$ control vs CKs 6H; Fig. 1c). Conversely, LPS (4H and 6H, $n = 34$ and 28, respectively) left the τ of the IPSCs unchanged (27.9 ± 7.1 ms LPS 4H; 28.1 ± 6.3 ms LPS 6H) in respect to control (29.1 ± 7.4 ms control, n = 37; Fig. 1c, bottom box plot and scaled averaged IPSCs are superimposed in the inset). The IPSC rise-time values (Additional file 3: Figure S2 C) were unaffected by all treatments. Since IPSC decay time may be developmentally regulated [32], we plotted the τ values detected in control and in CKs 4H and 6H against two time of growth in vitro. Bar plots in Fig. 1d show that CKs shortened the GABAergic current duration at any age of maturation in vitro, thus excluding a correlation between the CK modulation of IPSC decay time and the developmental stage of spinal cord slices in vitro.

We extended our characterization to the properties of miniature GABAergic currents (mPSCs; recorded in the presence of TTX). The results in this group of cells (Fig. 1e) confirmed that CKs affected mPSC decay kinetics (mPSCs τ value 40.9 ± 11.7 ms in control; 29.4 ± 11.6 ms in CKs 4H; 24.3 ± 6.4 ms in CKs 6H; $n = 9$, 7, 9, respectively; $^{*}P = 0.024$ control vs CKs 6H) with a trend similar to that of spontaneous IPSCs. mIPSC decay time remained unchanged upon LPS treatments (30.2 ± 5.9 ms control; 29.3 ± 4.3 ms LPS 4H; 30.2 ± 5.3 ms LPS 6H; $n = 5$, 5, 5, respectively; Fig. 1e, bottom) in accordance with the spontaneous IPSCs.

We next examined by immunofluorescence the presence and distribution of GABAergic neurons in spinal ventral horns, targeting either isoforms of GABA-synthesizing enzyme (glutamate decarboxylase, GAD), namely GAD65/67 [33]. We quantified and compared GAD65/67 labeling in all conditions (Additional file 4: Figure S3, A–D). Immunoreactivity for GAD65/67 was visible throughout the spinal explants where neurons

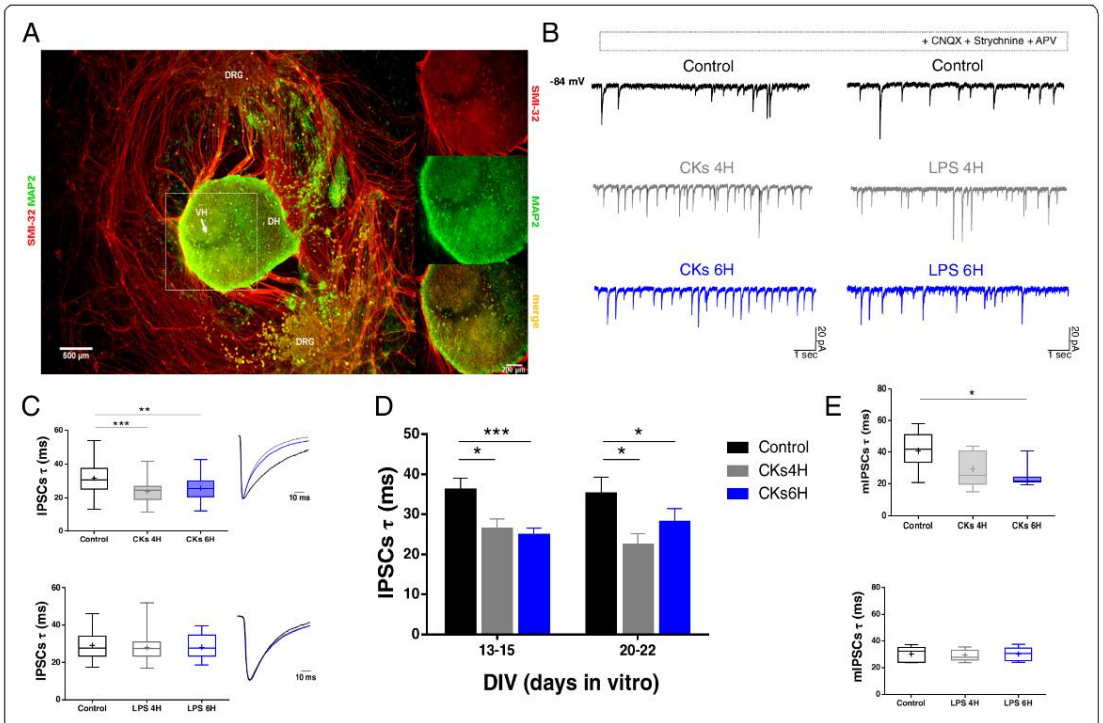

Fig. 1 Cytokines affect GABAergic synaptic current kinetics in organotypic spinal culture. **a** Low magnification micrograph of immunofluorescence labeling of organotypic spinal cord slice (14 DIV), SMI-32 (in red), and MAP 2 (in green) markers identify axons and mature neurons. The ventral area (localized by the *ventral fissure*, arrow) highlighted by the dashed square is shown at higher magnification in the right panels. VH = ventral horn, DH = dorsal horn, DRG = dorsal root ganglia. **b** Pharmacologically isolated IPSCs recorded from ventral interneurons at 14 DIV. Control current tracings are in black. CKs 4H (in gray) and 6H (in blue) (left) and LPS 4H (in gray) and 6H (in blue) (right) increased IPSC frequency. **c** Box plots summarize the decay time constant (τ) values of IPSCs from pooled experiments in CKs (top) or LPS (bottom); the insets show superimposed and scaled IPSC average tracings (same cells as in **b**); note the changes in IPSC duration in CKs (**$P < 0.01$; ***$P < 0.001$, one-way ANOVA). **d** Bar plot (mean ± SEM) of IPSCs τ values plotted against DIV; bins are at 13–15 DIV: 36.3 ± 2.7 ms control; 26.5 ± 2.2 ms CKs 4H; 24.5 ± 1.6 ms CKs 6H; $n = 14, 10, 15$, respectively; *$P = 0.011$ control vs CKs 4H; ***$P < 0.001$ control vs CKs 6H; bins at 20–22 DIV: 37.6 ± 3.6 ms control; 22.5 ± 2.6 ms CKs 4H; 26.2 ± 2.9 ms CKs 6H; $n = 8, 6, 6$, respectively; *$P = 0.011$ control vs CKs 4H; *$P = 0.041$ control vs CKs 6H (one-way ANOVA). **e** Box plots summarize the τ values of mIPSCs from pooled experiments in CKs (top) or LPS (bottom), note the changes in mIPSC duration in CKs. *$P = 0.024$ control vs CKs 6H, one-way ANOVA

were visualized using a specific marker (class III β-tubulin, Additional file 4: Figure S3 A and C). At lower magnification, scattered soma, extensive neural processes, and bouton-like structures (named clusters, see the "Methods" section) appeared to be stained for both GAD isoforms and were not affected by CK or LPS treatments, quantified in Additional file 4: Figure S3 B and D.

Resident neuroglia reactivity to CKs and LPS in spinal organotypic slices

In response to different microenvironment stimuli, microglia and astrocytes may switch to active states, highlighted by changes in cell function, number, and/or morphology. Microglia and astrocytes were visualized in organotypic spinal explants by Iba1 and GFAP co-immunolabeling, shown in Fig. 2 a and b.

CKs 4H and 6H promoted a significant increase in Iba1$^+$ cells (99.8 ± 5.5 cells/mm^2 control; 155.3 ± 21.5 cells/mm^2 CKs 4H; 183.7 ± 15.7 cells/mm^2 CKs 6H; *$P = 0.032$ control vs CKs 4H; ***$P < 0.001$ control vs CKs 6H; summarized in Additional file 1: Table S1 for 4H and in Fig. 2c, left, for 6H). The same treatments promptly induced a significant increase in GFAP intensity (158.1 ± 35.7% CKs 4H; 229.3 ± 37.3% CKs 6H; *$P = 0.024$ control vs CKs 4H, ***$P < 0.001$ vs CKs 6H; ***$P < 0.001$ CKs 4H vs CKs 6H; summarized in Additional file 1: Table S1 for 4H and Fig. 2c, right, for 6H). Differently, LPS, summarized for 4H in Additional file 1: Table S1 and in the plots in Fig. 2d

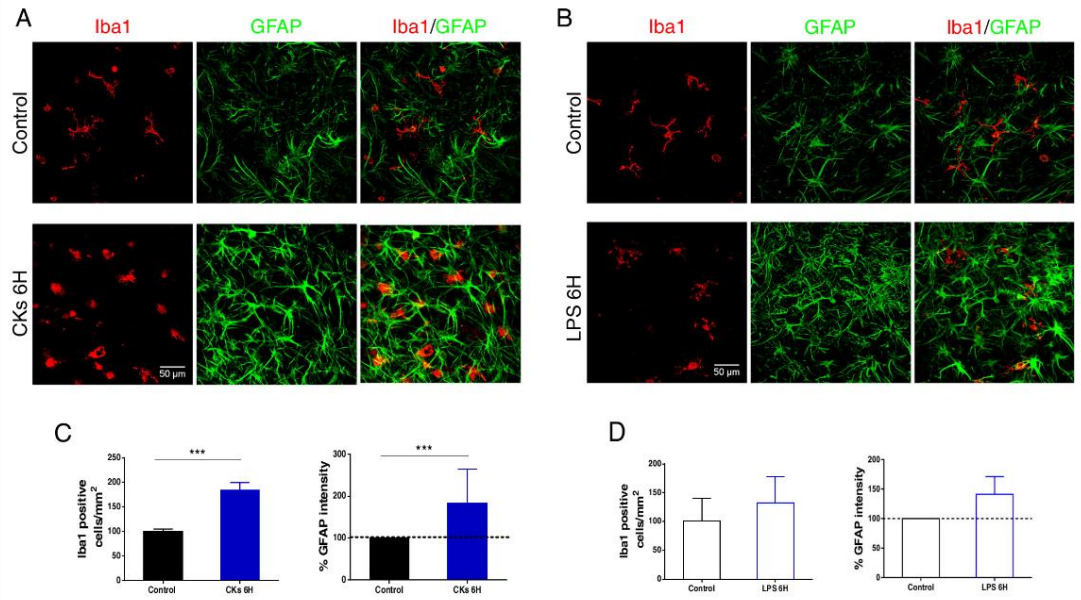

Fig. 2 CK and LPS modulation of resident microglia and astrocytes in organotypic spinal cultures. **a**, **b** Representative confocal images of organotypic spinal slices immunolabeled for Iba1 (in red) and GFAP (in green), visualizing microglia and astrocytes, respectively, prior and after CKs (in **a**) or LPS (in **b**) treatments (4H and 6H). **c**, **d** Bar plots summarize Iba1$^+$ cells/mm^2 and GFAP intensity (expressed as percentage of control) prior and after CKs (6H; in **c**) or LPS (6H; in **d**) treatments. Bar plots (mean ± SEM); $^{***}P < 0.001$, one-way ANOVA

for 6H, provoked only mild increases in Iba1$^+$ cells (100.8 ± 8.2 cell/mm^2 control; 112.8 ± 7.4 cell/mm^2 LPS 4H; 132.2 ± 11.7 cell/mm^2 LPS 6H) and in the GFAP intensity (110.4 ± 18.7% LPS 4H; 141.1 ± 15.1% LPS 6H).

We further assessed CK and LPS ability to shape the morphology of Iba1$^+$ microglia at 6H. To this aim, we quantified the total dendrite length [34] together with the transformation index (results summarized in Fig. 3a, b; [25]). Upon CKs 6H treatments, microglia showed a significant decrease in both the total dendrite lengths (270.3 ± 144.8 μm control; 93.8 ± 81.2 μm CKs 6H; $^{***}P <$ 0.001 control vs CKs 6H) and the transformation index (2.7 ± 2.4 control; 1.7 ± 0.7 CKs 6H; $^{**}P < 0.005$ control vs CKs 6H). In parallel, in slices stimulated by LPS, we observed, at 6H, changes in microglia morphology that seem to indicate a different stage of activation [35]. In fact, Fig. 3 a and b show a significant increment of the Iba1$^+$ cell dendrite length at LPS 6H (346.6 ± 194.9 μm control; 472.6 ± 255.9 μm LPS 6H; $^{***}P < 0.001$ control vs LPS 6H) and of the transformation index (7.2 ± 5.3 control; 12.2 ± 7.7 LPS 6H; $^{***}P < 0.001$ control vs LPS 6H). Finally, we evaluated and compared the production of cytokines and chemokines by spinal slices in response to pro-inflammatory stress at 6H (for CKs $n = 14$ slices and for LPS $n = 22$ slices, from 3 different culture series). The summarizing plots of Fig. 3c, d show that the exposure to CKs (c) and LPS (d) significantly increased, although to a different extent, the release of pro-inflammatory cytokines, measured in the supernatant, such as TNF-α, IL-6, and INF-γ, as well as the release of chemokines including CXCL1 and CXCL2 necessary for the recruitment of innate immune cells. Interestingly, IL-4 and IL-10 are significantly raised upon CK stimuli, but are not changed after LPS treatments. The different pro- and anti-inflammatory cytokine network, in addition to the production of chemokines, suggests the induction of alternative activation mechanisms in spinal slices stimulated by CKs and LPS at the time point (6H) analyzed.

In the central nervous system, LPS binds to the Toll-like receptors (TLRs), especially TLR4, expressed on the microglia surface. This signal involves several proteins resulting in the production and release of cytokines, chemokines, and other inflammatory factors [36]. Since LPS, differently from CKs [37], may not act directly on neurons, we tested whether a longer (24H) exposure to LPS may ultimately lead to changes in GABAergic transmission and kinetic. Figure 4 reports the effects of LPS 24H in terms of PSC frequency (21.7 ± 6.7 Hz control; 30.5 ± 5.0 Hz LPS 24H; $n = 8$ and 12, respectively; $^{**}P =$ 0.003 control vs LPS 24H; Fig. 4a), IPSC frequency (1.2 ± 0.8 Hz control; 2.5 ± 0.9 Hz LPS 24H; $^{**}P = 0.007$

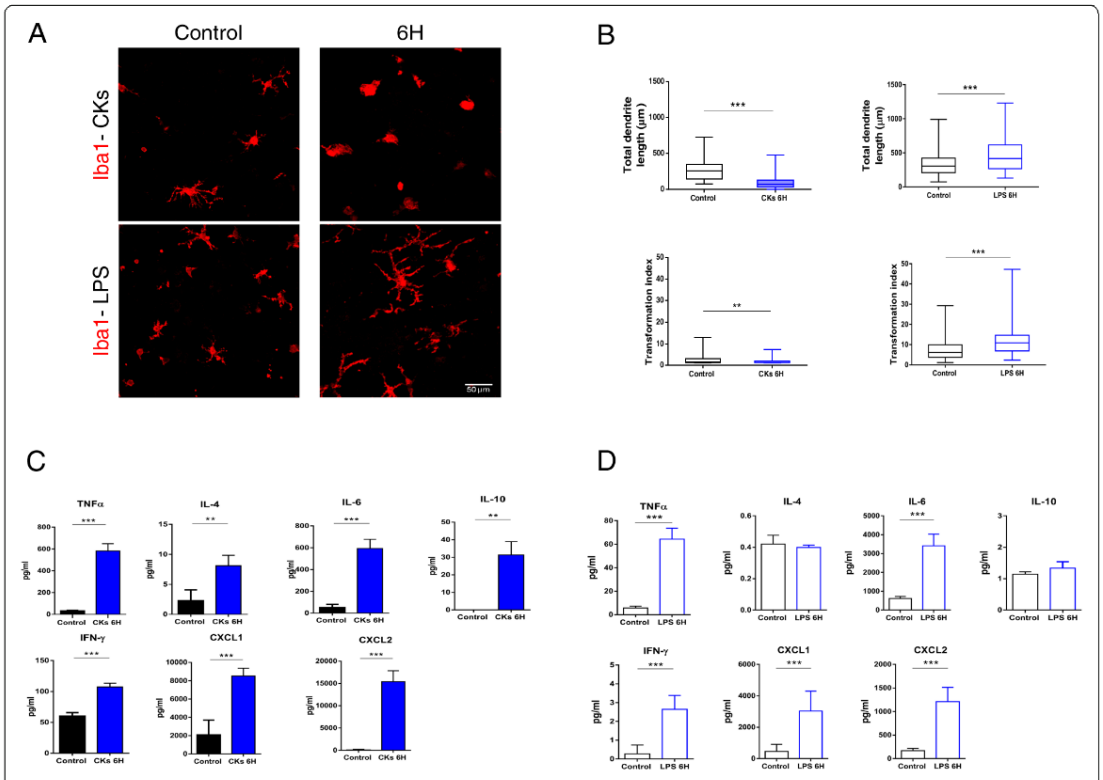

Fig. 3 CKs and LPS induce opposite changes in microglia morphology. **a** Representative confocal images comparing Iba1 immunolabeling in untreated (control) and CK- and LPS-treated (4H and 6H) cultures. **b** Box plots show pooled data from different experiments. Note the significant decrease in total dendrites length and transformation indices upon CKs 6H (left); on the opposite, a significant increase in total dendrites length and in the transformation indices is reported at LPS 6H (right). $^{**}P < 0.01$, $^{***}P < 0.001$, Kruskal-Wallis test (Dunn's post hoc test). **c**, **d** Production of cytokines (TNF-α; IL-4; IL-6; IL-10; INF-γ) and chemokines (CXCL1; CXCL2) determined by Milliplex assay of organotypic culture supernatants after incubation with CKs (**c**) and LPS (**d**) for 6H. Bar plot (mean ± SEM of 22 and 14 slices, respectively); $^{**}P < 0.01$, $^{***}P < 0.001$, one-way ANOVA

control vs LPS 24H; Fig. 4b), and IPSC decay time constant (32.7 ± 10.2 ms control; 29.7 ± 5.5 ms LPS 24H, Fig. 4c, scaled averaged IPSCs are superimposed in the inset). In addition, Iba1$^+$ cells at LPS 24H (Fig. 4 D) displayed the characteristic morphology with longer branching in ramified cells (quantified in plots of Fig. 4d, total dendrites length: 249.6 ± 96.0 µm control; 393.4 ± 216.9 µm LPS 24H; $^{***}P < 0.001$ control vs LPS 24H; transformation indices: 5.2 ± 3.1 control; 8.6 ± 7.1 LPS 24H). These results indicated that the kinetic of GABAergic currents was not modulated by longer incubation in this danger signal, and the effects on microglia dendrite lengths stabilized after 6H.

CKs modulate GABAergic current duration through changes in $GABA_AR$ subunits composition

We further explored the mechanisms responsible for IPSC shortening due to CKs. The decay of IPSCs is also faster, upon CK treatments, in unitary synaptic events (mIPSCs), ruling out the involvement of presynaptic processes affecting IPSC time course, such as neurotransmitter release synchronization. Moreover, the absence of changes in IPSC rise time (Additional file 3: Figure S2 C) suggests that differences in recording conditions, location of synapses or electronic filtering, are unlikely to have affected our observations.

Differences in the intracellular chloride concentration $[Cl^-]_i$ were reported to affect IPSC kinetics [38, 39]. We incubated organotypic slices with bumetanide (10 µM; 24H, $n = 11$), a blocker of NKCC1 activity [24], a membrane-protein described as the most abundant co-transporter determining intracellular chloride levels [40], to experimentally reduce $[Cl^-]_i$ prior to CKs 4H ($n = 10$; see sketch of the experimental settings in Fig. 5a).

Bumetanide per se induced an increase in PSC and IPSC frequencies that were slightly, although not significantly, further improved by CKs 4H (Fig. 5b for sample tracings and Additional file 5: Figure S4). More intriguingly, bumetanide

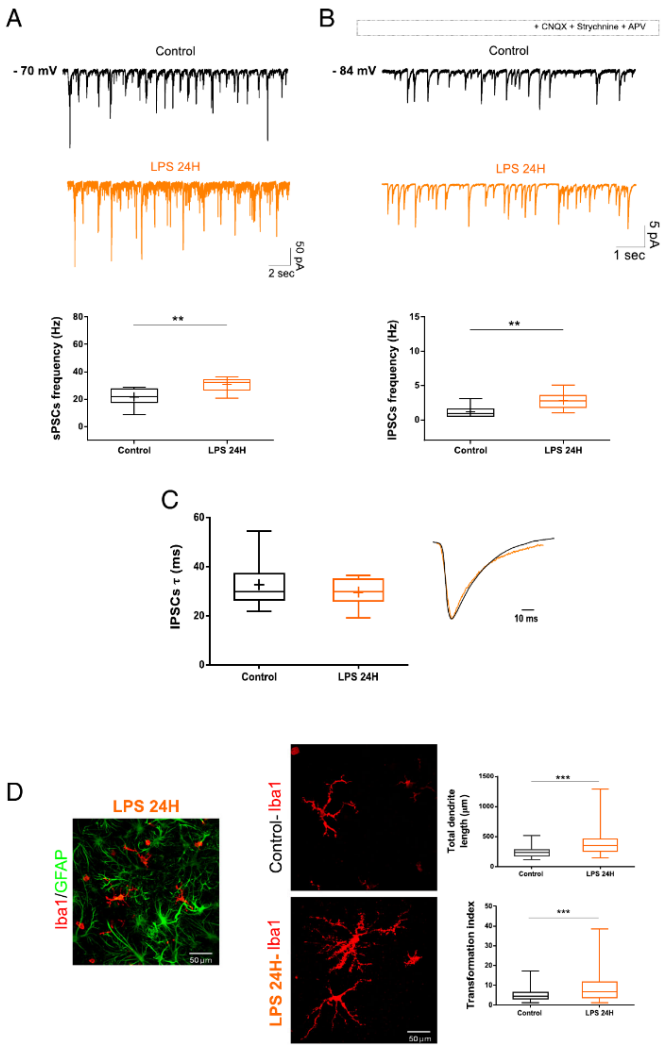

Fig. 4 Long-term exposure to LPS in organotypic spinal slices is not altering GABAergic currents. **a** Representative traces of spontaneous PSCs recorded from control (in black) and LPS 24H (in orange) ventral interneurons. The box plot shows a significant increase in PSC frequency upon LPS 24H. $^{**}P = 0.003$, Mann-Whitney test. **b** Pharmacologically isolated IPSCs are recorded from control (in black) and LPS 24H (in orange) ventral interneuron (same cells as in **a**). The box plot summarizes the IPSC frequency from pooled experiments and exhibits a significantly increased frequency brought about by LPS 24H. $^{**}P = 0.007$, Mann-Whitney test. **c** The box plot summarizes the values of τ for control and LPS; in the inset, averaged scaled and superimposed traces of the two conditions are shown. Note that no changes were detected in IPSC decay time constant. **d** Left, representative image of the LPS 24H-treated organotypic culture labeled with GFAP (green) and Iba1 (red). Right, high magnification Iba1 micrographs are shown (middle), and plots summarize the morphology changes of microglia upon LPS 24H. Note the significant increase in dendrites length (top) and in the transformation index (bottom); $^{***}P < 0.001$, Mann-Whitney test

reduced significantly the duration of GABAergic currents ($\tau = 33.1 \pm 8.1$ ms control; $\tau = 22.3 \pm 6.2$ ms BUM 24H; $^{**}P = 0.005$ control vs BUM 24H) that were not further shortened by CKs 4H ($\tau = 22.3 \pm 6.5$ ms BUM 24H + CKs 4H; $^{*}P = 0.012$ control vs BUM 24H + CKs 4H; Fig. 5c).

Figure 5 d shows the measurement of the reversal potential of IPSCs in control, BUM 24H, and BUM 24H + CKs 4H. The estimated E_{Cl} value in control (-48.5 ± 3.7 mV; $n = 7$) was close to the approximate theoretical value expected for the Cl^- equilibrium potential for our

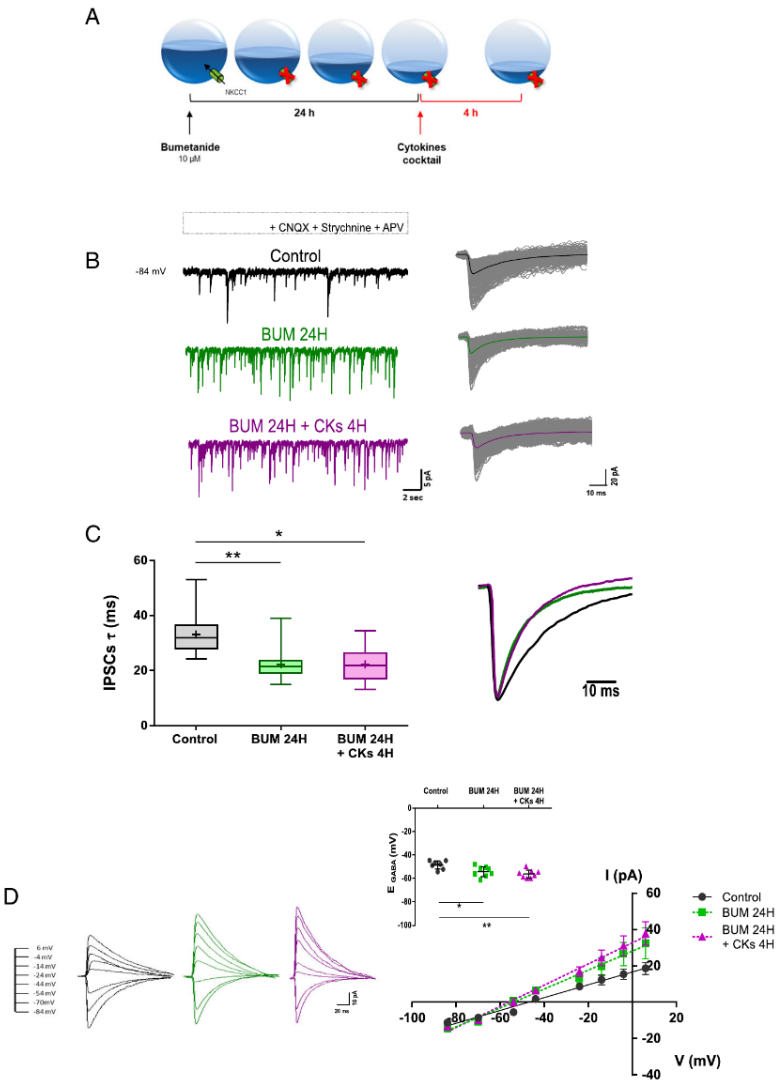

Fig. 5 Effects of CKs on GABAergic synaptic current duration in the presence of bumetanide. **a** Sketch of the protocol used to treat slices with bumetanide for 24H (BUM 24H) followed by CKs 4H. **b** Representative traces (left) and superimposed isolated events (right) of IPSCs in control, after BUM 24H (green), and BUM 24H + CKs 4H (magenta). **c** The box plot summarizes the IPSCs τ values measured in the three conditions; note the significant reduction in IPSCs τ in BUM 24H and BUM 24H + CKs 4H, in respect to control. Inset: superimposed averaged and scaled IPSCs in the three conditions. $^{*}P = 0.012$, $^{**}P = 0.005$, Kruskal-Wallis test. **d** Top, IPSCs averaged and superimposed traces recorded at different V_h in control (black), BUM 24H (green), and BUM 24H + CKs 4H (magenta). Bottom, I/V curves obtained by plotting $GABA_A$-IPSCs mean amplitude against V_h. Note in the inset the significant differences in the estimated IPSCs reversal potential (E_{GABA}) at BUM 24H and BUM 24H + CKs 4H, when compared to control. $^{*}P < 0.05$, $^{**}P < 0.01$, one-way ANOVA

intracellular and extracellular chloride concentrations (− 50 mV; [26]). However, the reversal potential was significantly shifted to more negative values by blocking NKCC1 (− 54.2 ± 4.3 mV BUM 24H, $n = 8$; $^{*}P = 0.025$ control vs BUM 24H), suggesting that local intracellular chloride concentrations are lower (estimated from 24 to 19 mM). It is important to note that in organotypic cultures, upon bumetanide treatments, the Cl^- reversal potential differed from the predicted theoretical value, suggesting a real shift in the internal chloride concentration as a result of reduced

co-transport [41, 42], regardless the 24 mM Cl^- intracellular pipette solution [17].

Pro-inflammatory CKs, in the presence of NKCC1 block, slightly increased such a shift only when compared to controls (− 56.2 ± 3.5 mV BUM 24H + CKs 4H; $n = 8$; $^{**}P = 0.003$ control vs BUM 24H + CKs 4H). The absence of significant changes in IPSC decay time constant and reversal once CKs were incubated in the presence of bumetanide might indicate an occluding mechanisms between CKs and bumetanide in regulating $[Cl^-]_i$.

To shed light in CK potential regulation of intracellular chloride, and thus of IPSCs τ, we estimated and compared E_{Cl} in control, CKs, and LPS treatments. Additional file 6: Figure S5 shows that the reversal potential of IPSCs was not altered by these treatments alone (− 52.0 ± 7.5 mV control; − 51.5 ± 5.2 mV CKs 4H; $n = 9$, 10, respectively; − 49.6 ± 7.8 mV control; − 49.7 ± 9.9 mV LPS 4H; $n = 13$, 8, respectively). Regardless of the similar E_{Cl} extrapolated in all the recording conditions, only CKs 4H induced the expected changes in the IPSC duration (τ = 31.8 ± 5.1 ms control; $\tau = 23.9 \pm 8.1$ ms CKs 4H; $^{*}P = 0.031$ control vs CKs 4H; Student t test; $\tau = 26.4 \pm 5.2$ ms control; τ = 26.2 ± 6.3 ms LPS 4H; respectively). These results show that changes in E_{Cl} might indeed modulate IPSC duration in the organotypic spinal interneurons; however, CKs apparently are not tuning the inhibitory current duration by shifts in the E_{Cl}.

A well-documented post-synaptic process that changes GABAergic inhibition is the switch in the α1-subunit expression reported to modulate IPSC kinetics, which become faster [43]. To address the potential changes in the receptor subunit composition due to CK treatment, we tested IPSC kinetics in the presence of zolpidem (100 nM; 15–20 min), an allosteric modulator of $GABA_AR$ subunits that at low concentrations is highly selective for the $GABA_AR$ α1 subunit [44]. Figure 6a shows sample superimposed isolated IPSCs recorded from control, CKs 4H, and CKs 6H, before and after zolpidem applications. Also, in this set of recordings, after CKs 4H and 6H, IPSCs τ was significantly reduced (33.3 ± 4.5 ms control; 25.4 ± 4.7 ms CKs 4H; 26.0 ± 4.0 ms CKs 6H; $n = 9$, 10, 9, respectively; $^{*}P = 0.019$ control vs CKs 4H; $^{*}P = 0.045$ control vs CKs 6H). Subsequent applications of zolpidem did not alter IPSCs τ in control (36.3 ± 3.9 ms), while significantly prolonged τ values detected in CKs 4H and 6H (34.5 ± 6.9 ms CKs 4H; 34.2 ± 6.0 ms CKs

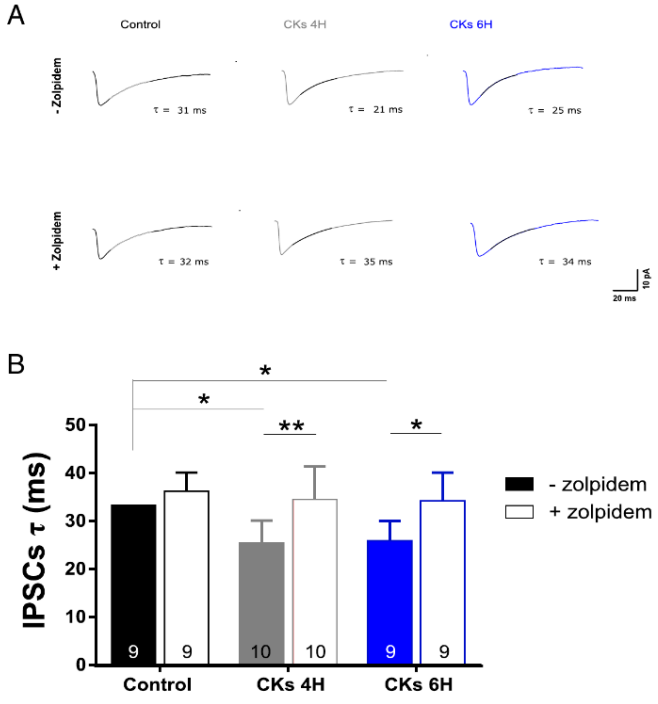

Fig. 6 Zolpidem effects on GABAergic synaptic current duration before and after CK treatments. **a** Sample tracings of averaged IPSCs recorded in control (black) and CKs (4H in gray and 6H in blue) in the presence (+) or in the absence (–) of zolpidem. Note the superimposed fitting used to calculate τ values. **b** Bar plot summarizes the τ values of IPSCs in control, CKs 4H, and CKs 6H, before and after bath application of zolpidem. Note that the significant decrease in IPSCs τ upon CKs treatments (4H and 6H) was reversed by zolpidem. $^{*}P < 0.05$, $^{**}P < 0.01$, one-way ANOVA

6H; $^{**}P = 0.003$ CKs 4H – Zolpidem vs CKs 4H + zolpidem; $^{*}P = 0.017$ CKs 6H -zolpidem vs CKs 6H + zolpidem), which did not differ anymore from control IPSCs (summarized in the bar plots of Fig. 6 B). These results strongly suggest that CK treatments regulated the duration of GABAergic inhibition via post-synaptic changes of the α1 subunit.

Discussion

Our study targets synaptic changes in response to local CNS tissue reactivity, experimentally induced by CKs or LPS and involving resident neuroglia. In particular, we used the spinal organotypic cultures to focus on the interplay between local inflammation and the dynamics of GABAergic currents, whose altered decay may represent a subtle alteration able to trigger neuronal network dysfunction, potentially involved in neurodegenerative processes [45–47]. The organotypic slice model represents a high-density cell system, where the 3D-architecture of specific resident cells, neuronal and non-neuronal, is preserved in a tissue culture setting [15–17, 48]. The main finding of the current work is that local inflammation in organotypic spinal slices induced by CKs and LPS stimulations boosts network activity already after 4H treatments, as shown by the augmented PSCs and IPSCs frequency; however, only tissue reactivity brought about by CKs specifically reduced GABAergic current duration. We adopted short-term treatments to trigger inflammatory responses, without affecting neuronal membrane properties or inducing direct neurotoxicity, yet still able to alter synaptic transmission [17, 49].

The ability of CKs, directly, or of LPS-activated immune cells, indirectly, to increase synaptic activity or neuronal excitability has been previously described using several experimental settings and in different CNS structures [5, 17, 30, 31, 50, 51]. Yet, mechanistically, the influence on synaptic function of acute or prolonged exposures to inflammatory milieus has led often to controversial results, involving the glutamatergic signaling system [6, 52, 53], or the inhibitory synaptic transmission [5, 30, 54], as well as neuronal excitability [31, 50, 55], clearly indicating the complexity of the signaling pathways activated upon inflammation. In addition, the output readout used in these studies, i.e., post-synaptic currents, might be misleading, due to the variable amount of homeostatic plasticity taking place once destabilizing influences alter synaptic transmission [56]. Regardless the mechanisms leading to improved synaptic activity, only the direct exposure to CKs regulated the GABAergic current decay, probably via a post-synaptic mechanisms, as indicated by the detected changes in mIPSC's τ [26, 57]. The absence of LPS ability, even upon prolonged exposure of the slices, to regulate the inhibitory current decay was apparently not due to a lack of LPS activation of inflammation, a notion supported by the LPS-mediated increase in synaptic activity and by the cytokines and chemokines produced by LPS-treated slices, despite the low GFAP-positive cell reactivity and the changes in microglia morphology detected by immunocytochemistry, different to those reported in CKs. To note, the morphology of resident neuroglia together with the small increase in GFAP expression upon LPS treatment may indicate a different state of activation, supported by a different profile of CK network and production, providing an alternative (i.e., to CKs), inflammation-mediated regulation of brain functions [35, 58]. LPS is experimentally used to mimic CNS bacterial inflammation [59], whereas CKs mimic the inflammatory network present when immune system intervenes in the CNS. These two functional conditions may affect synapses differently, and future investigations may allow elucidating CNS pathological conditions related to distinct etiologies. Indeed, we have to consider the diverse mechanisms of action triggered by CKs and LPS [60–63] which both act through precise receptors on microglia and neurons, affecting the microglia/neuron communication and function [64].

CK regulation of GABAergic current in the absence of changes in GABA synthesis is thus a specific feature of the selected CK cocktail, able to mimic an inflammatory reaction involved in neuropathy [2, 6, 17], and the mechanisms of this modulation might be a targetable pathway in spinal neuroinflammatory disease treatments.

We examined the main variables that might conceivably affect the kinetic properties of $GABA_AR$ and therefore the GABAergic-PSC time course. First, we excluded the possibility of differences in the intracellular chloride concentration, brought about by neuroinflammation [38, 65] that could affect IPSC kinetics [66], as confirmed by our experiments where NKCC1 was pharmacologically blocked, leading to a shift in Cl^- reversal potential. Our measurements show that the Cl^- reversal potential was similar in the cultures treated by CKs or LPS, in the absence of bumetanide, yet CKs still induced a significant shortening of the GABAergic current duration. In bumetanide-treated cultures, the Cl^- reversal potential differed from the predicted theoretical value. In our recording conditions, it is not possible to confirm a real shift in the internal chloride concentration as a result of the decreased influx [41, 42]. However, the detected shifts in bumetanide are consistent with a 19 mM Cl^- intracellular concentration.

An alternative process that changes IPSC current duration in the CNS is the $GABA_AR$ α-subunit composition [39, 67–69]. In particular, α1-subunit is responsible for fast deactivation, which results in faster-decaying currents [39, 69]. Our hypothesis, of an increased expression of α1-subunit upon CKs treatment, was supported by the efficacy of zolpidem [44] to prolong IPSC duration only in CK-treated slices.

Our results describe for the first time a selective mechanism that could be triggered during inflammatory stress. In particular, under pathological conditions, the switch of $GABA_AR$ α1-subunit would induce faster $GABA_AR$ decay time, weakening the IPSCs transmission. Therefore, lower IPSC duration could contribute to providing an aberrant excitatory transmission critical for pre-motor circuit tasks.

Conclusions

We exploited spinal cord explant cultures to investigate two diverse immune conditions in the CNS, characterized by different inflammatory networks and products, thus providing alternative inflammation-mediated regulation of the CNS functions. We have shown that these two functional conditions affect inhibitory synapses differently, and we hypothesized that the mechanisms of this modulation might be a targetable pathway in spinal neuroinflammatory disease treatments.

Additional files

Additional file 1: Table S1. Neuroglial cell reactivity upon 4-h treatments in CKs and LPS. (PDF 1613 kb)

Additional file 2: Figure S1. CKs and LPS increase sPSC frequency in organotypic slices A-B, Representative current tracings of sPSCs recorded in control (black) and after incubation in CKs (4H in gray and 6H in blue; left) or in LPS (4H in gray and 6H in blue; right). C-D, Box plots summarize the increase in sPSC frequency (20.3 ± 9.5 Hz control; 27.9 ± 9.4 Hz CKs 4H; 28.8 ± 9.4 Hz CKs 6H; ***$P < 0.001$ control vs CKs 4H and control vs CKs 6H, one-way ANOVA) and in LPS (21.4 ± 9.7 control; 28.4 ± 10.4 LPS 4H; 33.3 ± 9.8 LPS 6H; **$P = 0.008$ control vs LPS 4H; ***$P < 0.001$ control vs LPS 6H, one-way ANOVA) treatments. (PDF 37 kb)

Additional file 3: Figure S2. CKs and LPS increase IPSC frequency in organotypic slices A–C. Box plots illustrate the mean value of IPSCs frequency (A), amplitude (B), and rise time (C) upon CK and LPS treatments. A significant increase was observed in the IPSC frequency at CKs 4H and 6H, when compared to control (3.3 ± 1.5 Hz control; 4.7 ± 1.9 Hz CKs 4H; 4.6 ± 2.0 Hz CKs 6H; $n = 40, 33, 37$, respectively; **$P = 0.003$ control vs CKs 4H and **$P = 0.006$ vs CKs 6H, one-way ANOVA) and at LPS 4H and 6H when compared to their relative control (1.7 ± 0.9 Hz control; 3.1 ± 2.6 Hz LPS 4H; 3.4 ± 2.7 Hz LPS 6H; $n = 34, 33, 27$, respectively; *$P = 0.002$, control vs LPS 4H, and **$P = 0.001$ vs LPS 6H, one-way ANOVA). IPSC amplitude (17.5 ± 10.5 pA control; 19.4 ± 9.1 pA CKs 4H; 17.0 ± 11.2 pA CKs 6H; 15.7 ± 8.9 pA control; 11.3 ± 4.5 pA LPS 4H; 13.1 ± 7.3 pA LPS 6H) and rise time (2.5 ± 0.8 ms control; 2.1 ± 0.8 ms CKs 4H; 2.6 ± 1.4 ms CKs 6H; 2.6 ± 1.0 ms control; 2.5 ± 1.0 ms LPS 4H; 2.6 ± 0.9 ms LPS 6H) were unaffected by CK or LPS treatments. (PDF 6885 kb)

Additional file 4: Figure S3. GAD65/67 immunoreactivity in organotypic slices before and after CK or LPS treatments A and C. Representative images of spinal slices labeled for β-tubulin III (in blue) and GAD65/67 (in red) show GABAergic neurons in untreated (control) and CK- and LPS-treated (4H and 6H) ventral area of spinal organotypic slices (14 DIV) B and D. Bar plots summarize the normalized GAD65/67 clusters (1483 ± 62.2 control; 1503 ± 49.9 CKs 4H; 1403 ± 27.2 CKs 6H; 1295 ± 45.3 control; 1300 ± 46.3 LPS 4H; 1382 ± 54.4 LPS 6H) and the GAD65/67 intensity in a.u. (379.1 ± 29.4 control; 423.9 ± 40.8 CKs 4H; 383.9 ± 38.5 CKs 6H; 417.3 ± 46.9 control; 391.3 ± 58.4 LPS 4H; 433.3 ± 46.5 LPS 6H). (PDF 28 kb)

Additional file 5: Figure S4 Spontaneous PSC and IPSC frequency in bumetanide 24 h before and after CKs 4H. **A** Left, box plots of PSCs frequency values from control, bumetanide-treated slices prior and after CKs. Note the significant increase in PSC frequency BUM 24H and BUM 24H + CKs 4H compared to control (24.4 ± 7.8 Hz control; 37.1 ± 11.4 Hz BUM 24H; 42.6 ± 11.2 Hz BUM 24H + CKs 4H; $n = 9, 10, 9$, respectively; *$P = 0.033$ control vs BUM 24H; **$P = 0.003$ control vs BUM 24H + CKs 4H, one-way ANOVA). Right, box plots of IPSCs frequency values upon BUM 24H and BUM 24H + CKs 4H compared to control (3.1 ± 1.4 Hz control; 6.0 ± 2.8 Hz BUM 24H; 6.6 ± 2.5 Hz BUM 24H + CKs 4H; $n = 10, 11, 10$, respectively; *$P = 0.019$ control vs BUM 24H; **$P = 0.005$ control vs BUM 24H + CKs 4H, one-way ANOVA). (PDF 278 kb)

Additional file 6: Figure S5. E_{GABA} estimated in control, CKs 4H and LPS 4H. IPSCs averaged and superimposed traces (top) recorded at different V_h in control, CKs 4H, and LPS 4H. Bottom, I/V curves were obtained by plotting $GABA_A$-PSCs mean amplitude against Vh. Inset, note the similar (E_{GABA}) in all conditions. *$P < 0.05$, **$P < 0.01$, one-way ANOVA. (PDF 13 kb)

Abbreviations

APV: (2*R*)-amino-5-phosphonovaleric acid; BSA: Bovine serum albumin; BUM: Bumetanide; CKs: Cytokines; CNQX: 6-Cyano-7-nitroquinoxaline-2,3-dione; DH: Dorsal horn; DIV: Days in vitro; DRG: Dorsal root ganglia; FBS: Fetal bovine serum; GAD: Glutamate decarboxylase; GFAP: Glial fibrillary acidic protein; GM-CSF: Granulocyte-macrophage colony-stimulating factor; Iba1: Ionized calcium-binding adapter molecule 1; IL-1β: Interleukin-1beta; LPS: Lipopolysaccharide; MAP 2: Microtubule-associated protein 2; mPSCs: Miniature post-synaptic currents; PBS: Phosphate-buffered saline; PSCs: Post-synaptic currents; RT: Room temperature; SMI-32: Neurofilament H non-phosphorylated; TNF-α: Tumor-necrosis factor-alfa; TTX: Tetrodotoxin; VH: Ventral horn

Acknowledgements

The authors would like to thank M. Grandolfo for providing technical support with immunofluorescence labeling, confocal microscopy, and image analysis.

Authors' contributions

VG, GP, and MM performed the electrophysiology and immunohistochemistry experiments and analysis. VG contributed to the experimental design. EB and AA performed the Milliplex experiments and analysis. CB and LB conceived the study, design the experiments, interpreted the data, and wrote the manuscript. All authors read and approved the final manuscript.

Funding

We acknowledge the financial support from the European Union's Horizon 2020 research and innovation program under grant agreements No. 696656 and No. 785219 Graphene Flagship.

Availability of data and materials

The datasets supporting the conclusion of this article are included within the article (and its additional files). The datasets generated and/or analyzed during the current study are stored in a public repository and are available from the corresponding authors on reasonable request.

Ethics approval and consent to participate

All experiments were performed in accordance with the EU guidelines (2010/63/UE) and Italian law (Decree 26/14) and were approved by the local authority veterinary service and by our institution (SISSA) ethical committee. All efforts were made to minimize animal suffering and to reduce the number of animals used. Animal use was approved by the Italian Ministry of Health, in agreement with the EU Recommendation 2007/526/CE.

Consent for publication

Not applicable.

Competing interests

The authors declare that they have no competing interests.

Author details

[1]International School for Advanced Studies (SISSA/ISAS), 34136 Trieste, Italy. [2]Department of Life Sciences, University of Trieste, 34127 Trieste, Italy. [3]Department NEUROFARBA, University of Florence, 50139 Florence, Italy. [4]Dipartimento di Medicina Sperimentale e Clinica, University of Florence,

50139 Florence, Italy. [5]Present address: Wolfson Centre for Age Related Disease, King's College London, Guy's Campus, London SE1 1UL, UK.

Received: 15 February 2019 Accepted: 11 June 2019
Published online: 25 June 2019

References

1. Chen WW, Zhang X, Huang WJ. Role of neuroinflammation in neurodegenerative diseases (review). Mol Med Rep. 2016;13:3391–6.
2. Mandolesi G, Gentile A, Musella A, Fresegna D, De Vito F, Bullitta S, Sepman H, Marfia GA, Centonze D. Synaptopathy connects inflammation and neurodegeneration in multiple sclerosis. Nat Rev Neurol. 2015;11:711–24.
3. Pozzi D, Menna E, Canzi A, Desiato G, Mantovani C, Matteoli M. The communication between the immune and nervous systems: the role of IL-1β in synaptopathies. Front Mol Neurosci. 2018;11:111.
4. Musella A, Gentile A, Rizzo FR, De Vito F, Fresegna D, Bullitta S, Vanni V, Guadalupi L, Stampanoni Bassi M, Buttari F, Centonze D, Mandolesi G. Interplay between age and neuroinflammation in multiple sclerosis: effects on motor and cognitive functions. Front Aging Neurosci. 2018;10:238.
5. Kawasaki Y, Zhang L, Cheng JK, Ji RR. Cytokine mechanisms of central sensitization: distinct and overlapping role of interleukin-1beta, interleukin-6, and tumor necrosis factor-alpha in regulating synaptic and neuronal activity in the superficial spinal cord. J Neurosci. 2008;28:5189–94.
6. Centonze D, Muzio L, Rossi S, Cavasinni F, De Chiara V, Bergami A, Musella A, D'Amelio M, Cavallucci V, Martorana A, Bergamaschi A, Cencioni MT, Diamantini A, Butti E, Comi G, Bernardi G, Cecconi F, Battistini L, Furlan R, Martino G. Inflammation triggers synaptic alteration and degeneration in experimental autoimmune encephalomyelitis. J Neurosci. 2009;29:3442–52.
7. Glass CK, Saijo K, Winner B, Marchetto MC, Gage FH. Mechanisms underlying inflammation in neurodegeneration. Cell. 2010;140:918–34.
8. Hellstrom IC, Danik M, Luheshi GN, Williams S. Chronic LPS exposure produces changes in intrinsic membrane properties and a sustained IL-beta-dependent increase in GABAergic inhibition in hippocampal CA1 pyramidal neurons. Hippocampus. 2005;15:656–64.
9. Viviani B, Bartesaghi S, Gardoni F, Vezzani A, Behrens MM, Bartfai T, Binaglia M, Corsini E, Di Luca M, Galli CL, Marinovich M. Interleukin- 1beta enhances NMDA receptor-mediated intracellular calcium increase through activation of the Src family of kinases. J Neurosci. 2003;23:8692e8700.
10. Murray CA, McGahon B, McBennett S, Lynch MA. Interleukin-1 beta inhibits glutamate release in hippocampus of young, but not aged, rats. Neurobiol Aging. 1997;18:343–8.
11. Zeise ML, Espinoza J, Morales P, Nalli A. Interleukin-1beta does not increase synaptic inhibition in hippocampal CA3 pyramidal and dentate gyrus granule cells of the rat in vitro. Brain Res. 1997;768:341–4.
12. Wang S, Cheng Q, Malik S, Yang J. Interleukin-1β inhibits γ-aminobutyric acid type a (GABAA) receptor current in cultured hippocampal neurons. JPet. 2000;292:497–504.
13. Luk WP, Zhang Y, White TD, Lue FA, Wu C, Jiang CG, Zhang L, Moldofsky H. Adenosine: a mediator of interleukin-1beta-induced hippocampal synaptic inhibition. J Neurosci. 1999;19:4238–44.
14. Ikegaya Y, Delcroix I, Iwakura Y, Matsuki N, Nishiyama N. Interleukin-1beta abrogates long-term depression of hippocampal CA1 synaptic transmission. Synapse. 2003;47:54–7.
15. Avossa D, Rosato-Siri MD, Mazzarol F, Ballerini L. Spinal circuits formation: a study of developmentally regulated markers in organotypic cultures of embryonic mouse spinal cord. Neuroscience. 2003;122:391–405.
16. Furlan F, Taccola G, Grandolfo M, Guasti L, Arcangeli A, Nistri A, et al. ERG conductance expression modulates the excitability of ventral horn GABAergic interneurons that control rhythmic oscillations in the developing mouse spinal cord. J Neurosci. 2007;27:919–28.
17. Medelin M, Giacco V, Aldinucci A, Castronovo G, Bonechi E, Sibilla A, et al. Neuro-immune crosstalk in organotypic spinal slices: investigating the protective role of an NGF-mimetic. Molecular Brain. 2018;11:3.
18. Kiehn O, Hounsgaard J, Sillar KT. Basic building blocks of vertebrate spinal central pattern generators. In: Stein PSG, et al., editors. Neurons, networks and motor behaviour. Cambridge: The MIT Press; 1997. p. 47–59.
19. Li X, Tupper JC, Bannerman DD, Winn RK, Rhodes CJ, Harlan JM. Phosphoinositide 3 kinase mediates Toll-like receptor 4-induced activation of NF-kappa B in endothelial cells. Infect Immun. 2003;71:4414–20.
20. Vereker E, Campbell V, Roche E, McEntee E, Lynch MA. Lipopolysaccharide inhibits long term potentiation in the rat dentate gyrus by activating caspase-1. J Biol Chem. 2000;275:26252–8.
21. Usmani S, Aurand ER, Medelin M, Fabbro A, Scaini D, Laishram J, et al. 3D meshes of carbon nanotubes guide functional reconnection of segregated spinal explants. Sci Adv. 2016;2:e1600087.
22. Ifergan I, Davidson TS, Kebir H, Xu D, Palacios-Macapagal D, Cann J, Rodgers JM, Hunter ZN, Pittet CL, Beddow S, Jones CA, Prat A, Sleeman MA, Miller SD. Targeting the GM-CSF receptor for the treatment of CNS autoimmunity. J Autoimmun. 2017;84:1–11.
23. Hanisch UK. Microglia as a source and target of cytokines. Glia. 2002; 40:140–55.
24. Dzhala VI, Talos DM, Sdrulla DA, Brumback AC, Mathews GC, Benke TA, Delpire E, Jensen FE, Staley KJ. NKCC1 transporter facilitates seizures in the developing brain. Nat Med. 2005;11:1205–13 Epub 2005 Oct 9.
25. Caldeira C, Oliveira AF, Cunha C, Vaz AR, Falcão AS, Fernandes A, Brites D. Microglia change from a reactive to an age-like phenotype with the time in culture. Front Cell Neurosci. 2014;2(8):152.
26. Medelin M, Rancic V, Cellot G, Laishram J, Veeraraghavan P, Rossi C, et al. Altered development in GABA co-release shapes glycinergic synaptic currents in cultured spinal slices of the SOD1G93A mouse model of ALS. J Physiol. 2016;594:3827–40.
27. Galante M, Nistri A, Ballerini L. Opposite changes in synaptic activity of organotypic rat spinal cord cultures after chronic block of AMPA/kainate or glycine and GABAA receptors. J Physiol. 2000;523(Pt 3):639–51.
28. Maric D, Maric I, Wen X, Fritschy JM, Sieghart W, Barker JL, Serafini R. GABAA receptor subunit composition and functional properties of Cl- channels with differential sensitivity to zolpidem in embryonic rat hippocampal cells. J Neurosci. 1999;15(19):4921–37.
29. Chen L, Savio Chan C, Yung WH. Electrophysiological and behavioral effects of zolpidem in rat globus pallidus. Exp Neurol. 2004;186:212–20.
30. Zhang H, Dougherty PM. Acute inhibition of signalling phenotype of spinal GABAergic neurons by tumour necrosis factor-alpha. J Physiol. 2011;589:4511–26.
31. Zhang H, Nei H, Dougherty PM. A p38 mitogen-activated protein kinase-dependent mechanism of disinhibition in spinal synaptic transmission induced by tumor necrosis factor-α. J Neurosci. 2010;30:12844–55.
32. Liu Q, Wong-Riley MTT. Developmental changes in the expression of GABAA receptor subunits α1, α2, and α3 in the rat pre-Bötzinger complex. J Appl Physiol. 2004;10:1152.
33. Pribiag H, Stellwagen D. TNF-α downregulates inhibitory neurotransmission through protein phosphatase 1-dependent trafficking of GABA(A) receptors. J Neurosci. 2013;33:15879–93.
34. Puram SV, Riccio A, Koirala S, Ikeuchi Y, Kim AH, Corfas G, Bonni A. A TRPC5-regulated calcium signaling pathway controls dendrite patterning in the mammalian brain. Genes Dev. 2011;25:2659–73.
35. Mathieu P, Battista D, Depino A, Roca V, Graciarena M, Pitossi F. The more you have, the less you get: the functional role of inflammation on neuronal differentiation of endogenous and transplanted neural stem cells in the adult brain. J Neurochem. 2010;112:1368–85.
36. Rahimifard M, Maqbool F, Moeini-Nodeh S, Niaz K, Abdollahi M, Braidy N, Nabavi SM, Nabavi SF. Targeting the TLR4 signaling pathway by polyphenols: a novel therapeutic strategy for neuroinflammation. Ageing Res Rev. 2017;36:11–9.
37. Schäfers M, Sorkin L. Effect of cytokines on neuronal excitability. Neurosci Lett. 2008;437:188–93.
38. Funk K, Woitecki A, Franjic-Würtz C, Gensch T, Möhrlen F, Frings S. Modulation of chloride homeostasis by inflammatory mediators in dorsal root ganglion neurons. Mol Pain. 2008;4:32.
39. Moroni M, Meyer JO, Lahmann C, Sivilotti LG. In glycine and GABA(A) channels, different subunits contribute asymmetrically to channel conductance via residues in the extracellular domain. J Biol Chem. 2011;286:13414–22.
40. Ben-Ari Y. NKCC1 chloride importer antagonists attenuate many neurological and psychiatric disorders. Trends Neurosci. 2017;40:536–54.
41. DeFazio RA, Keros S, Quick MW, Hablitz JJ. Potassium-coupled chloride cotransport controls intracellular chloride in rat neocortical pyramidal neurons. J Neurosci. 2000;20:8069–76.
42. Ostroumov A, Simonetti M, Nistri A. Cystic fibrosis transmembrane conductance regulator modulates synaptic chloride homeostasis in motoneurons of the rat spinal cord during neonatal development. Dev Neurobiol. 2011;71:253–68.

43. Vicini S, Ferguson C, Prybylowski K, Kralic J, Morrow AL, Homanics GE. GABA(A) receptor alpha1 subunit deletion prevents developmental changes of inhibitory synaptic currents in cerebellar neurons. J Neurosci. 2001;21:3009–16.
44. Perrais D, Ropert N. Effect of zolpidem on miniature IPSCs and occupancy of postsynaptic GABAA receptors in central synapses. J Neurosci. 1999;19:578–88.
45. Ransohoff RM. How neuroinflammation contributes to neurodegeneration. Science. 2016;353:777–83.
46. Giovannetti EA, Fuhrmann M. Unsupervised excitation: GABAergic dysfunctions in Alzheimer's disease. Brain Res. 2019;1707:216–26.
47. Liberman AC, Trias E, da Silva Chagas L, Trindade P, Dos Santos Pereira M, Refojo D, Hedin-Pereira C, Serfaty CA. Neuroimmune and inflammatory signals in complex disorders of the central nervous system. Neuroimmunomodulation. 2018;25:246–70.
48. Masuch A, Shieh CH, van Rooijen N, van Calker D, Biber K. Mechanism of microglia neuroprotection: involvement of P2X7, TNFα, and valproic acid. Glia. 2016;64:76–89.
49. Pascual O, Ben Achour S, Rostaing P, Triller A, Bessis A. Microglia activation triggers astrocyte-mediated modulation of excitatory neurotransmission. Proc Natl Acad Sci U S A. 2012;109:E197–205.
50. Gao F, Liu Z, Ren W, Jiang W. Acute lipopolysaccharide exposure facilitates epileptiform activity via enhanced excitatory synaptic transmission and neuronal excitability in vitro. Neuropsychiatr Dis Treat. 2014;10:1489–95.
51. Igelhorst BA, Niederkinkhaus V, Karus C, Lange MD, Dietzel ID. Regulation of neuronal excitability by release of proteins from glial cells. Philos Trans R Soc Lond Ser B Biol Sci. 2015;370(1672).
52. Centonze D, Muzio L, Rossi S, Furlan R, Bernardi G, Martino G. The link between inflammation, synaptic transmission and neurodegeneration in multiple sclerosis. Cell Death Differ. 2010;17:1083–91.
53. Rossi S, Furlan R, De Chiara V, Motta C, Studer V, Mori F, Musella A, Bergami A, Muzio L, Bernardi G, Battistini L, Martino G, Centonze D. Interleukin-1β causes synaptic hyperexcitability in multiple sclerosis. Ann Neurol. 2012;71:76–83.
54. Rossi S, Muzio L, De Chiara V, Grasselli G, Musella A, Musumeci G, Mandolesi G, De Ceglia R, Maida S, Biffi E, Pedrocchi A, Menegon A, Bernardi G, Furlan R, Martino G, Centonze D. Impaired striatal GABA transmission in experimental autoimmune encephalomyelitis. Brain Behav Immun. 2011;25:947–56.
55. Zhou Y, Tang H, Liu J, Dong J, Xiong H. Chemokine CCL2 modulation of neuronal excitability and synaptic transmission in rat hippocampal slices. J Neurochem Volume. 2010;116:406–14.
56. Turrigiano G. Homeostatic synaptic plasticity: local and global mechanisms for stabilizing neuronal function. Cold Spring Harb Perspect Biol. 2012;4:a005736.
57. Balakrishnan V, Kuo SP, Roberts PD, Trussell LO. Slow glycinergic transmission mediated by transmitter pooling. Nat Neurosci. 2009;12:286–94.
58. Letournel-Boulland ML, Fages C, Rolland B, Tardy M. Lipopolysaccharides (LPS), up-regulate the IL-1-mRNA and down-regulate the glial fibrillary acidic protein (GFAP) and glutamine synthetase (GS)-mRNAs in astroglial primary cultures. Eur Cytokine Netw. 1994;5:51–6.
59. Kuhn SA, van Landeghem FK, Zacharias R, Färber K, Rappert A, Pavlovic S, Hoffmann A, Nolte C, Kettenmann H. Microglia express GABA(B) receptors to modulate interleukin release. Mol Cell Neurosci. 2004;25:312–22.
60. Pocock JM, Kettenmann H. Neurotransmitter receptors on microglia. Trends Neurosci. 2007;30:527–35.
61. Fogal B, Hewett SJ. Interleukin-1beta: a bridge between inflammation and excitotoxicity? J Neurochem. 2008;106:1–23.
62. Probert L. TNF and its receptors in the CNS: the essential, the desirable and the deleterious effects. Neuroscience. 2015;302:2–22.
63. Becher B, Tugues S, Greter M. GM-CSF: from growth factor to central mediator of tissue inflammation. Immunity. 2016;45:963–73.
64. Szepesi Z, Manouchehrian O, Bachiller S, Deierborg T. Bidirectional microglia-neuron communication in health and disease. Front Cell Neurosci. 2018;12:323.
65. Coull JAM. Trans-synaptic shift in anion gradient in spinal lamina I neurons as a mechanism of neuropathic pain. Nature. 2003;424:938–42.
66. Houston CM, Bright DP, Sivilotti LG, Beato M, Smart TG. Intracellular chloride ions regulate the time course of GABA-mediated inhibitory synaptic transmission. J Neurosci. 2009;29:10416–23.
67. Dunning DD, Hoover CL, Soltesz I, Smith MA, O'Dowd DK. GABA(A) receptor-mediated miniature postsynaptic currents and alpha-subunit expression in developing cortical neurons. J Neurophysiol. 1999;82:3286–97.
68. Hutcheon B, Morley P, Poulter MO. Developmental change in GABAA receptor desensitization kinetics and its role in synapse function in rat cortical neurons. J Physiol. 2000;522:3–17.
69. Dixon C, Sah P, Lynch JW, Keramidas A. GABAA receptor α and γ subunits shape synaptic currents via different mechanisms. J Biol Chem. 2014;289:5399–411.

Publisher's Note

2. Inflammatory threats modulate glial cells activity in organotypic spinal slices: the role of Connexin43 hemichannels in Ca^{2+} signaling

Inflammatory threats modulate glial cells activity in organotypic spinal slices: the role of Connexin43 hemichannels in Ca^{2+} signaling.

Giulia Panattoni[1], Roberta Amoriello[1,2], Clara Ballerini[2] and Laura Ballerini[1]

[1] International School for Advanced Studies (SISSA/ISAS), 34136 Trieste, Italy

[2] Dipartimento di Medicina Sperimentale e Clinica, University of Florence, 50139 Florence, Italy

*Corresponding authors: Laura Ballerini, International School for Advanced Studies (SISSA), 34136 Trieste, Italy Email: laura.ballerini@sissa.it ; Clara Ballerini: Dipartimento di Medicina Sperimentale e Clinica, University of Florence, 50139 Florence, Italy Email: clara.ballerini@unifi.it

Keywords

Pro-inflammatory cytokines, LPS, live imaging, neuroinflammation, gap junctions, hemichannels, spinal neurons, immune resident cells.

Abstract

Neuroinflammation is a characterizing trait of various central nervous system (CNS) pathologies, from neurodegenerative diseases to neuropsychiatric disorders. In the effort of dissecting the impact of immune status alterations on neural circuit function, we focused our study on the effects of local inflammation in a controlled micro-environment where neurons and neuroglial cells maintain their appropriate organization: the organotypic spinal cord slices. These cultures, developed from the spinal cord of mouse embryos, represent a complex *in vitro* model where sensory-motor cytoarchitecture, synaptic properties and spinal cord resident cells, are retained in a 3D fashion.

The model has been exploited to mainly investigate the astrocytes calcium signaling tuned by the diverse types of inflammation and the mechanisms which modulate the calcium release and its spreading in the inflamed environment. For the purpose, organotypic spinal cord slices are cultured for two or three weeks *in vitro* (WIV). Then, they are exposed for 6 hours to a cocktail of cytokines (CKs), composed by tumor necrosis factor alpha (TNF-α), interleukin-1 beta (IL-1 β) and granulocyte macrophage-colony stimulating factor (GM-CSF), or to lipopolysaccharide (LPS). By live calcium imaging, we document an increase in the occurrence of calcium oscillations displayed by the astrocytes located in the ventral horn. By several pharmacological treatments, we demonstrated that the connexin 43 (Cx43) hemichannels have a pivotal role in the calcium intercellular communication, while the Cx43 gap junction communication is reduced by the inflammatory treatments.

Introduction

Neuroinflammation is a characterizing feature occurring in and contributing to CNS pathologies such as amyotrophic lateral sclerosis (ALS) and multiple sclerosis (MS)[1,2]. In the CNS, successful inflammatory responses exert a protective homeostatic action, on the contrary, protracted tissue reactivity sustains unregulated cytokine/chemokine release and chronic inflammation, which has been proposed as a major cause of disease progression[3]. In the last decade, several studies documented, associated to neuroinflammatory processes, the emergence of synaptic dysfunction, i.e. synaptopathy[4,5]. Indeed, the emergent activity of neural circuits may be altered acutely and chronically by inflammatory milieus activating intricate signaling pathways, orchestrated by various cell phenotypes, ultimately responsible for intercellular communication and contributing to the propagation of the inflammatory damage in the CNS. In this picture, astrocytes, the key cellular partners to neurons, play both beneficial roles, such as recovery of extracellular ionic homeostasis limiting inflammation[6] and deleterious ones, such as hypertrophy with increased astrogliosis[7,8]. Knowing how astrocytes perform such signalling might allow to selectively promote beneficial functions and inhibit adverse ones in diseased CNS.

We recently investigated the effects on spinal synaptic outputs of different inflammatory threats, focusing on the consequences of local inflammation in a controlled micro-environment: the organotypic slice cultures developed from the embryonic mouse spinal cord explants[9–11]. Core features of this *in vitro* model are the 3D organization of spinal cord resident cells and the preserved sensory-motor cytoarchitecture[11–13]. This model allows the study of spinal cord

alterations induced by inflammation, addressing the role of resident cells: neuronal and not neuronal populations. By the use of spinal cord explant cultures, we reported the ability of two diverse immune conditions to improve network excitability by specific synaptic mechanisms[11]. In the present study, we exploit spinal slice cultures to explore astrocyte recruitment upon exposure (6 hours) to pro-inflammatory CKs cocktail (TNF-α, IL-1β and GM-CSF[4,14,15]) or to LPS, a potent trigger of cytokine release[16,17] largely adopted to elucidate the mechanisms of brain inflammation. In our previous experiments, CKs and LPS treatments mediated an increase in cytokines and chemokines production, although differently regulating the morphology of resident neuroglia, suggestive of diverse activation states[11]. In reactive tissues, astrocytes can be neuroprotective or neurotoxic, depending on the context, and Ca^{2+} signaling is a key process in these roles[18]. Reactive astrocytes are known to increase dynamic Ca^{2+} signals, shown to be crucial to intracellular signaling and intercellular communication[19]. Such calcium dynamics was reported to vary in distinct pathological models and regions, indicating that aberrant Ca^{2+} signals may depend on the context conditions[18].

To examine astrocytes responses to inflammation, we monitor live Ca^{2+} signals within the spinal cord cultured microcircuits. We focus on astrocytes located in the ventral horn within pre-motor networks and we compared their calcium signaling when activated by CKs or LPS. We document the timing and appearance of intracellular calcium oscillations upon CKs or LPS exposure, such episodes are generated by each treated astrocyte independently from the ongoing synaptic activity. We further show, by pharmacological treatments, that CKs and LPS induced calcium release from endoplasmic reticulum, mitochondria and that astrocyte reactivity is tuned by gap junctions (GJs) and hemichannels (HCs) activation.

Results

Sulforhodamine-positive glial cells display slow spontaneous Ca^{2+} activity

The presence of GFAP-positive astrocytes has long been described in cultured spinal explants ventral horns[11–13], as confirmed by Fig. 1A, where numerous astrocytes are shown within the ventral area of a spinal organotypic culture after 2 WIV. We labeled by fluorescent dye Fluo-4 AM cells in organotypic spinal cord and dorsal root ganglia (DRG) co-cultures to simultaneously visualize within the sampled area (visual field 330 × 330 μm^2, Fig. 1B) of the ventral horn pre-motor circuit[11], neuronal and glial cells calcium signaling. To reliably identify astrocytes for physiological measurements of calcium dynamics, we took advantage of a widely used astrocyte marker, sulforhodamine (SR101; 1 μM, Fig. 1C)[20–22] enabling the detection of

living astrocytes during *ex vivo* calcium imaging experiments, in combination with the calcium dye Fluo-4 AM. As shown in Fig. 1C (top panels) and in the corresponding sample tracings of spontaneous fluorescent recordings in Fig. 1D (top), the imaging of visually identified small neurons close to the ventral fissure[23] resulted in SR101-negative cells highly active in control saline solution, with fast (4.12 ± 0.63 s; n = 14 cells) calcium episodes which were silenced upon application of tetrodotoxin (TTX, 1 μM; fast voltage-gated sodium channel blocker to remove action potentials[23]), confirming their neuronal identity. Differently, closely located SR101-positive cells (Fig. 1C, bottom panels) were spontaneously less active (Fig. 1D, bottom tracings) and typically displayed slow (21.6 ± 1.55 s; n = 42 cells) and rare episodes of spontaneous activity, which were resistant to TTX application and allowed identifying glial cells calcium dynamics. In these conditions, we never observed short-lasting Ca^{2+} transients (less than 8 s)[24,25], altogether these observations suggested that these active cells were likely to be non-neuronal. In subsequent experiments we used the spatial location, the slow kinetic and the TTX resistance to identify glial calcium signaling.

CKs and LPS treatments affect Ca^{2+} transients in organotypic spinal slices

To investigate the ability of inflammation to impact calcium dynamics in glial cells, organotypic spinal explants (2-3 WIV) were treated (6H, see Methods) with two danger signals triggering different, although well characterized, inflammatory states in these cultures[2,3]: a pro-inflammatory cocktail of CK (10 ng/mL; TNF-α, IL-1 β and GM-CSF)[13,11] and the LPS (1 μg/mL)[11,17] stimuli. First, we monitored ventral neurons calcium signaling and we compared Control recordings of fluorescent tracings with the activity from neurons after CKs or LPS treatments. In the supplementary Fig. S1A, snapshots of neurons stained with membrane permeable dye Fluo4-AM are visualized in all conditions. Neurons, in CKs and LPS treated slices (n = 9, 7 respectively; supplementary Fig. S1B, sample fluorescent tracings) displayed a significant increase in the frequency of spontaneous calcium oscillations, when compared to Control (n = 7; 0.24 ± 0.014 Hz Control, 0.31 ± 0.023 Hz CKs and 0.39 ± 0.03 Hz LPS; ***P < 0.001 Control vs LPS 6H and **P = 0.0052 Control vs CKs, Kruskal-Wallis test; box plot in Fig. S1C). This boost in activity was accompanied by increased synchronization, measured among simultaneously recorded cells (see Methods and supplementary Fig. S2A-B). Such an enhanced calcium dynamics probably reflect the high degree of spontaneous synaptic activity typical of spinal cord preparations when inflammatory states are activated[2,3] and was not further examined. Calcium signaling due to synaptic activity was removed by TTX application, as shown in Fig. 1D, and we next explored glial cells activity and in particular how astrocytes

respond to the localized inflammation, since it is known that astrocytes as well can display spontaneous calcium oscillations[26–28].

Calcium dynamics in glial cells was measured always in the presence of TTX and in Control slices (n = 8) was characterized by the sporadic (on average 2.1 ± 0.29 active cells per recorded field) appearance of slow oscillations, quantified by inter events intervals (IEIs) of 51.3 ± 5.4 s (Fig. 2 A-D). Upon CKs (n = 7) and LPS (n = 7) treatments, an increased number of active cells per recorded field was detected in respect to Control (4.5 ± 0.56 in CKs and 5.8 ± 1.16 in LPS; $^{**}P = 0.003$ Control vs LPS and $^{*}P = 0.04$ Control vs CKs, one-way ANOVA test; bar plot in Fig. 2C) displaying calcium oscillations characterized by a significant reduction in the IEIs when compared to the Control ones (36.5 ± 4.3 s in CKs and 31.1 ± 2.5 s in LPS; $^{***}P < 0.001$ Control vs LPS 6H and $^{**}P = 0.005$ Control vs CKs, Kruskal-Wallis test; cumulative probability plot and box plot in Fig. 2 D). Glial cell calcium oscillations were also analyzed for their synchronicity among simultaneously recorded cells. To this aim we measured in each slice (n = 3, Control CKs and LPS) the activity of distant (see Methods and supplementary Fig.S2) pairs of active glial cells (n = 6, 20 and 22 pairs in Control, CKs and LPS). Interestingly, increase active cells during inflammatory threats, regardless the triggering by CKs or LPS, were significantly less synchronized when compared to Control ones (0.04483 ± 0.01662 pair p-value Control; 0.2139 ± 0.02114 pair p-value CKs 6H; 0.3310 ± 0.01788 pair p-value LPS 6H, $^{***}P < 0.001$ Control vs LPS and $^{**}P = 0.0025$ Control vs CKs, one-way ANOVA test; $\chi_2 = 7.73$, $^{*}P = 0.02$, Fisher's exact test; supplementary Fig. S2C-D). It is well reported that GJs are responsible for the synchronization of glial calcium activity[29–31] and that during diverse pathological conditions the calcium events are less synchronized than in physiological states[32].

Intracellular stores and gap-junction dependence of glial calcium signals

In order to explore the nature of the observed oscillatory patterns, in Control as well as in CKs and LPS, we investigated the dependence on intracellular calcium stores of these activities. We assessed the contribution of internal Ca^{2+} sources from the mitochondria and the endoplasmic reticulum (sketched in Fig. 3A). To explore the mitochondrial contribution, we used the protonophore carbonyl cyanide 3-chlorophenylhydrazone (CCCP, 2 μM)[5] to dissipate the proton gradient across the inner mitochondrial membrane and disrupt the Ca^{2+} uptake. After CCCP application, Ca^{2+} transients completely disappeared, this response did not differ among the three experimental conditions (n = 8, 7 and 5, Control, CKs and LPS, respectively; Fig. 3B). Next, we explored the contribution of intracellular Ca^{2+} source, namely the endoplasmic

reticulum. Application of the non-competitive inhibitor of the sarco/endoplasmic reticulum Ca^{2+} ATPase (SERCA) thapsigargin (TG, 5 μM) blocked all calcium transients in the three conditions (n = 8, 9 and 5 slices, Control, CKs and LPS, respectively; Fig. 3C). These results suggest that spontaneous intracellular Ca^{2+} transients in single astrocytes in Control as well as in neuroinflammed tissues strongly rely on intracellular calcium sources.

In tissue cultures, Ca^{2+} events can propagate among a network of astrocytes via GJs[33], allowing synchronization of the calcium activity. GJs are formed by the docking of two HCs and unapposed HCs, not assembled into GJs and usually closed, are present in the plasma membrane. Unapposed HCs may be activated in response to inflammation stimuli[34], thereby allowing ionic and molecular exchange between the intra- and extracellular environment. In the absence of neurotransmitter activation, cultured explant did not show propagated calcium signals among astrocytes, however astroglial cells usually express connexins that support long-range communication. GJs and connexins are also known to have an enhanced turnover in the inflamed tissues[30,31,35].

We used carbenoxolone (CBX 200 μM, 10 min), a well-known GJs uncoupler[23,36,37] and a blocker of active HCs[38] to test the functional role of GJs and HCs in the observed slow kinetic calcium events. In virtually all recorded Control slices (8 out of 9 slices) CBX completely silenced glial cells displaying spontaneous calcium activity. Similarly, in CKs and LPS treated slices (n = 6 and 9, respectively) the presence of active glial cells was strongly reduced (activity was abolished in 3 slices out of 6 and in 3 slices out of 9, CKs and LPS respectively) after CBX (**P = 0.008 CKs vs CKs +CBX and **P = 0.005 LPS vs LPS CBX, one-way ANOVA test). These results are summarized in Fig. 4A (bar plot, left). In Fig. 4A (right), the box plot shows the calcium episodes IEIs, prior and after CBX, in CKs and LPS treated slices which retained calcium activity in the presence of this blocker (35.7 ± 1.9 and 30.1 ± 1.8, respectively CKs and LPS and 43.1 ± 7.9 and 56 ± 8.2, respectively CKs+CBX and LPS+CBX; **P = 0.008 LPS vs LPS+CBX, Kruskal-Wallis test). The relatively higher presence of active cells after CBX in CKs and LPS slices suggests that, in these cells, GJs contribute to calcium dynamics, but that this is not the only mechanism involved[39,40]. Since both GJs and HCs in astrocytes in culture are mainly composed by Cx43 protein[16] to address potential changes in the expression of Cx43 we used immunoblotting analysis under the three different experimental conditions. The western blot (WB) in Fig. 4B shows the protein bands of the three experimental conditions (n = 8, 7 and 8 slices, Control, CKs and LPS, respectively), we observed that CKs and LPS treatments significantly (**P = 0.004 Control vs LPS and *P = 0.03 Control vs CKs, one-way ANOVA test; bar plot in Fig. 4 B) reduced the expression of Cx43, in respect to Control, in

agreement with previous works[41-35]. It has been shown that proinflammatory CKs released by activated microglia, inhibit GJs mediated by Cx43, whereas opening HCs, a pathway enabling release of active molecules[41]. In the presence of reduced Cx43 expression, CKs and LPS might still enhance calcium activity in astrocytes by the opening of HCs.

We used the fluorescent dye ethidium bromide (EtBr), a tool adopted to investigate HCs and GJs permeability[37,41,42], to assess the presence of changes in HC and GJs activity upon CKs and LPS exposures. Control and treated slices (n = 5, 8, 7, control, CKs and LPS, respectively) were incubated (30 min) with EtBr (5 μM), as shown in Fig. 4C and quantified in the bar plot (normalized to GFAP-positive cells: 0.41 ± 0.03 Control; 0.77 ± 0.02 CKs; 0.76 ± 0.04 LPS; *** $P < 0.0001$, one-way ANOVA test). When Control and treated slices were pre-incubated (30 min; n = 5, 9, 5, control, CKs and LPS, respectively) with CBX, the dye uptake in treated slices was significantly reduced (0.33 ± 0.03 Control+CBX; 0.36 ± 0.04 CKs+CBX, 0.36 ± 0.05 LPS+CBX).

Since the pharmacology and dynamics of live calcium imaging together with the EtBr uptake and WB analysis apparently supported an increase in the permeability of Cx43 HCs in parallel with GJs inhibition, upon CKs and LPS treatments, we decided to gain more insights on the role of activated HCs in astrocytes calcium dynamics in Control and treated slices (n = 3 all groups) by preincubating with Gap27 (500 μM; 30 min), a Cx43 peptide blocker[41] known to inhibit HCs opening triggered by chemical or electrical stimuli[43]. In the presence of this blocker, live imaging of ventral neurons indicated that, although reduced when compared to that recorded in the absence of Gap27, neuronal calcium activity was still augmented by inflammatory treatments (supplementary Fig. S3).

In TTX, upon Gap27 treatment, we did not observe any residual calcium activity in astrocytes in untreated or treated cultures (Fig. 5A). Thus, activated HCs are instrumental in astrocyte signaling and enhanced activity upon inflammation, and such astrocyte activity is only partially contributing to the increase in neuronal calcium dynamics due to the inflammatory threats.

Discussion

In the current study we strengthen the role of active HCs in the generation of inflammation-induced calcium dynamics in resident spinal cord astrocytes. We target spinal tissue reactivity, experimentally induced by pro-inflammatory treatments and involving local neuroglia. We imaged, in the spinal organotypic cultures, calcium signaling from glial cells located close to ventral interneurons, identified upon specific labeling[20], displaying calcium episodes resistant

to synaptic activity removal and characterized by low pace kinetics[44]. We adopted the organotypic slice model, a well characterized cell system[11–13,45], where the 3D-architecture of specific resident cells, neuronal and non-neuronal, can be directly investigated after pro-inflammatory treatments[11,13]. We ignite inflammatory responses by adopting two different acute (6 hours) stresses known to alter synaptic transmission, to trigger different pro- and anti-inflammatory cytokine and chemokines network and to induce different changes in the morphology of GFAP-positive astrocytes and microglia, suggestive of different states of activation[11,13]. LPS, a toll- like receptors (TLR) agonist, in particular of TLR4, expressed on the microglia surface, that influence cytokine production and immune cell function mimicking systemic inflammation[11,13,17] and a cytokines cocktail know to exert pro-inflammatory effects in the CNS of multiple sclerosis animal models[4,11,13–15]. Despite the induction of alternative activation mechanisms by CKs and LPS[11,13], these two functional conditions similarly enhanced both the number of active glial cells and their oscillatory activity, within the neuronal circuit. We focus on aberrant calcium signals when recorded in the absence of neuronal synaptic activity and restricted to a precise anatomical area, since to understand the functional implications of such signaling requires considering the heterogeneity of reactive cells and of CNS circuits. Apparently, although representing distinct etiologies in the pathology of neuroinflammation, the used danger signals affect glia communication similarly and reactive astrocytes rapidly increase their calcium signals, in frequency and in terms of number of active cells, suggesting that both CKs and LPS promote a similar downstream signaling to translate inflammation into functional changes. In both conditions, aberrant calcium signals occurred spontaneously and relay on Ca^{2+} release from the mitochondria and from the endoplasmic reticulum. In both CKs and LPS treated spinal slices, reactive astrocytes are less synchronized, and indeed WB analysis confirms a reduction in Cx43 protein detection. However, CBX drastically reduces the amounts of active cells in a large number of slices. Our results support the suggestion that Cx43 functions are regulated in an opposite manner by inflammatory stresses, namely with a reduction in GJs channel formation and an increase in permeable HCs unapposed channels[41]. The increase cellular uptake of the non-fluorescent permeability tracer EtBr in CKs and LPS is reduced by CBX applications, thus indicating an increased activity of HC upon neuroinflammatory stresses. Indeed, cell death and plasma membrane rupture could influence this dye distribution, however our GFAP counterstaining confirm the presence of intact astrocytes, in addition we have previously shown that both treatments, despite inducing a clear inflammatory reaction, did not affect cell viability[11,13]. In this scenario, only prolonged CBX treatments enable the blockage of EtBr influx. HCs role as membrane pathways for

signaling mechanisms and diffusion of small molecules or ions (including Ca^{2+}) can be regulated by pro-inflammatory CKs[41,46]. HCs might not be the exclusive membrane pathway contributing to the calcium response, however the use of a mimetic peptide which successfully inhibits abnormal opening of Cx43 HCs[43,47] and displays a better selectivity than general inhibitors such as CBX[48] completely removed astrocyte calcium activity, suggesting that HCs opening is instrumental in such responses or is crucially recruiting other channels.

Calcium-dependent glia signaling is a highly investigated and well characterized feature of astrocytes, nonetheless its key mechanisms and contribution to inflammatory pathology are still under debate[49,50]. The finding that in spinal cord circuits local reactive astrocytes display similar calcium signals, but diverse hypertrophy[11,13] may provide insight into the role of these functional changes. In both the pathological conditions, astrocytes Cx43 HC permeability, key to intracellular signaling including calcium oscillations[51,52], is enhanced while apparently GJ intercellular trafficking is restricted.

Conclusions

In this work we confirmed that the organotypic slices system represents an excellent setting, thanks to which it is possible to dissect how the inflammatory environment interferes with the spinal circuits function, due to the easy accessibility of the resident cells and to the long lasting of the cultures. In fact, we exploited these cultures to investigate whole network changes of a precise region of interest under pathological conditions and we were able to mimic two different kind of inflammation. The main finding of the current work is that local inflammation in organotypic spinal slices, induced by CKs and LPS, was able to regulate the astrocytes function, acting at the calcium signaling level, modulating the permeability of the HCs and altering the GJs communication. In conclusion, expanding our knowledge on the interplay between astrocytes and neurons in the spinal circuits and understanding the role of the occurring Ca^{2+} oscillations during pathological conditions represent the starting point for developing new therapies and strategies, essential for investigating the spinal neurodegenerative disorders.

Materials and Methods

Organotypic spinal cord cultures and pro-inflammatory treatments

All experiments were performed in accordance with the EU guidelines (2010/63/UE) and Italian law (Decree 26/14) and were approved by the local authority veterinary service and by our institution (SISSA) ethical committee. All efforts were made to minimize animal suffering and to reduce the number of animals used. Animal use was approved by the Italian Ministry of Health (no. 22DABNQYA), in agreement with the EU Recommendation 2007/526/CE. Organotypic spinal cord and DRG slices were obtained from mouse embryos (C57BL/6J) at E12-13 of gestation as previously described[12,13,11]. Briefly, pregnant mice were sacrificed by CO_2 overdose and fetuses delivered by caesarean section. Isolated fetuses were decapitated and their backs were isolated from low thoracic and high lumbar regions and transversely sliced (275 μm) with a tissue chopper. After dissecting the spinal cord slices and the DRG from the surrounding tissue, slices were embedded into a thick matrix obtained by chicken plasma (Sigma) and thrombin (Sigma) clot. Slices were cultured in plastic tubes with 1 mL medium. The tubes were kept in a roller drum rotating 120 times per hour in an incubator at 37 °C in the presence of humidified atmosphere, with 5 % CO_2. Experiments were performed on spinal cultures at 2-3 weeks in vitro (WIV) treated for 6 hours with two different inflammatory paradigms[11,13]: i) a cocktail of the mouse recombinant cytokines (10 ng/mL each) TNF-α (R&D Systems, #210-TA/CF), IL-1β (R&D Systems, #M15330), and granulocyte-macrophage colony stimulating factor (GM-CSF; R&D Systems, #P04141)[13,11,53]; ii) lipopolysaccharide (LPS; 1 μg/mL, Sigma, O55:B5)[11]. CKs or LPS were removed after the incubation times, prior to live cell imaging recordings, immunoblotting analysis and immunostaining analysis.

Lentiviruses preparations and organotypic slices infection

The lentiviruses were generated and titrated as previously described[54]. Lentiviral vectors employed in this study include: LV_pGfap-rtTA2S-M2 (LV-Gfap) [built by transferring the pGfap-containing, MluI/BamHI 1.2 kb fragment taken from pAAV-GFAP-hChR2(H134R)-EYFP plasmid (Addgene #27054) into MluI/BamHI-cut LV_pTa1-rtTA/M2[54], in place of pTa1, upstream of rtTAM2-cds] and LV_TREt-mCherry. The 8-14 DIV slices were infected with 5 μL of the plasmids, whose titres were 4×10^6 and 1×10^7 respectively. 2 μg/mL doxycycline were administered every two days (TetON system).

Live cell Ca^{2+} Imaging

Organotypic spinal cord cultures were loaded with 4 µM Fluo-4 AM (Molecular Probes); 11.6 µL of DMSO (Sigma-Aldrich) were added to the stock 50 µg of the dye and cultures were incubated with a final concentration of 4 µM for 1h in the roller drum at 37 °C, 5 % CO_2. After dye loading, a de-esterification period followed, cultures were maintained in extracellular saline solution, also used as recording solution, composed of (mM): 150 NaCl, 4 KCl, 1 $MgCl_2$, 2 $CaCl_2$, 10 HEPES, 10 glucose (pH adjusted to 7.35 with 2 M NaOH), in the same incubator for 30 min. The samples were mounted in a recording chamber placed on an inverted microscope (Nikon Eclipse Ti-U), where they were continuously perfused (5 mL/minute flow rate) at room temperature (RT) with the recording saline solution. The dye was excited at 488 nm with a mercury lamp and the emission was detected at 520 nm. Neurons and glial cells (the focus was set and maintained in a slice layer where both neurons and glial cells could be detected) at the premotor region in the ventral zone of the slice were observed with a 40 × objective (PlanFluor, 0.60 NA)[23]. Images were constantly acquired at 6.67 fps every 150 ms using an ORCA-Flash4.0 V2 sCMOS camera (Hamamatsu) and the set-up was controlled by HCImage Live software. Basal activity was recorded for 10 minutes in the presence of saline solution in order to check the spontaneous activity of the network; subsequently in the presence of different drugs, diluted in recording solution at the following concentrations (in µM): 1 tetrodotoxin (TTX, fast voltage-gated Na^+ channel blocker, Latoxan), 2 carbonyl cyanide 3-chlorophenylhydrazone (CCCP, mitochondrial protonophore, Sigma), 5 thapsigargin (TG, SERCA inhibitor, Sigma), 200 carbenoxolone (CBX, gap junction uncoupler, Sigma). For the Gap27 experiments, the Connexin43 mimetic Gap27 (500 µM; GeneCust) was dissolved in the saline solution and incubated for 30 minutes prior to recordings. The recorded images were analyzed selecting ROIs around dye positive cells with Fiji software. The corresponding traces were extracted with Clampfit software (pClamp suite, 10.6 version; Axon Instruments) and analyzed off-line. Ca^{2+} transients were expressed as $\Delta F/F_0$, where ΔF is the fluorescence rise over baseline, and F_0 is the baseline fluorescence level, calculated as:

$$100 \times \frac{F - F_0}{F_0}$$

(F, fluorescence value; F_0, baseline fluorescence). F_0 was calculated as the median of the frame fluorescence values.

Sulforhodamine 101 (SR101) staining protocol

In order to confirm that the Ca^{2+} activity detected in the presence of TTX was the one of glial cells and in particular, of astrocytes, the slices were incubated for 20 minutes in the recording solution containing 1 μM SR101 at 37 °C, after the incubation with the calcium dye. The slices were then washed with the recording solution for 10 minutes at 37 °C, to allow the washout of excess dye from the extracellular space. The dye was excited at 594 nm with a mercury lamp.

Western blotting analysis

After corresponding treatments, organotypic spinal cultures (4 slices per condition) were scraped in 200 μL of Lysis buffer (10 mM Tris-HCl, 150 mM NaCl, 0.5 % NP40, 0.5 % DOC, protease inhibitor cocktail). Samples were triturated using 200-μL pipette and 1-mL syringe pass tissue suspension through a 26-gauge needle until all tissue were lysed. Subsequently samples were subjected 3 freeze-thaw cycles of 1 minute each at – 80 °C, sonicated at 50 % amplitude for 30 seconds and centrifuged at 100 × g at 4 °C for 5 minutes. Proteins concentration of the lysate were determined using the bicinchoninic acid assay (Thermofisher Scientific). Samples were prepared adding 2 × Leammli buffer (10 % SDS, 20 % glycerol, 125 mM Tris-HCl, 0.01 % bromophenol blue, 1 M DTT) to 20 μg of proteins and denatured boiling at 100 °C for 5 minutes. SDS-PAGE gels were prepared in relation to the molecular weight of the protein of interest (12 % polyacrylamide separating gel). Samples were run at 120 V at room temperature and transferred onto Immun-Blot PVDF (Polyvinylidene difluoride) membrane (Millipore) by electroblotting at 100 V for 1 hour and 30 minutes at 4 °C. Membranes were blocked in 5 % BSA in TBS-T for 1 hour and incubated overnight at 4 °C with anti-Cx43 (rabbit monoclonal, 1:8000, Abcam). The day after, the primary antibody was recovered, the washed membranes in TBS-T were incubated with secondary antibody (Alexa goat anti-rabbit horseradish peroxidase-conjugated, 1:1000, Invitrogen) at RT for 1 hour and washed again. As housekeeping protein normalizer was used anti-β-Tubulin III (mouse monoclonal, 1:1000, Sigma) conjugated with the proper secondary antibody (Alexa goat anti-mouse horseradish peroxidase-conjugated, 1:1000, Invitrogen) at RT for 1 hour. Subsequently, the membranes were washed with TBS-T and developed by enhanced chemiluminescence (ECL Western Blotting Substrate, Thermofisher) using the UViTEC Cambridge system. The quantified band intensity of three replicates were analyzed using Uviband Analysis, Image quantification Software. Ordinary one-way ANOVA and Tukey Multiple comparisons test was performed in order to examine change in protein expression. Results were plotted as Mean ± S.E.M.

Ethidium bromide uptake and immunofluorescence analysis

For dye uptake experiments, cultures were exposed to 5 μM EtBr (Sigma) for 10 min at 37 °C. In order to investigate the contribution of GJs and HCs to the dye uptake, an independent experiment was performed where slices were incubated with CBX for 10-15 min prior to EtBr+CBX for additional 30 min. EtBr is permeable through membrane but can transit through HCs and becomes more fluorescent after binding to DNA. After 30 min exposure to EtBr, the slices were washed in extracellular saline solution for 15 minutes, fixed in 4 % formaldehyde (prepared from fresh paraformaldehyde; PFA, Sigma) in PBS 1 × for 1 hour at RT and washed in PBS. Free aldehyde groups were quenched in 0.1 M glycine in PBS for 10 minutes. Slices were permeabilized and blocked in PBS 1 ×, 10 % FBS (Sigma), 5 % BSA (Sigma), and 0.3 % Triton-X 100 (Sigma) at RT for 1 hour, and then incubated over night at 4 °C with anti-GFAP (mouse monoclonal, 1:200, Sigma) primary antibody. Subsequently, the slices were PBS-washed and incubated with secondary antibody Alexa 488 goat anti-mouse (1:500, Invitrogen) and DAPI (1:500, Thermo Fisher Scientific) diluted in blocking solution for 2h at RT, in the dark. Samples were mounted on glass coverslips using Fluoromount-G aqueous mounting medium (Thermo Fisher Scientific). Images were acquired using Nikon C2 Confocal microscopes with Ar/Kr, He/NE, and UV laser with 40 × oil objectives (1.4 N.A.) using oil mounting medium (1.515 refractive index). Confocal sections were acquired every 0.5 μm up to a total *Z*-stack thickness of 20 μm in sequential mode with lasers (488 nm for GFAP and 561 nm for EtBr). For each condition, we performed 3 independent cultures (3 slices/series), and from each slice ≥ 3 fields were randomly acquired. Offline analysis of the image Z-stack was performed using the Volocity3D Image Analysis Software. The "$GFAP^+$ objects" and the "$EtBr^+$ objects" were determined after thresholding images. With the Volocity tool "Intersect objects" we determined the number of "$EtBr^+$ astrocytes". EtBr uptake was expressed as the ratio between the "$EtBr^+$ astrocytes" over the total number of astrocytes ("$GFAP^+$ objects").

Statistical analysis and analysis of synchronization

All values from samples subjected to the same experimental protocols were pooled together and results are presented as mean ± S.E.M., if not stated otherwise. A statistically significant difference between three data sets was assessed by one-way ANOVA for parametric data or Kruskal-Wallis test for non-parametric ones. In addition, differences in the relative cumulative frequency distribution were obtained using the paired Kolmogorov–Smirnov test. Statistical significance was determined at $p < 0.05$.

In box-plots, the thick horizontal bar indicates the median value, the cross indicates the mean value, the boxed area extends from the 25th to 75th percentiles while whiskers from the 5th to the 95th percentiles.

The correlation between the oscillatory activities of two neighbor cells in the same slice was assessed by cross correlation analysis. The synchronization analysis was based on a bootstrapping method modified from Usmani et al.[55]. With this analysis, 200.000 - time windows are generated from each pair of traces and used to obtain a "real CCF (cross-correlation factor)" distribution with its mean/median, then compared with the distribution of "randomly generated CCFs" obtained by shuffling the 200.000 - time windows. The extent of the area of the "random CCFs" distribution that exceeded the mean/median of the "real CCFs" allowed the calculation of a p-value. Significantly (*$p < 0.05$) correlated pairs were considered synchronized and their count over the total number of cell pairs analyzed was plotted as percentage of correlated pairs. The distribution of the *p*-values was also plotted. For estimating significantly synchronous slices in the three groups, we performed a homogeneity test with the Fisher's exact test.

More in detail, we measured three slices per experimental condition and we obtained the measurements from non-overlapping neurons or glial cells. Here, we found that paired neurons (n = 135, 135 and 156 pairs in Control, CKs and LPS) in all the three different experimental conditions are synchronized (0.004 ± 0.001 pair *p*-value Control; 0.001 ± 0.0002 pair *p*-value CKs 6H; 0.001 ± 0.0002 pair *p*-value LPS 6H, Kruskal-Wallis test and Fisher's exact test; S2 B upper and below), with no significant differences among the groups. Glial cells analysis is reported in the Results.

Abbreviations

ALS: amyotrophic lateral sclerosis;

CBX: carbenoxolone;

CCCP: 2 carbonyl cyanide 3-chlorophenylhydrazone;

CCF: cross correlation coefficient.

CKs: cytokines;

CNS: central nervous system;

Cx43: connexin 43;

DRG: dorsal root ganglia;

ER: endoplasmic reticulum;

EtBr: ethidium bromide;

GM-CSF: granulocyte-macrophage colony-stimulating factor;

GJs: gap junctions;

HCs: hemichannels;

IL-1β: interleukin 1 beta;

LPS: lipopolysaccharide;

MS: multiple sclerosis;

RT: room temperature;

SERCA: sarco-Endoplasmic Reticulum

SR101: sulforhodamine 101;

TG: tapsigargin;

TLR: toll-like receptor;

TNF-α: tumor necrosis factor alpha;

TTX: tetrodotoxin;

WIV: weeks *in vitro*;

WB: western blot;

LV-Gfap: LV_pGfap-rtTA2S-M2.

Ethics approval

All experiments were performed in accordance with the EU guidelines (2010/63/UE) and Italian law (Decree 26/14) and were approved by the local authority veterinary service and by our institution (SISSA) ethical committee. All efforts were made to minimize animal suffering and to reduce the number of animals used. Animal use was approved by the Italian Ministry of Health (no. 22DABNQYA), in agreement with the EU Recommendation 2007/526/CE.

Availability of data and material

The datasets supporting the conclusion of this article are included within the article (and its additional files). The datasets generated and/or analysed during the current study are stored in a public repository and are available from the corresponding author on reasonable request.

Competing interests

The authors declare that they have no competing interests.

Funding

We acknowledge financial support from the European Union's Horizon 2020 research and innovation program under grant agreements no. 785219 and no. 881603 Graphene Flagship.

Authors' contributions

G.P. performed cell biology, live imaging, and immunofluorescence experiments and analysis; R.A. performed the Milliplex experiments and analysis. L.B. and C.B. conceived the study, the experimental design and wrote the manuscript.

Acknowledgements

The authors would like to thank M. Grandolfo for providing technical support with immunofluorescence labelling, confocal microscopy and image analysis and M. Santo for assistance in lentivirus preparation and infections.

References

1. Kempuraj, D. *et al.* Neuroinflammation Induces Neurodegeneration. *J. Neurol. Neurosurg. spine* **1**, 1–15 (2016).
2. Puentes, F., Malaspina, A., Van Noort, J. M. & Amor, S. Non-neuronal cells in ALS: Role of glial, immune cells and blood-CNS barriers. *Brain Pathol.* **26**, 248–257 (2016).
3. Glass, C. K., Saijo, K., Winner, B., Marchetto, M. C. & Gage, H. Mechanisms Underlying Inflammation in Neurodegeneration. *Nih* **140**, 918–934 (2010).
4. Centonze, D. *et al.* Inflammation triggers synaptic alteration and degeneration in experimental autoimmune encephalomyelitis. *J. Neurosci.* **29**, 3442–3452 (2009).
5. Mandolesi, G. *et al.* Synaptopathy connects inflammation and neurodegeneration in multiple sclerosis. *Nat. Rev. Neurol.* **11**, 711–724 (2015).
6. Mader, S. & Brimberg, L. Aquaporin-4 Water Channel in the Brain and Its Implication for Health and Disease. *Cells* **8**, 90 (2019).
7. Farina, C., Aloisi, F. & Meinl, E. Astrocytes are active players in cerebral innate immunity. *Trends Immunol.* **28**, 138–145 (2007).
8. Sofroniew, M. V. Molecular dissection of reactive astrogliosis and glial scar formation. *Trends in Neurosciences* (2009) doi:10.1016/j.tins.2009.08.002.
9. Gähwiler, B. H. Organotypic monolayer cultures of nervous tissue. *J. Neurosci. Methods* **4**, 329–342 (1981).
10. Gähwiler, B. H., Capogna, M., Debanne, D., McKinney, R. A. & Thompson, S. M. Organotypic slice cultures: a technique has come of age. *Trends Neurosci.* **20**, 471–477 (1997).
11. Giacco, V. *et al.* Cytokine inflammatory threat, but not LPS one, shortens GABAergic synaptic currents in the mouse spinal cord organotypic cultures. *J. Neuroinflammation* **16**, (2019).
12. Avossa, D., Rosato-Siri, M. D., Mazzarol, F. & Ballerini, L. Spinal circuits formation: A study of developmentally regulated markers in organotypic cultures of embryonic

mouse spinal cord. *Neuroscience* **122**, 391–405 (2003).

13. Medelin, M. *et al.* Bridging pro-inflammatory signals, synaptic transmission and protection in spinal explants in vitro. *Mol. Brain* **11**, 1–14 (2018).

14. Pascual, O., Achour, S. Ben, Rostaing, P., Triller, A. & Bessis, A. Microglia activation triggers astrocyte-mediated modulation of excitatory neurotransmission. *Proc. Natl. Acad. Sci. U. S. A.* **109**, (2012).

15. Rossi, S. *et al.* Interleukin-1β causes synaptic hyperexcitability in multiple sclerosis. *Ann. Neurol.* **71**, 76–83 (2012).

16. Vereker, E., Campbell, V., Roche, E., McEntee, E. & Lynch, M. A. Lipopolysaccharide inhibits long-term potentiation in the rat dentate gyrus by activating caspase-1. *J. Biol. Chem.* **275**, 26252–8 (2000).

17. Li, X. *et al.* Phosphoinositide 3 Kinase Mediates Toll-Like Receptor 4-Induced Activation of NF- κ B in Endothelial Cells. **71**, 4414–4420 (2003).

18. Shigetomi, E., Saito, K., Sano, F. & Koizumi, S. C. Aberrant calcium signals in reactive astrocytes: A key process in neurological disorders. *Int. J. Mol. Sci.* **20**, (2019).

19. Araque, A. *et al.* Gliotransmitters travel in time and space. *Neuron* **81**, 728–739 (2014).

20. Rasmussen, R., Nedergaard, M. & Petersen, N. C. Sulforhodamine 101, a widely used astrocyte marker, can induce cortical seizure-like activity at concentrations commonly used. *Sci. Rep.* **6**, 1–9 (2016).

21. Hülsmann, S., Hagos, L., Heuer, H. & Schnell, C. Limitations of sulforhodamine 101 for brain imaging. *Front. Cell. Neurosci.* **11**, 1–6 (2017).

22. Schnell, C., Hagos, Y. & Hulsmann, S. Active Sulforhodamine 101 Uptake into Hippocampal Astrocytes. *PLoS One* **7**, 1–13 (2012).

23. Fabbro, A., Pastore, B., Nistri, A. & Ballerini, L. Activity-independent intracellular Ca2+ oscillations are spontaneously generated by ventral spinal neurons during development in vitro. *Cell Calcium* **41**, 317–329 (2007).

24. Garaschuk, O., Linn, J., Eilers, J. & Konnerth, A. Large-scale oscillatory calcium waves in the immature cortex. *Nat. Neurosci.* **3**, 452–459 (2000).

25. Hirase, H., Qian, L., Barthó, P. & Buzsáki, G. Calcium dynamics of cortical astrocytic networks in vivo. *PLoS Biol.* **2**, 494–499 (2004).

26. Petravicz, J., Fiacco, T. A. & McCarthy, K. D. Loss of IP3 receptor-dependent Ca2+ increases in hippocampal astrocytes does not affect baseline CA1 pyramidal neuron synaptic activity. *J. Neurosci.* **28**, 4967–4973 (2008).

27. Shigetomi, E. *et al.* Imaging calcium microdomains within entire astrocyte territories and endfeet with GCaMPs expressed using adeno-associated viruses. *J. Gen. Physiol.* **141**, 633–647 (2013).

28. Agarwal, A. *et al.* Transient Opening of the Mitochondrial Permeability Transition Pore Induces Microdomain Calcium Transients in Astrocyte Processes. *Neuron* **93**, 587-605.e7 (2017).

29. Giaume, C. *et al.* Gap Junctions in Cultured Astrocytes : Currents and Characterization of Protein Single-Channel. **6**, 133–143 (1991).

30. Ren, J., Momose-Sato, Y., Sato, K. & Greer, J. J. Rhythmic neuronal discharge in the medulla and spinal cord of fetal rats in the absence of synaptic transmission. *J. Neurophysiol.* **95**, 527–534 (2006).

31. Hjorth, J., Blackwell, K. T. & Kotaleski, J. H. Gap junctions between striatal fast-spiking interneurons regulate spiking activity and synchronization as a function of cortical activity. *J. Neurosci.* **16**, 5276–5286 (2009).

32. Yin, J. & VanDongen, A. Enhanced Neuronal Activity and Asynchronous Calcium Transients Revealed in a 3D Organoid Model of Alzheimer's Disease. (2020) doi:10.1101/2020.07.07.192781.

33. Cornell-Bell, A. H., Finkbeiner, S. M., Cooper, M. S. & Smith, S. J. Glutamate induces calcium waves in cultured astrocytes: Long-range glial signaling. *Science (80-.).* **247**, 470–473 (1990).

34. Orellana, J. A. *et al.* Modulation of brain hemichannels and gap junction channels by pro-inflammatory agents and their possible role in neuro- degeneration. *Antioxid. Redox Signal.* **11**, 369–399 (2009).

35. Liao, C. K., Jeng, C. J., Wang, H. S., Wang, S. H. & Wu, J. C. Lipopolysaccharide induces degradation of connexin43 in rat astrocytes via the ubiquitin-proteasome proteolytic pathway. *PLoS One* **8**, 1–11 (2013).

36. Wang, N. *et al.* Connexin targeting peptides as inhibitors of voltage- and intracellular Ca2+-triggered Cx43 hemichannel opening. *Neuropharmacology* **75**, 506–516 (2013).

37. Yin, X. *et al.* Roles of astrocytic connexin-43, hemichannels, and gap junctions in oxygen-glucose deprivation/reperfusion injury induced neuroinflammation and the possible regulatory mechanisms of salvianolic acid B and carbenoxolone. *J. Neuroinflammation* **15**, 1–24 (2018).

38. Chever, O., Lee, C. Y. & Rouach, N. Astroglial connexin43 hemichannels tune basal excitatory synaptic transmission. *J. Neurosci.* **34**, 11228–11232 (2014).

39. Weissman, T. A., Riquelme, P. A., Ivic, L., Flint, A. C. & Kriegstein, A. R. Calcium waves propagate through radial glial cells and modulate proliferation in the developing neocortex. *Neuron* **43**, 647–661 (2004).

40. Kurth-Nelson, Z. L., Mishra, A. & Newman, E. A. Spontaneous glial calcium waves in the retina develop over early adulthood. *J. Neurosci.* **29**, 11339–11346 (2009).

41. Retamal, M. A. *et al.* Cx43 hemichannels and gap junction channels in astrocytes are regulated oppositely by proinflammatory cytokines released from activated microglia. *J. Neurosci.* **27**, 13781–13792 (2007).

42. Contreras, J. E. *et al.* Metabolic inhibition induces opening of unapposed connexin 43 gap junction hemichannels and reduces gap junctional communication in cortical astrocytes in culture. *Proc. Natl. Acad. Sci. U. S. A.* **99**, 495–500 (2002).

43. Wang, N. *et al.* Connexin mimetic peptides inhibit Cx43 hemichannel opening triggered by voltage and intracellular Ca2+ elevation. *Basic Res. Cardiol.* **107**, 17 (2012).

44. Deitmer, J. W., Verkhratsky, A. & Lohr, C. Calcium signalling in glial cells. *Pharmacogn. Mag.* **24**, 405–416 (1998).

45. Furlan, F. *et al.* ERG conductance expression modulates the excitability of ventral horn GABAergic interneurons that control rhythmic oscillations in the developing mouse spinal cord. *J. Neurosci.* **27**, 919–928 (2007).

46. Sáez, P. J., Shoji, K. F., Aguirre, A. & Sáez, J. C. Regulation of Hemichannels and Gap Junction Channels by Cytokines in Antigen-Presenting Cells. *Mediators Inflamm.* **2014**, (2014).

47. Evans, W. H. & Leybaert, L. Mimetic Peptides as Blockers of Connexin Channel-Facilitated Intercellular Communication. *Cell Commun. Adhes.* **14**, 265–273 (2007).

48. Davidson, J. S., Baumgarten, I. M. & Harley, E. H. Reversible inhibition of intercellular junctional communication by glycyrrhetinic acid. *Biochem. Biophys. Res. Commun.* **134**, 29–36 (1986).

49. Nedergaard, M., Rodríguez, J. J. & Verkhratsky, A. Glial calcium and diseases of the nervous system. *Cell Calcium* **47**, 140–149 (2010).

50. Shigetomi, E., Saito, K., Sano, F. & Koizumi, S. Aberrant Calcium Signals in Reactive Astrocytes: A Key Process in Neurological Disorders. *Int. J. Mol. Sci.* **20**, 996 (2019).

51. Stout, C. E., Costantin, J. L., Naus, C. C. G. & Charles, A. C. Intercellular calcium signaling in astrocytes via ATP release through connexin hemichannels. *J. Biol. Chem.* **277**, 10482–10488 (2002).

52. Orellana, J. A., Sánchez, H. A., Schalper, K. A., Figueroa, V. & Sáez, J. C. Regulation of Intercellular Calcium Signaling Through Calcium Interactions with Connexin-Based Channels BT - Calcium Signaling. in (ed. Islam, M. S.) 777–794 (Springer Netherlands, 2012). doi:10.1007/978-94-007-2888-2_34.

53. Hanisch, U. K. Microglia as a source and target of cytokines. *Glia* **40**, 140–155 (2002).

54. Brancaccio, M., Pivetta, C., Granzotto, M., Filippis, C. & Mallamaci, A. Emx2 and Foxg1 inhibit gliogenesis and promote neuronogenesis. *Stem Cells* **28**, 1206–1218 (2010).

55. Usmani, S. *et al.* 3D meshes of carbon nanotubes guide functional reconnection of segregated spinal explants. *Sci. Adv.* **2**, 1–10 (2016).

56. Streit, J. Regular Oscillations of Synap tic Activity in Spinal Networks In Vitro. **70**, (1993).

57. Ballerini, L., Galante, M., Grandolfo, M. & Nistri, A. Generation of rhythmic patterns of activity by ventral interneurones in rat organotypic spinal slice culture. 459–475 (1999).

Figure 1

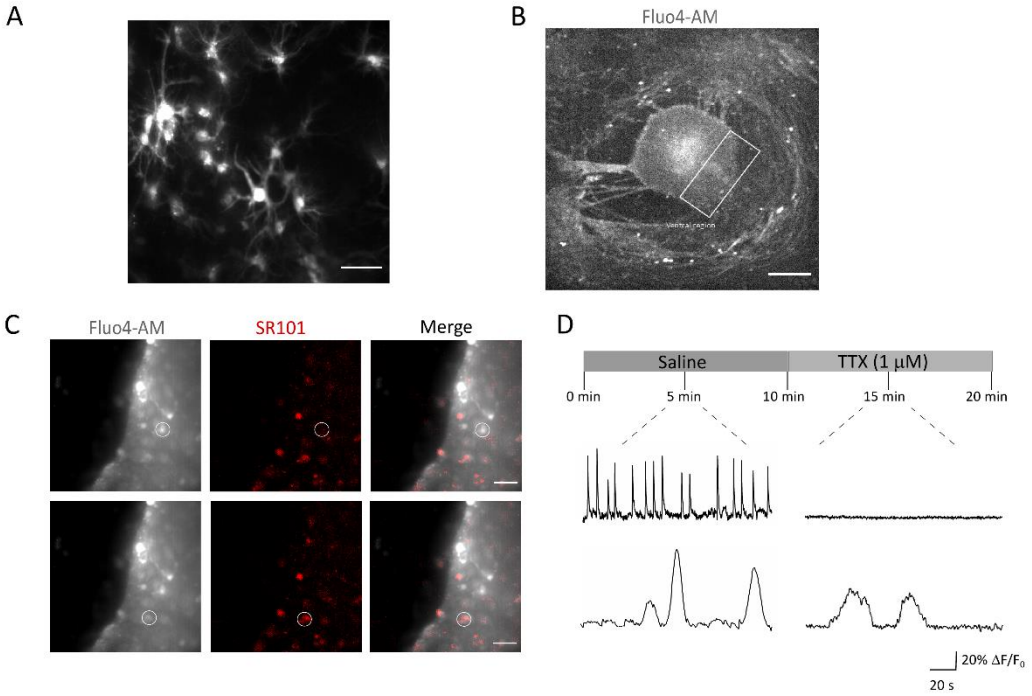

Figure 2

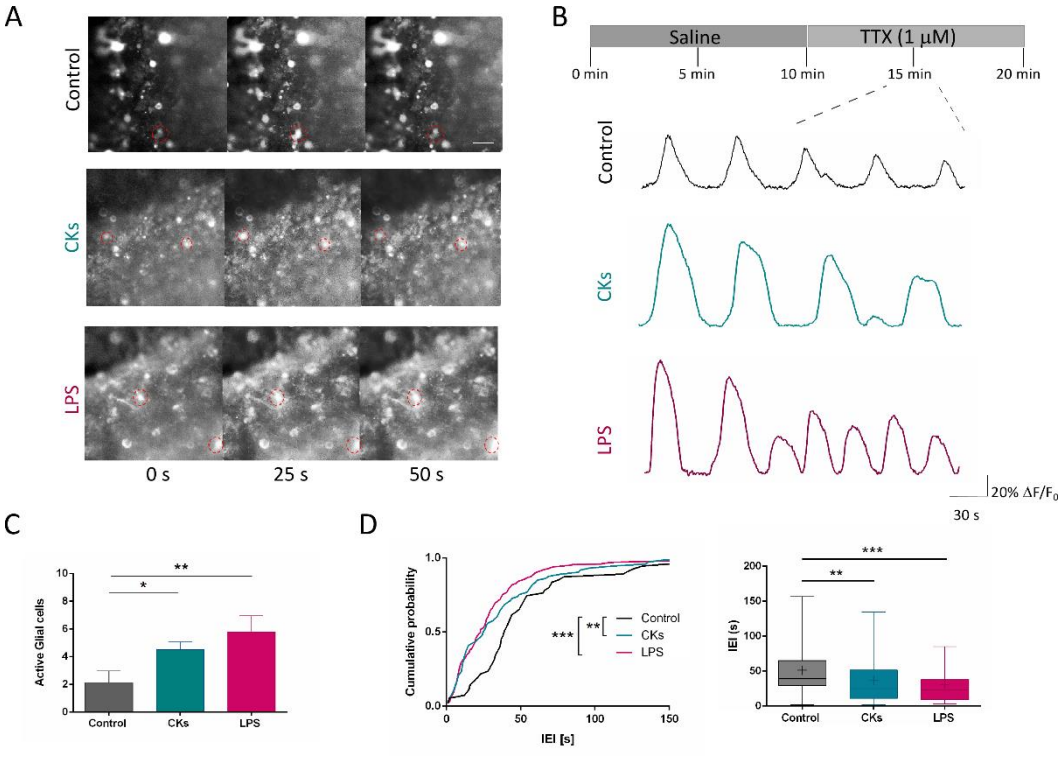

Figure 3

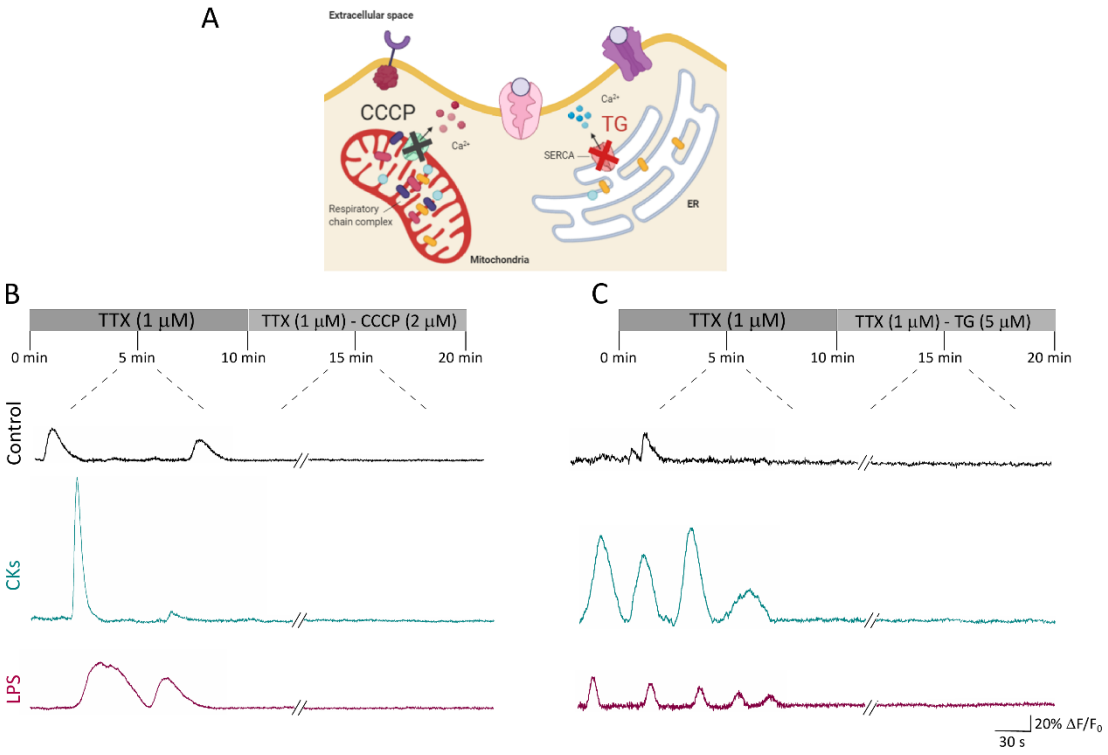

Figure 4

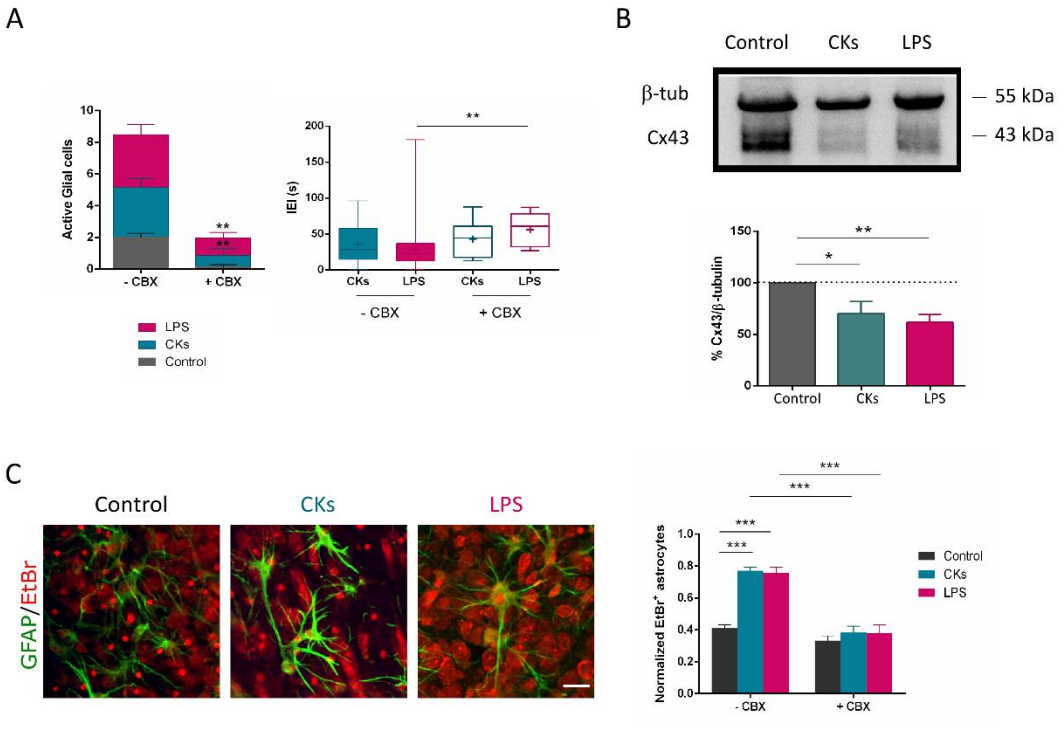

Figure 5

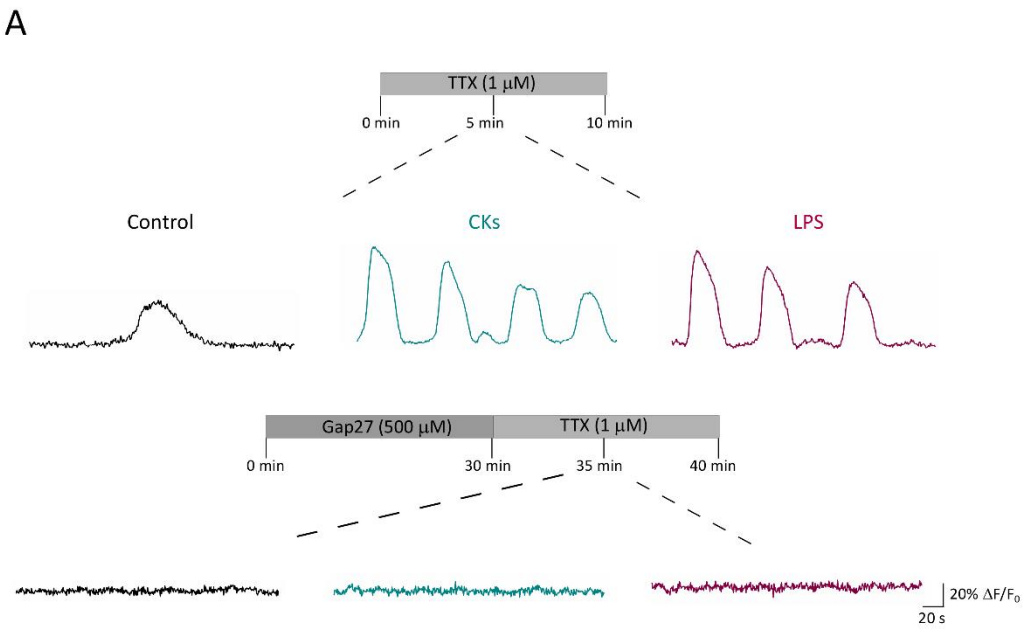
A
TTX (1 µM)
0 min
5 min
10 min
Control
CKs
LPS
Gap27 (500 µM)
TTX (1 µM)
0 min
30 min
35 min
40 min
20% ΔF/F0
20 s

Supplementary Figure 1

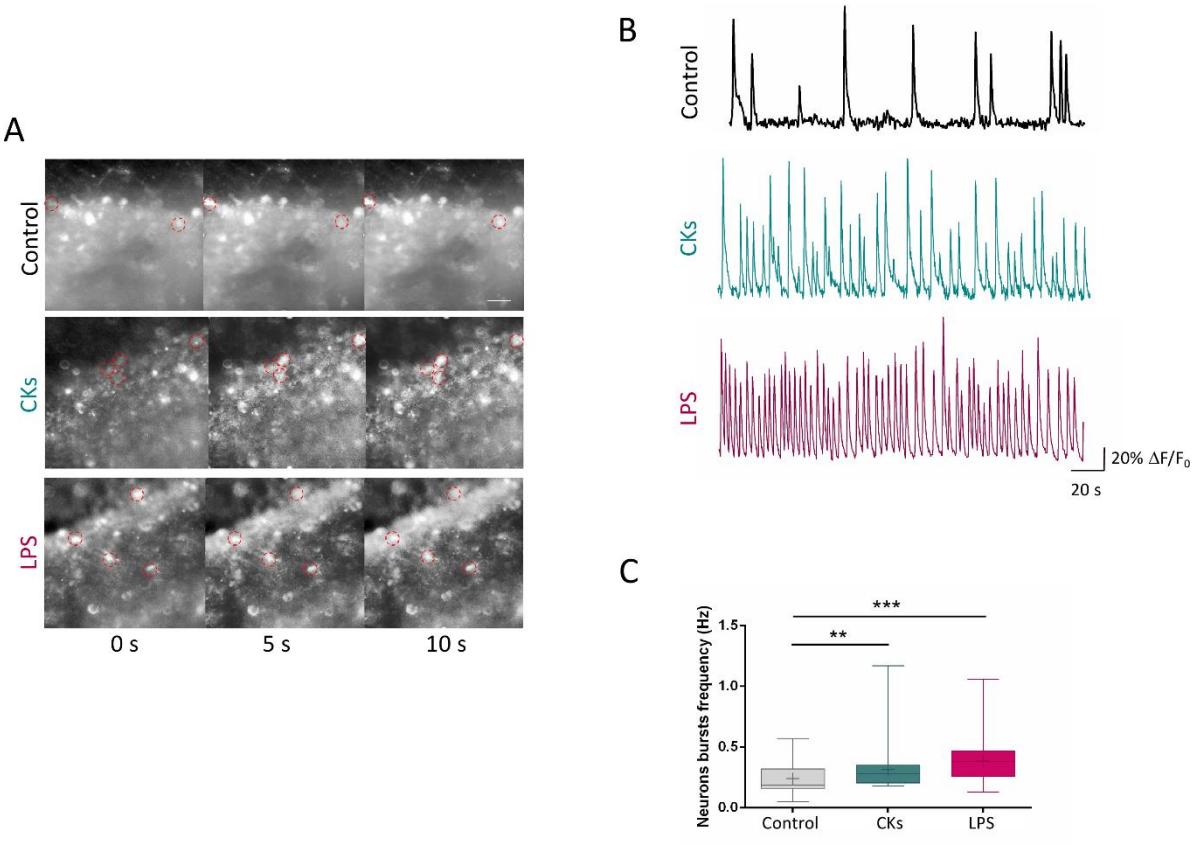

Supplementary Figure 2

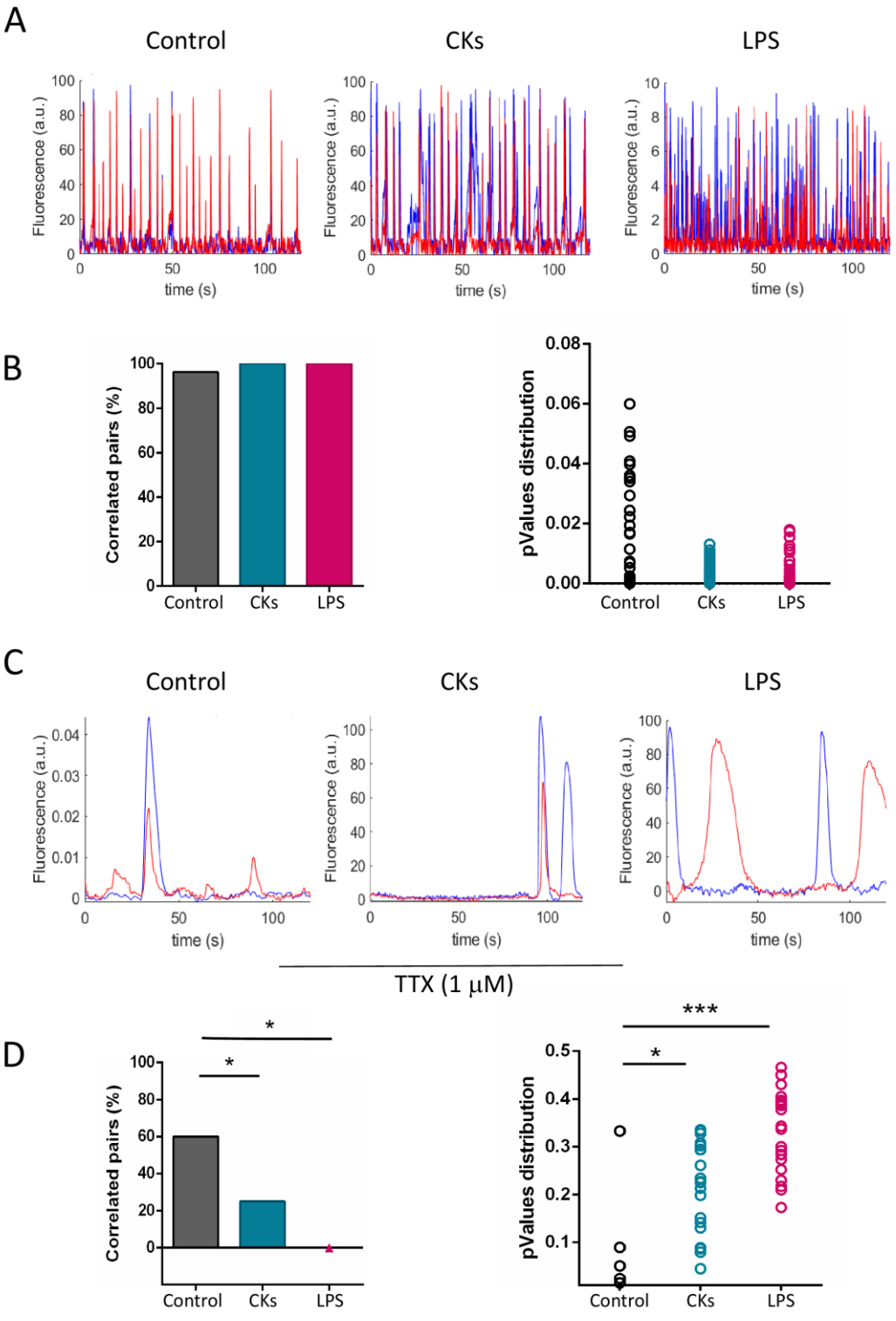

Supplementary Figure 3

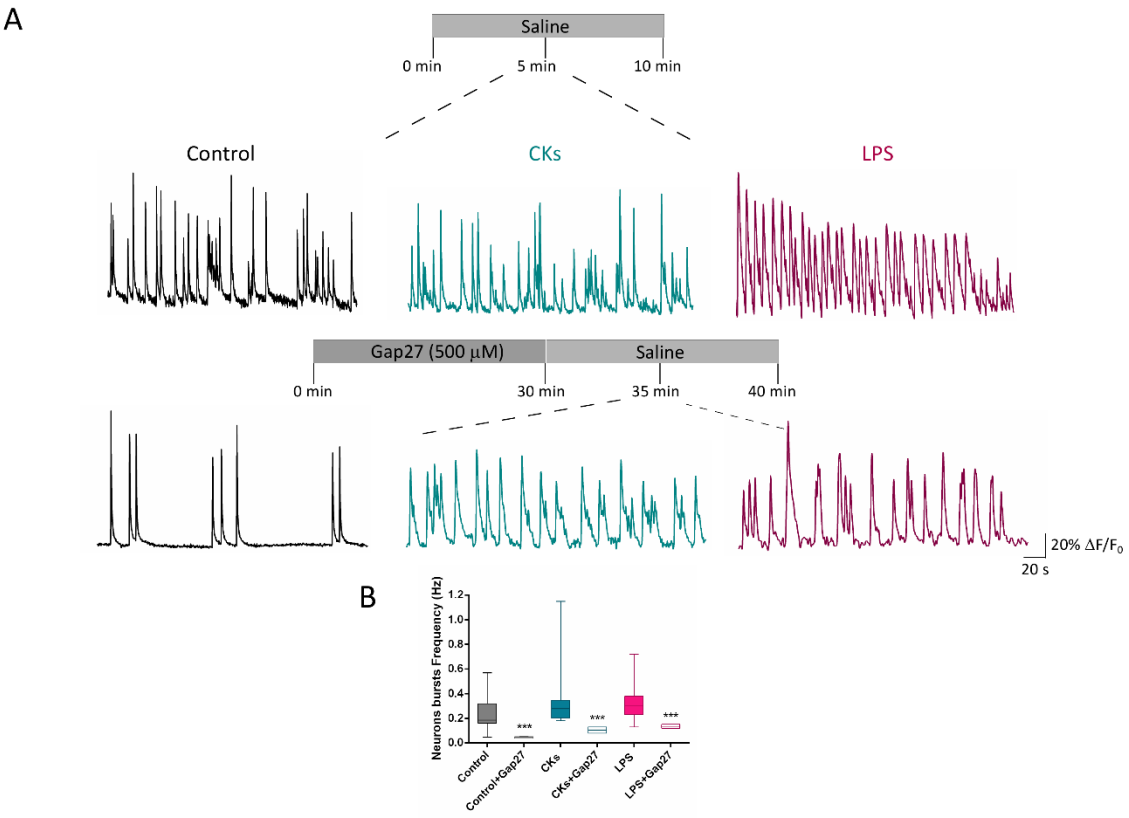

Figure Legends

Figure 1. SR101-positive glial cells display spontaneous, slow Ca^{2+} oscillations **A.** Representative image of LV-Gfap-Cherry expressing astrocytes in the ventral-horn of the organotypic spinal slice, in grey scale. Scale bar 50 μm. **B.** Representative fluorescent image at low magnification (4×) of a spinal organotypic slice (2 WIV) loaded with the calcium dye Fluo4-AM (4 μM). The ventral region (white frame) is identified by the ventral fissure. Scale bar, 500 μm. **C.** CCD-camera snapshots visualize cells located at the border of the ventral region and loaded with Fluo4-AM, in grey (left), and with SR101, in red (middle). Merged images on the right. Scale bars, 50 μm. **D.** Top, representative fluorescent tracing of spontaneous neuronal Ca^{2+} activity, prior and after 1 μM tetrodotoxin (TTX), recorded from SR101 negative cell (same as in in C). Bottom, representative fluorescent tracing of astrocytes Ca^{2+} oscillations, before and after the application of TTX, recorded from SR101 positive cell (same as in in C).

Figure 2. CKs and LPS enhance spinal astrocytes calcium dynamics **A.** Representative snapshots (40× magnification) of the ventral area of organotypic spinal slices (2 WIV) loaded with Fluo-4 AM; frames were taken at variable time intervals (0, 25 and 50 seconds) in three different experimental conditions (Control, CKs and LPS). Scale bar 50 μm. **B.** Representative fluorescent tracings depicting glial cells calcium oscillations in Control (black), CKs and LPS (6H, blue and purple, respectively), all recorded in the presence of TTX. **C.** The bar plot summarizes the number of spontaneously active glial cells/field. **$p<0.01$ and *$p<0.05$, one-way ANOVA. **D.** Cumulative distributions and box plot quantify the IEIs (s) of the recorded calcium activity in all conditions. ***$p<0.001$ and **$p<0.01$, in the cumulative plot Kolmogorov-Smirnov test and in the Box plot, Kruskal-Wallis test.

Figure 3. Intracellular calcium sources sustain calcium dynamics in astrocytes **A.** Sketch of the intracellular calcium sources. **B.** Fluorescent tracings from representative glial cells prior and after CCCP (2 μM) mitochondrial uncoupler administration in Control (black), CKs and LPS (blue and purple, respectively). **C.** Fluorescent tracings from representative glial cells prior and after Thapsigargin (TG, 5 μM) administration in Control (black), CKs and LPS (blue and purple, respectively). All recordings were performed in the presence of TTX. Note the removal of calcium activity in all cases.

Figure 4. Cx43 GJs and HCs role in the increased calcium dynamics in CKs and LPS
A. The bar plot shows the amount of active glial cells in Control (gray), CKs (blue) and LPS (purple) before and after the administration of carbenoxolone (CBX, 200 μM). Note the significant decrease in the number of the active glial cells upon CBX exposure. **p<0.01 one-way ANOVA. The box plot (right) compares IEI values in residual active cells before and after CBX application. **B.** Western blot experiments and (bar plot) analysis for the protein Cx43 in Control, CKs and LPS treated slices. Values are expressed as % of Control. *p<0.01 and *p<0.05, one-way ANOVA. **C.** Representative high magnification (40×) confocal images of EtBr uptake (30 min, in red) in astrocytes (GFAP, in green) induced by CKs and LPS treatments, scale bar 25 μm. Right, EtBr uptake is quantified in the bar plot, normalized to the total number of astrocytes/field, in the absence or in the presence of CBX pre-incubation (30 min). ***p<0.001, one-way ANOVA.

Figure 5. Incubation in the analogous peptide blocker of HCs permeability and GJs completely removed calcium activity in astrocytes
A. Representative glial cells calcium oscillations in Control (black) and after CKs and LPS (blue and purple, respectively). Upon 30 minutes incubation in Gap27 (500 μM) glial cells activity was completely removed in all conditions. All were performed in TTX.

Supplementary Information

Supplementary Figures

Figure S1. Pro-inflammatory treatments boost neuronal calcium signaling
A. Representative snapshots (40 × magnification) of the ventral area of organotypic spinal slices (2 WIV) loaded with Fluo-4 AM; frames were taken at variable time intervals (0, 5 and 10 seconds) in three different experimental conditions (Control, CKs and LPS). Scale bar 50 μm. **B.** Representative fluorescent tracings depicting neuronal spontaneous activity as calcium transients in control (black) and after CKs and LPS (blue and purple, respectively). **C.** The box plot summarizes the frequency values of calcium events in all conditions. ***p<0.001 and **p<0.01, Kruskal-Wallis.

Figure S2. Synchrony among neurons or astrocytes calcium signaling upon CKs and LPS
A. Two example fluorescent tracings, obtained from two neurons located in the same visual

field in the ventral horn of organotypic slices (2 WIV) in Control, CKs and LPS. The fluorescent recordings show calcium oscillations and the synchrony between recorded neurons was determined by computing their Pearson correlation coefficient in time windows that were randomly sampled from the all duration of the recording. **B.** The bar plot shows the % of correlated pairs in Control, CKs and LPS. Kruskal-Wallis test. The aligned dot plot shows the p values distributions obtained by the comparison of correlated pairs of traces. Fisher's exact test. **C.** Two example fluorescent tracings, obtained from two astrocytes located in the same visual field in the ventral horn of organotypic slices (2 WIV) in Control, CKs and LPS. The fluorescent recordings show calcium oscillations in the presence of TTX and the synchrony between recorded astrocytes was determined by computing their Pearson correlation coefficient in time windows that were randomly sampled from the all duration of the recording. **D.** The bar plot summarizes the % of correlated pairs detected in all conditions. ***$p<0.001$ and *$p<0.05$, one-way ANOVA. The aligned dot plot (right) shows the p values distribution obtained by the comparison of correlated pairs of traces. *$p<0.05$ Fisher's exact.

Figure S3. Gap27 treatment modulates neuronal calcium oscillations
A. Representative fluorescent recordings of spontaneous neuronal calcium episodes in Control (black) and after CKs and LPS (blue and purple, respectively), prior and after Gap27 (500 μM) treatment. **B.** The box plot summarizes the frequency values of calcium episodes in untreated and treated slices before and after Gap27 (n = 3, 3 and 3 Control, CKs and LPS; 0.06 ± 0.001 Hz Control+Gap27, 0.10 ± 0.005 Hz CKs 6H+Gap27, 0.14 ± 0.003 Hz LPS 6H+Gap27; ***p< 0.001, Kruskal-Wallis test).

Discussion

In several neuro-pathological conditions, including neurodegenerative diseases and neuropsychiatric disorders, neuroglia play a central role, contributing to neuronal damage by developing inflammatory responses within the CNS[2]. Trying to dissect the impact of the immune status alteration on spinal circuits function, we focused the attention on the effect of a localized and acute inflammation in a controlled micro-environment, provided by the organotypic spinal cord slice cultures, developed from the embryonic mouse spinal cords. The slices *in vitro* maintain their original sensory-motor cytoarchitecture and dorsal-ventral orientation. Furthermore, synaptic properties and spinal cord resident cells, encompassing heterogeneous neuronal phenotypes and neuroglia, are retained in a 3D-fashion[111,143,144]. Here, like in our previous work[111], we adopted short-term treatments with a specific cytokines cocktail in order to trigger inflammatory responses, without affecting neuronal membrane properties or inducing direct neurotoxicity, which would eventually have led to neuronal death, but still able to alter synaptic transmission. The peculiar cocktail was composed by IL-1β, a well-known determinant of neuropathy, TNF-α, present during Th1/Th17-mediated inflammatory reactions and GM-CSF, able in targeting resident microglial cells[102,126,228]. These cytokines are key factors known to affect neuronal functions and to mediate the harmful action of microglia in experimental animal models of MS[111]. By the use of this model, we reported the emergence of the so-called “synaptopathy” in pre-motor circuits following CKs transient exposure, characterized by an increase in the sPSCs

frequencies and a speeding up of the decay phase of GABAergic inhibitory currents, accompanied by a marked production of pro-inflammatory cytokines and chemokines[111]. It is well reported in literature that some of the main pro-inflammatory cytokines are able to modulate both glutamatergic and GABAergic transmissions, acting directly on the neurotransmitter receptors or on their re-uptake[103–106]. Pro-inflammatory cytokines have been already tested on brain slices to evaluate their effects on synaptic activity since they are over-expressed in pathological conditions. Centonze and coworkers treated a microglia cell line with a cytokines mix composed by TNF-α, IL-1β and INF-γ, known to peak during the acute phase of the EAE. They showed that TNF-α released from activated microglia might be a good candidate for the induction of the synaptic dysfunctions in EAE[102,229]. Thanks to these previous observations, in the work we are presenting here, we decided to compare the effects on synaptic transmission and on resident immune cells reactivity of two different experimental paradigms, LPS, a common inductor of inflammation, used to investigate microglia reactivity, able to trigger the release of pro-inflammatory cytokines[128] and the above-mentioned CKs cocktail. Since the LPS effects on neurons might be indirect, because LPS is known to induce the release of different molecules, including for instance TNF-α and IL-1β, but also others such as IL-6 and NO after binding TLR4 mainly on microglia, we decided to perform a longer LPS treatment (24 h), even maintaining the 4 and 6 hours treatments as well, both for the CKs and LPS paradigms[44]. On the other hand, with the CKs treatment we were able to detect direct effects on neurons since they display CKs receptors. The main finding of the present work is that the localized inflammation induced by LPS or CKs altered the synaptic transmission, already after 4 hours treatment, shown by the increase in the sPSCs and IPSCs

frequencies. This result represented the starting point for the analysis of the observed behavior, followed by the dissection of the inhibitory currents. We pharmacologically isolated the GABAergic component, finding that only the CKs treatment was effective in speeding up the current decay, probably via a post-synaptic mechanism, as demonstrated by the changes in the mIPSC's τ[153]. On the contrary, LPS, even upon prolonged exposure of the slices, was not able to induce a reduction in the decay currents, although the LPS treated slices produced several pro-inflammatory cytokines and chemokines and microglia expressed the TLR4, necessary to let LPS exert its inflammatory role (see the Appendix 1). The next step was to check the involvement of glial cells in mediating synaptic activity, focusing on their morphology. Also in this case, the treatment with CKs was more effective than the one with LPS, but, despite the low GFAP-positive cell reactivity after the LPS treatment, we were able to detect marked changes (although opposite) in the microglia morphology after the administration of both of the paradigms. In fact, we could observe the typical amoeboid microglia (marker of phagocytic microglia)[48] after the CKs treatment and a more ramified microglia after the LPS one, which may indicate that probably we were facing two different stages of glial cells activation, supported also by the different cytokines and chemokines profile production[32,230]. In fact, since CKs and LPS simulate different inflammatory conditions (the typical inflammatory responses of the CNS immune system and the bacterial inflammation, respectively), it may be that they affect synapses in a different way and following different pathways[231].

Once determined that the resident immune system was involved in the synaptic transmission alteration, at least for what the CKs treatment concerned, we focused again

on the GABAergic current component and in particular in the mechanisms responsible for IPSCs shortening. Since the differences in the intracellular Cl^- concentration have been reported to affect IPSCs kinetics[232], we administered the CKs treated slices with a blocker of the NKCC1 activity, bumetanide, to reduce the internal Cl^- concentration, but with this experiment we excluded the possibility of such differences in the Cl^- concentration, known to occur during neuroinflammation, which could have affected the IPSCs kinetics[232,233]. Finally, the last process involved in the change of the IPSCs current duration we considered in our work was the analysis of $GABA_AR$ α-subunit composition, taking into account that the α1-subunit was responsible for fast deactivation and for faster-decay currents[234–236]. Our experiments with the allosteric modulator of $GABA_AR$ subunits, zolpidem, suggested that the CKs treatment was effective in prolonging IPSCs duration. In conclusion, we can assert that the mechanism of switch of the $GABA_AR$ subunit, which is regulated by the inflammatory milieu and in particular by the CKs cocktail, which contributes to shortens the GABAergic currents decay, might disrupt and weaken the IPSCs transmission.

In the second part of the project, we focused again on the main characters of the neuroinflammatory process: neuroglia. For the first time, we approached to the analysis of these cells, in this complex *in vitro* system, exploiting live cell Ca^{2+} imaging techniques, focusing on the Ca^{2+} activity of the astrocytes, since it is well known that they display spontaneous Ca^{2+} oscillations, as well as neurons. With this method we aimed to have a better and wider overview on the spinal network activity, since using Ca^{2+} imaging it is possible to record the activity of a large number of cells simultaneously. Moreover, with the live imaging it was possible to record from astrocytes, on the contrary to the patch-

clamp techniques, since they are located in the deeper layers of the organotypic slice and it is quite difficult to detect them and record from them with a patch pipette. It is also important to consider that calcium has been implicated in the etiology of inflammation, since it is well known that calcium signaling is required for the activation of several immune cells[237,238], and it has been observed that in MS, T cells are not able to properly exert their role of reducing calcium influx[239]. Finally, it is important to characterize the calcium signaling in inflammatory conditions since it is now clear that calcium is involved in neurodegeneration, which, among other things, can be induced by neuroinflammation. In these experiments we exposed again the slices to both of the inflammatory paradigms for 6 hours, because, even if LPS did not induce the shortening of the $GABA_AR$-mediated currents, it was for sure a trigger for the inflammatory processes, as demonstrated by the cytokines and chemokines released by the glial cells in the inflamed slices. Even if a Ca^{2+} signaling characterization in the spinal slices has already been performed in our lab[189,190], here we described for the first time glia activity in an inflammatory environment. As expected, given the results of the previously mentioned work, we observed that the two treatments induced an increase in the frequency of the Ca^{2+} events, that are also synchronized among them, due to the weak presence of inhibition in spinal slices, cultured for two weeks[150,240,241]. We then moved to the main focus of the investigation, the astrocytes activity, obtained after blocking the neuronal firing, with the application of TTX, from the sulforhodamine 101-positive cells[242]. We observed a dysregulation of the astrocytes oscillatory activity after both of the inflammatory treatments, given by the increase in the number of active astrocytes and by the reduction in the number of IEIs, which means that the inflamed astrocytes display more oscillations, given by the increase

in the calcium concentration, in the same range time, when compared to the non-inflamed tissue. It was already confirmed by literature, that the increase in the astrocytes calcium activity was related to the pathogenesis of neurodegenerative diseases[185–187], also because the increase is firstly given by a rise in the internal Ca^{2+} concentration, to which glutamate receptors, such as the AMPA receptors, are very sensitive[243]. In our case, we demonstrated that mitochondria and endoplasmic reticulum accounted for the release of the ion and eventually for the increase in the Ca^{2+} concentration, which was not dependent by the inflammatory environment. In order to better characterize the observed calcium oscillations and to understand not only their source, but also their way of spreading, we analyzed them for their synchronicity among simultaneously recorded cells, since it is well reported that GJs are responsible for the synchronization of the calcium activity and that during inflammatory conditions the calcium events are less synchronized than in physiological conditions[13,244,245]. As expected, we found that the astrocytes in the inflamed slices are less synchronized than in the control condition, and that, when we applied the GJs uncoupler CBX, the astrocytes calcium activity was reduced in an inflamed-dependent manner, which means that the astrocytes are more active in the CKs and LPS treated slices. Then, when we applied Gap27, a specific astrocytes-GJs blocker[246], which targeted the Cx43-GJs and HCs[13], we obtained the complete lack of astrocytes activity in all the three experimental conditions, with a mechanism independent from the inflammatory environment, meaning that probably the GJs involved in the spreading of the calcium waves are mainly made of Cx43. Moreover we also observed a disruption in the neuronal activity. In fact, the neuronal transients showed low frequency and a burst-like feature, probably due to the lack of K^+ buffering,

induced by Gap27[247]. Another point we considered was that during inflammatory conditions the protein turnover is higher than in physiological conditions and this is the same for the Cx proteins which constitute the GJs[206]. For this reason, we decided to analyze the expression of Cx43, revealing that in the inflamed tissues there were a reduced amount of protein, which may imply that probably the protein is degraded faster during inflammation. Despite this, such a reduction could not explain the enhanced calcium activity previously observed. In order to explain the increase in the astrocytes calcium activity, in the presence of a reduced expression of Cx43, we hypothesize that this could be due to changes in the pores permeability[203,226,248]. Taking advantage of a commonly used fluorescent dye, ethidium bromide, able to cross the GJs and HCs pores, we demonstrated that in the inflamed tissues the dye uptake was higher when compared to the control tissue, but also that the uptake was comparable to the control when the inflamed tissues were pre-incubated with CBX. This might indicate that the inflammatory treatments induce a change in the GJs and HCs pores capacitance, responsible for the observed increase in the calcium activity.

In conclusion, we can assert that in this case CKs and LPS act in the same way in increasing the astrocytes Ca^{2+} signaling, likely modulating the permeability of the GJs and HCs pores, responsible for the spreading of the calcium waves, between close cells.

Conclusions

In this work we confirmed that the organotypic slices system represents an excellent setting, thanks to which we were able to dissect how the inflammatory environment interferes with the spinal circuits function, due to the easy accessibility of the resident cells and to the long lasting of the cultures. In fact, we exploited these cultures to investigate both the synaptic and whole network changes of a precise region of interest under physiological and pathological conditions, since we were able to mimic two different kind of inflammation. The main findings of this work are that only in the CKs treated slices, the interneurons GABAergic transmission is altered and more precisely the final result was that the cytokines cocktail induced the weakening of the IPSCs transmission in the spinal circuits, which could be detrimental for the correct tuning of the synaptic transmission. On the other hand, we found that both of the inflammatory treatments were able to regulate the astrocytes function, regardless of GFAP expression or microglia morphology differences, acting at the calcium signaling level, modulating the permeability of GJs and HCs. In this case it is possible to have a dysregulation in the calcium transmission, which can eventually lead to excitotoxicity and neurodegeneration. In conclusion, expanding our knowledge on the cross-talk between glial cells and neurons in the spinal circuits, and understanding the mechanisms which promote the dysregulation of the inhibitory transmission and of the astrocyte calcium signaling in pathological condition, represent the starting point for developing new therapies and strategies, essential for investigating the spinal neurodegenerative disorders.

Bibliography

1. Markowitz, A. J. B., White, M. G., Kolson, D. L. & Jordan-Sciutto, K. L. Cellular interplay between neurons and glia: toward a comprehensive mechanism for excitotoxic neuronal loss in neurodegeneration. *Cellscience* **4**, 111–146 (2007).
2. Kempuraj, D. *et al.* Neuroinflammation Induces Neurodegeneration. *J. Neurol. Neurosurg. spine* **1**, 1–15 (2016).
3. Shabab, T., Khanabdali, R., Moghadamtousi, S. Z., Kadir, H. A. & Mohan, G. Neuroinflammation pathways: a general review. *Int. J. Neurosci.* **127**, 624–633 (2017).
4. Xie, L. & Yang, S.-H. INTERACTION OF ASTROCYTES AND T CELLS IN PHYSIOLOGICAL AND PATHOLOGICAL CONDITIONS. *Brain Res.* 63–73 (2015) doi:10.1016/j.brainres.2015.03.026.INTERACTION.
5. Glass, C. K., Saijo, K., Winner, B., Marchetto, M. C. & Gage, H. Mechanisms Underlying Inflammation in Neurodegeneration. *Nih* **140**, 918–934 (2010).
6. Anrather, J. & Iadecola, C. Inflammation and Stroke: An Overview. *Neurotherapeutics* **13**, 661–670 (2016).
7. Ransohoff, R. M. How neuroinflammation contributes to neurodegeneration. *Science (80-.).* **353**, 777–782 (2016).
8. Troncoso-Escudero, P., Parra, A., Nassif, M. & Vidal, R. L. Outside in: Unraveling the role of neuroinflammation in the progression of Parkinson's disease. *Front. Neurol.* **9**, 1–15 (2018).
9. Somjen, G. G. Nervenkitt: Notes on the history of the concept of neuroglia. *Glia* **1**, 2–9 (1988).
10. Garwood, C. J. *et al.* Review: Astrocytes in Alzheimer's disease and other age-associated dementias: a supporting player with a central role. *Neuropathol. Appl. Neurobiol.* **43**, 281–298 (2017).
11. Jäkel, S. & Dimou, L. Glial Cells and Their Function in the Adult Brain : A Journey through the History of Their Ablation. **11**, 1–17 (2017).
12. Eng, L. F. Glial Fibrillary Acidic Protein (GFAP)" the Major Protein of Glial Intermediate Filaments in Differentiated Astrocytes. **8**, 203–214 (1985).
13. Giaume, C. *et al.* Gap Junctions in Cultured Astrocytes : Currents and Characterization of Protein Single-Channel. **6**, 133–143 (1991).
14. Kimelberg, H. K. Functions of mature mammalian astrocytes: A current view.

Neuroscientist **16**, 79–106 (2010).

15. W. Lloyd Andriezen. THE NEUROGLIA ELEMENTS IN THE HUMAN BRAIN. *Br. Med. J.* (1893).

16. Şovrea, A. & Boşca, A. Astrocytes reassessment - an evolving concept part one: embryology, biology, morphology and reactivity. *J. Mol. Psychiatry* **1**, 18 (2013).

17. Kessaris, N., Pringle, N. & Richardson, W. D. Specification of CNS glia from neural stem cells in the embryonic neuroepithelium. *Philos. Trans. R. Soc. B Biol. Sci.* **363**, 71–85 (2008).

18. Haber, M., Zhou, L. & Murai, K. K. Cooperative Astrocyte and Dendritic Spine Dynamics at Hippocampal Excitatory Synapses. **26**, 8881–8891 (2006).

19. Norenberg, M. . & Martinez-Hernandez, A. FINE STRUCTURAL LOCALIZATION OF GLUTAMINE SYNTHETASE IN ASTROCYTES OF RAT BRAIN. *Brain Res.* **161**, 303–310 (1979).

20. Sagare, A. P. *et al.* neurodegeneration in mice. *Nat. Commun.* **4**, 1–14 (2013).

21. Nett, W. J., Oloff, S. H. & Mccarthy, K. D. Hippocampal astrocytes in situ exhibit calcium oscillations that occur independent of neuronal activity. *J. Neurophysiol.* **87**, 528–537 (2002).

22. Danbolt, N. C. Glutamate uptake. **65**, 1–105 (2001).

23. Kettenmann, H., Kirchhoff, F. & Verkhratsky, A. Microglia: New Roles for the Synaptic Stripper. *Neuron* **77**, 10–18 (2013).

24. Lawson, L. J., Perry, V. H., Dri, P. & Gordon, S. Heterogeneity in the distribution and morphology of microglia in the normal adult mouse brain. *Neuroscience* **39**, 151–170 (1990).

25. Hanisch, U. K. & Kettenmann, H. Microglia: Active sensor and versatile effector cells in the normal and pathologic brain. *Nat. Neurosci.* **10**, 1387–1394 (2007).

26. Grassivaro, F. *et al. Convergence between microglia and peripheral macrophages phenotype during development and neuroinflammation*. (2019).

27. Salter, M. W. & Stevens, B. Microglia emerge as central players in brain disease. *Nat. Med.* **23**, 1018–1027 (2017).

28. Li, Q. & Barres, B. A. Microglia and macrophages in brain homeostasis and disease. *Nat. Rev. Immunol.* **18**, 225–242 (2018).

29. Peferoen, L., Kipp, M., van der Valk, P., van Noort, J. M. & Amor, S. Oligodendrocyte-microglia cross-talk in the central nervous system. *Immunology* **141**, 302–313 (2014).

30. Weikert, U. & Simons, A. G. Myelin pruning during Development. **100**, 120–134 (2019).

31. Bodea, G.-L. *et al.* Neurodegeneration by the activation of the Microglial Complement-Phagosome Pathway. *J. Neurosci.* **34**, 8546–8556 (2014).

32. Madry, C. *et al.* Microglial Ramification, Surveillance, and Interleukin-1β Release Are Regulated by the Two-Pore Domain K+ Channel THIK-1. *Neuron* **97**, 299-312.e6 (2018).

33. Garner, K. M., Amin, R., Johnson, R. W., Scarlett, E. J. & Michael, D. Microglia priming by interleukin-6 signaling is enhanced in aged mice. 90–99 (2019) doi:10.1016/j.jneuroim.2018.09.002.Microglia.

34. Yeung, M. S. Y. *et al.* Dynamics of oligodendrocyte generation and myelination in the human brain. *Cell* (2014) doi:10.1016/j.cell.2014.10.011.

35. van Tilborg, E. *et al.* Origin and dynamics of oligodendrocytes in the developing brain: Implications for perinatal white matter injury. *Glia* **66**, 221–238 (2018).

36. Simons, M. & Nave, K. A. Oligodendrocytes: Myelination and axonal support. *Cold Spring Harb. Perspect. Biol.* **8**, 1–16 (2016).

37. Trajkovic, K. *et al.* Neuron to glia signaling triggers myelin membrane exocytosis from endosomal storage sites. *J. Cell Biol.* **172**, 937–948 (2006).

38. Hildebrand, C., Remahl, S., Persson, H. & Bjartmar, C. Myelinated nerve fibres in the CNS. *Prog. Neurobiol.* **40**, 319–384 (1993).

39. Feltri, M. L., Poitelon, Y. & Previtali, S. C. How Schwann Cells Sort Axons: New concepts. *Neuroscientist* **22**, 252–265 (2016).

40. Jessen, K. R. & Mirsky, R. The success and failure of the schwann cell response to nerve injury. *Front. Cell. Neurosci.* **13**, 1–14 (2019).

41. Jessen, K. R. & Mirsky, R. The repair Schwann cell and its function in regenerating nerves. *J. Physiol.* **594**, 3521–3531 (2016).

42. Louveau, A., Harris, T. H. & Kipnis, J. Revisiting the Mechanisms of CNS Immune Privilege. *Trends Immunol.* **36**, 569–577 (2015).

43. Aarli, J. A. The immune system and the nervous system. 137–154 (1983).

44. Kumar, H., Kawai, T. & Akira, S. Pathogen Recognition by the Innate Immune System. **0185**, (2011).

45. Ajami, B., Bennett, J. L., Krieger, C., Tetzlaff, W. & Rossi, F. M. V. Local self-renewal can sustain CNS microglia maintenance and function throughout adult life. *Nat. Neurosci.* **10**, 1538–1543 (2007).

46. Lyman, M., Lloyd, D. G., Ji, X., Vizcaychipi, M. P. & Ma, D. Neuroinflammation: The role and consequences. *Neurosci. Res.* **79**, 1–12 (2014).

47. Davalos, D. *et al.* ATP mediates rapid microglial response to local brain injury in vivo. *Nat. Neurosci. Neurosci.* **8**, 752–758 (2005).

48. Palpagama, T. H., Waldvogel, H. J., Faull, R. L. M. & Kwakowsky, A. The Role of Microglia and Astrocytes in Huntington's Disease. *Front. Mol. Neurosci.* **12**, 1–15 (2019).

49. No Title. http://jonlieffmd.com/wp-content/uploads/2013/12/Ramified-.jpg.

50. Ransohoff, R. M. A polarizing question: Do M1 and M2 microglia exist. *Nat. Neurosci.* **19**, 987–991 (2016).

51. Okubo, M. *et al.* Macrophage-Colony Stimulating Factor Derived from Injured Primary Afferent Induces Proliferation of Spinal Microglia and Neuropathic Pain in Rats. *PLoS One* **11**, e0153375 (2016).

52. Soto-Díaz, K., Juda, M. B., Blackmore, S., Walsh, C. & Steelman, A. J. TAK1 inhibition in mouse astrocyte cultures ameliorates cytokine-induced chemokine production and neutrophil migration. *J. Neurochem.* 1–13 (2019) doi:10.1111/jnc.14930.

53. Farina, C., Aloisi, F. & Meinl, E. Astrocytes are active players in cerebral innate immunity. *Trends Immunol.* **28**, 138–145 (2007).

54. Sofroniew, M. V. Molecular dissection of reactive astrogliosis and glial scar formation. *Trends in Neurosciences* (2009) doi:10.1016/j.tins.2009.08.002.

55. Liddelow, S. A. *et al.* Neurotoxic reactive astrocytes are induced by activated microglia. *Nature* **541**, 481–487 (2017).

56. Mader, S. & Brimberg, L. Aquaporin-4 Water Channel in the Brain and Its Implication for Health and Disease. *Cells* **8**, 90 (2019).

57. Madsen, P. M. *et al.* Oligodendrocytes modulate the immune-inflammatory response in EAE via TNFR2 signaling. *Brain Behav. Immun.* (2019) doi:10.1016/j.bbi.2019.11.017.

58. Philips, T. & Robberecht, W. Neuroinflammation in amyotrophic lateral sclerosis: role of glial activation in motor neuron disease. *Lancet Neurol.* **10**, 253–263 (2011).

59. Holtmann, H. & Resch, K. Cytokines. *Naturwissenschaften* **83**, 178–187 (1996).

60. Borsini, A., Zunszain, P. A., Thuret, S. & Pariante, C. M. The role of inflammatory cytokines as key modulator of neurogenesis. *Trends Neurosci.* **38**, 145–157 (2015).

61. Domingues, C., da Cruz e Silva, O. A. B. & Henriques, A. G. Impact of Cytokines and Chemokines on Alzheimer's Disease Neuropathological Hallmarks. *Curr. Alzheimer Res.* **14**, 870–882 (2017).

62. Holmes, C. *et al.* Systemic inflammation and disease progression in Alzheimer disease. *Neurology* **73**, 768 LP – 774 (2009).

63. Cunningham, C. Microglia and Neurodegeneration : The Role of Systemic

Inflammation. 90, 71–90 (2013).

64. Goldgaber, D. *et al.* Interleukin 1 regulates synthesis of amyloid beta-protein precursor mRNA in human endothelial cells. *Proc. Natl. Acad. Sci.* 86, 7606 LP – 7610 (1989).

65. Griffin, W. S. T., Liu, L., Li, Y., Mrak, R. E. & Barger, S. W. Interleukin-1 mediates Alzheimer and Lewy body pathologies. 9, 1–9 (2006).

66. Chakrabarty, P. *et al.* Massive gliosis induced by interleukin-6 suppresses Aβ deposition in vivo: evidence against inflammation as a driving force for amyloid deposition. *FASEB J.* 24, 548–559 (2009).

67. Grassi, F. *et al.* TNF-a increases the frequency of spontaneous miniature synaptic currents in cultured rat hippocampal neurons. 659, 226–230 (1994).

68. Yamamoto, M. *et al.* Interferon-gamma and tumor necrosis factor-alpha regulate amyloid-beta plaque deposition and beta-secretase expression in Swedish mutant APP transgenic mice. *Am. J. Pathol.* 170, 680–692 (2007).

69. Naves, R. *et al.* The Interdependent, Overlapping, and Differential Roles of Type I and II IFNs in the Pathogenesis of Experimental Autoimmune Encephalomyelitis. *J. Immunol.* 191, 2967 LP – 2977 (2013).

70. Yang, J. *et al.* Silencing IFN- γ Binding/Signaling in Astrocytes versus Microglia Leads to Opposite Effects on Central Nervous System Autoimmunity. (2020) doi:10.4049/jimmunol.1303321.

71. Chao, C. C. *et al.* Transforming growth factor beta in Alzheimer's disease. *Clin. Diagn. Lab. Immunol.* 1, 109 LP – 110 (1994).

72. Hochman Shawn. Spinal Cord. *Curr. Biol.* 17, 1–11 (2007).

73. Jessell TM. Neuronal specification in the spinal cord:inductive signals and transcriptional codes. *Nat. Rev. Genet.* 1, 20–29 (2000).

74. Gutierrez-Mecinas, M., Polgár, E., Bell, A. M., Herau, M. & Todd, A. J. Substance P-expressing excitatory interneurons in the mouse superficial dorsal horn provide a propriospinal input to the lateral spinal nucleus. *Brain Struct. Funct.* 223, 2377–2392 (2018).

75. Eccles, J. C., Eccles, R. M. & Magni, F. CENTRAL INHIBITORY ACTION ATTRIBUTABLE TO PRESYNAPTIC DEPOLARIZATION PRODUCED BY MUSCLE AFFERENT VOLLEYS. *J. Physiol.* 159, 147–166 (1961).

76. Engelman, H. S. & MacDermott, A. B. Presynaptic ionotropic receptors and control of transmitter release. *Nat. Rev. Neurosci.* 5, 135–145 (2004).

77. Colloca, L. *et al.* Neuropathic pain. *Nat. Rev. Dis. Prim.* 3, 1–20 (2017).

78. Steuer, I. & Guertin, P. A. Central pattern generators in the brainstem and spinal cord: An overview of basic principles, similarities and differences. *Rev. Neurosci.*

(2018) doi:10.1515/revneuro-2017-0102.

79. Kiehn, O. L. E. & Kjaerulff, O. L. E. Distribution of Central Pattern in the Spinal Cord of Limbed Vertebrates a. *Ann. N. Y. Acad. Sci.* **860**, 110–129 (1998).

80. Minassian, K., Hofstoetter, U. S., Dzeladini, F., Guertin, P. A. & Ijspeert, A. The Human Central Pattern Generator for Locomotion: Does It Exist and Contribute to Walking? *Neuroscientist* **23**, 649–663 (2017).

81. Badhiwala, J. H., Ahuja, C. S. & Fehlings, M. G. Time is spine: A review of translational advances in spinal cord injury. *J. Neurosurg. Spine* **30**, 1–18 (2019).

82. Hara, M. *et al.* Interaction of reactive astrocytes with type i collagen induces astrocytic scar formation through the integrin-N-cadherin pathway after spinal cord injury. *Nat. Med.* **23**, 818–828 (2017).

83. Buss, A. *et al.* Gradual loss of myelin and formation of an astrocytic scar during Wallerian degeneration in the human spinal cord. *Brain* **127**, 34–44 (2004).

84. Gaudet, A. D. & Fonken, L. K. Glial Cells Shape Pathology and Repair After Spinal Cord Injury. 554–577 (2018).

85. Beck, K. D. *et al.* Quantitative analysis of cellular inflammation after traumatic spinal cord injury: Evidence for a multiphasic inflammatory response in the acute to chronic environment. *Brain* **133**, 433–447 (2010).

86. Yuan, Y. M. & He, C. The glial scar in spinal cord injury and repair. *Neurosci. Bull.* **29**, 421–435 (2013).

87. Rowland Lewis P. *Merritt's Textbook of Neurology*. (1995).

88. Pearn, J. Incidence, prevalence, and gene frequency studies of chronic childhood spinal muscular atrophy. *J. Med. Genet.* **15**, 409 LP – 413 (1978).

89. Papadimitriou, D. *et al.* Inflammation in ALS and SMA: Sorting out the good from the evil. *Neurobiol. Dis.* **37**, 493–502 (2010).

90. Frakes, A. E. *et al.* Microglia induce motor neuron death via the classical NF-κB pathway in amyotrophic lateral sclerosis. *Neuron* **81**, 1009–1023 (2014).

91. Cassina, P. *et al.* Peroxynitrite triggers a phenotypic transformation in spinal cord astrocytes that induces motor neuron apoptosis. *J. Neurosci. Res.* **67**, 21–29 (2002).

92. Ponath, G. *et al.* Myelin phagocytosis by astrocytes after myelin damage promotes lesion pathology. *Brain* **140**, 399–413 (2017).

93. Elieh-Ali-Komi, D. & Cao, Y. Role of Mast Cells in the Pathogenesis of Multiple Sclerosis and Experimental Autoimmune Encephalomyelitis. *Clin. Rev. Allergy Immunol.* **52**, 436–445 (2017).

94. Baranzini, S. E. *et al.* Genetic variation influences glutamate concentrations in brains of patients with multiple sclerosis. *Brain* **133**, 2603–2611 (2010).

95. Stadelmann, C. *et al.* BDNF and gp145trkB in multiple sclerosis brain lesions: neuroprotective interactions between immune and neuronal cells? *Brain* **125**, 75–85 (2002).

96. Merrill, J. E., Ignarro, L. J., Sherman, M. P., Melinek, J. & Lane, T. E. Microglial cell cytotoxicity of oligodendrocytes is mediated through nitric oxide. *J. Immunol.* **151**, 2132 LP – 2141 (1993).

97. Selmaj, K. W., Farooq, M., Norton, W. T., Raine, C. S. & Brosnan, C. F. Proliferation of astrocytes in vitro in response to cytokines. A primary role for tumor necrosis factor. *J. Immunol.* **144**, 129 LP – 135 (1990).

98. Vezzani, A. & Viviani, B. Neuromodulatory properties of inflammatory cytokines and their impact on neuronal excitability. *Neuropharmacology* (2015) doi:10.1016/j.neuropharm.2014.10.027.

99. Mandolesi, G. *et al.* Synaptopathy connects inflammation and neurodegeneration in multiple sclerosis. *Nat. Rev. Neurol.* **11**, 711–724 (2015).

100. Dutta, R. *et al.* Demyelination causes synaptic alterations in hippocampi from multiple sclerosis patients. *Ann. Neurol.* **69**, 445–454 (2011).

101. Kawasaki, Y., Zhang, L., Cheng, J. K. & Ji, R. R. Cytokine mechanisms of central sensitization: Distinct and overlapping role of interleukin-1β, interleukin-6, and tumor necrosis factor-α in regulating synaptic and neuronal activity in the superficial spinal cord. *J. Neurosci.* **28**, 5189–5194 (2008).

102. Centonze, D. *et al.* Inflammation triggers synaptic alteration and degeneration in experimental autoimmune encephalomyelitis. *J. Neurosci.* **29**, 3442–3452 (2009).

103. Stellwagen, D., Beattie, E. C., Seo, J. Y. & Malenka, R. C. Differential regulation of AMPA receptor and GABA receptor trafficking by tumor necrosis factor-α. *J. Neurosci.* **25**, 3219–3228 (2005).

104. Zou, J. Y. & Crews, F. T. TNF-alpha potentiates neurotoxicity by inhibiting glutamate uptake in organotypic brain slice cultures: neuroprotection by NF-kB inhibition. *Brain Res.* **1034**, 11–24 (2005).

105. Takeuchi, H. *et al.* TNF-alpha induces neurotoxicity via glutamate release from hemichannels of activated microglia in an autocrine manner. *J. Biol. Chem.* **281**, 21363–21368 (2006).

106. Pribiag, H. & Stellwagen, D. Tnf-α downregulates inhibitory neurotransmission through protein phosphatase 1-dependent trafficking of GABAA receptors. *J. Neurosci.* **33**, 15879–15893 (2013).

107. Yan, X. & Weng, H. R. Endogenous interleukin-1β in neuropathic rats enhances glutamate release from the primary afferents in the spinal dorsal horn through coupling with presynaptic N-methyl-D-aspartic acid receptors. *J. Biol. Chem.* **288**, 30544–30557 (2013).

108. Yan, X. *et al.* Interleukin-1beta released by microglia initiates the enhanced glutamatergic activity in the spinal dorsal horn during paclitaxel-associated acute pain syndrome. *Glia* **67**, 482–497 (2019).

109. Boakye, P. A. *et al.* Receptor dependence of BDNF actions in superficial dorsal horn: Relation to central sensitization and actions of macrophage colony stimulating factor 1. *J. Neurophysiol.* **121**, 2308–2322 (2019).

110. Alford, S., Schwartz, E. & Prisco, G. V. D. I. The Pharmacology of Vertebrate Spinal Central Pattern Generators. **9**, 217–228 (2003).

111. Medelin, M. *et al.* Bridging pro-inflammatory signals, synaptic transmission and protection in spinal explants in vitro. *Mol. Brain* **11**, 1–14 (2018).

112. Steinman, L. Inflammatory Cytokines at the Summits of Pathological Signal Cascades in Brain Diseases. *Sci. Signal.* **6**, (2013).

113. Bushong, E. A., Martone, M. E., Jones, Y. Z. & Ellisman, M. H. Protoplasmic astrocytes in CA1 stratum radiatum occupy separate anatomical domains. *J. Neurosci.* **22**, 183–192 (2012).

114. Theodosis, D. ., Poulain, D. A. & Oliet, S. H. R. Activity-dependent structural and functional plasticity of astrocyte-neuron interactions. *Physiol. Rev.* **88**, 983–1008 (2008).

115. Hamilton, N. B. & Attwell, D. Do astrocytes really exocytose neurotransmitters? *Nat. Rev. Neurosci.* **11**, 227–238 (2010).

116. Araque, A., Parpura, V., Sanzgiri, R. P. & Haydon, P. G. Tripartite synapses: Glia, the unacknowledged partner. *Trends Neurosci.* **22**, 208–215 (1999).

117. Pascual, M., Ibanez, F. & Guerri, C. Exosomes as mediators of neuron-glia communication in neuroinflammation. *Neural Regen. Res.* **15**, 796–801 (2019).

118. Ma, B. *et al.* Gap junction coupling confers isopotentiality on astrocyte syncytium. *Glia* **64**, 214–226 (2016).

119. Karwoski, C. J., Lu, H. K. & Newman, E. A. Spatial buffering of light-evoked potassium increases by retinal Muller (glial) cells. *Science (80-.).* **244**, 578 LP – 580 (1989).

120. Bellot-Saez, A., Kékesi, O., Morley, J. W. & Buskila, Y. Astrocytic modulation of neuronal excitability through K+spatial buffering. *Neurosci. Biobehav. Rev.* **77**, 87–97 (2017).

121. Kaiser, M. *et al.* Progressive loss of a glial potassium channel (KCNJ10) in the spinal cord of the SOD1 (G93A) transgenic mouse model of amyotrophic lateral sclerosis. *J. Neurochem.* **99**, 900–912 (2006).

122. Basso, M. *et al.* Mutant copper-zinc superoxide dismutase (SOD1) induces protein secretion pathway alterations and exosome release in astrocytes: Implications for disease spreading and motor neuron pathology in amyotrophic

lateral sclerosis. *J. Biol. Chem.* **288**, 15699–15711 (2013).

123. Bianco, F. *et al.* Astrocyte-derived ATP induces vesicle shedding and IL-1 beta release from microglia. *J. Immunol.* **174**, 7268–7277 (2005).

124. Wake, H., Moorhouse, A. J., Jinno, S., Kohsaka, S. & Nabekura, J. Resting microglia directly monitor the functional state of synapses in vivo and determine the fate of ischemic terminals. **29**, 3974–3980 (2009).

125. Yoshiyama, Y. *et al.* Synapse Loss and Microglial Activation Precede Tangles in a P301S Tauopathy Mouse Model. *Neuron* **53**, 337–351 (2007).

126. Pascual, O., Achour, S. Ben, Rostaing, P., Triller, A. & Bessis, A. Microglia activation triggers astrocyte-mediated modulation of excitatory neurotransmission. *Proc. Natl. Acad. Sci. U. S. A.* **109**, (2012).

127. Hu, S., Sheng, W. S., Ehrlich, L. C., Peterson, P. K. & Chao, C. C. Cytokine effects on glutamate uptake by human astrocytes. *Neuroimmunology* **7**, 153–159 (2000).

128. Li, X. *et al.* Phosphoinositide 3 Kinase Mediates Toll-Like Receptor 4-Induced Activation of NF- B in Endothelial Cells. **71**, 4414–4420 (2003).

129. Nguyen, M. D., D'Aigle, T., Gowing, G., Julien, J. P. & Rivest, S. Exacerbation of motor neuron disease by chronic stimulation of innate immunity in a mouse model of amyotrophic lateral sclerosis. *J. Neurosci.* **24**, 1340–1349 (2004).

130. Li, B. *et al.* The NADPH oxidase is involved in lipopolysaccharide-mediated motor neuron injury. *Brain Res.* **1226**, 199–208 (2008).

131. Ravikumar, M., Jain, S., Miller, R. H., Capadona, J. R. & Selkirk, S. M. An organotypic spinal cord slice culture model to quantify neurodegeneration. *J. Neurosci. Methods* **211**, 280–288 (2012).

132. Cantaut-Belarif, Y. *et al.* Microglia control the glycinergic but not the GABAergic synapses via prostaglandin E2 in the spinal cord. *J. Cell Biol.* **216**, 2979–2989 (2017).

133. Olson, J. K. & Miller, S. D. Microglia initiate central nervous system innate and adaptive immune responses through multiple TLRs. *J. Immunol.* **173**, 3916–3924 (2004).

134. Korgaonkar, A. A. *et al.* TLR4 signaling in neurons enhances calcium-permeable AMPAR currents and drives post-traumatic epileptogenesis. *Ann. Neurol.* 497–515 (2020) doi:10.1002/ana.25698.

135. Spicarova, D., Nerandzic, V. & Palecek, J. Modulation of spinal cord synaptic activity by tumor necrosis factor α in a model of peripheral neuropathy. *J. Neuroinflammation* **8**, 177 (2011).

136. Kim, Y. S. *et al.* Correction of humoral derangements from mutant superoxide dismutase 1 spinal cord. *Ann. Neurol.* **60**, 716–728 (2006).

137. Cho, S., Wood, A. & Bowby, M. R. Brain slices as models for neurodegenerative disease and screening platforms to identify novel therapeutics. *Curr. Neuropharmacol.* 5, 19–33 (2007).

138. Jarjour, A. A., Zhang, H., Bauer, N., French-Constant, C. & Williams, A. In vitro modeling of central nervous system myelination and remyelination. *Glia* 60, 1–12 (2012).

139. Sundstrom, L., Morrison, B., Bradley, M. & Pringle, A. Organotypic cultures as tools for functional screening in the CNS. *Drug Discov. Today Targets* 10, 993–1000 (2005).

140. Gähwiler, B. H., Capogna, M., Debanne, D., McKinney, R. A. & Thompson, S. M. Organotypic slice cultures: a technique has come of age. *Trends Neurosci.* 20, 471–477 (1997).

141. Stoppini, L., Buchs, P. A. & Muller, D. A simple method for organotypic cultures of nervous tissue. *J. Neurosci. Methods* 37, 173–182 (1991).

142. Rosato-Siri, M., Grandolfo, M. & Ballerini, L. Activity-dependent modulation of GABAergic synapses in developing rat spinal networks in vitro. *Eur. J. Neurosci.* 16, 2123–2135 (2002).

143. Avossa, D., Rosato-Siri, M. D., Mazzarol, F. & Ballerini, L. Spinal circuits formation: A study of developmentally regulated markers in organotypic cultures of embryonic mouse spinal cord. *Neuroscience* 122, 391–405 (2003).

144. Furlan, F. *et al.* ERG conductance expression modulates the excitability of ventral horn GABAergic interneurons that control rhythmic oscillations in the developing mouse spinal cord. *J. Neurosci.* 27, 919–928 (2007).

145. Streit, J., Spenger, C. & Lüscher, H. R. An organotypic spinal cord - dorsal root ganglion - skeletal muscle coculture of embryonic rat. II. Functional evidence for the formation of spinal reflex arcs in vitro. *Eur. J. Neurosci.* 3, 1054–1068 (1991).

146. Wu, W. L., Zinskind-Conhaim, L. & Sweet, M. A. Early development of glycine- and GABA-mediated synapses in rat spinal cord. *J. Neurosci.* 12, 3935–3945 (1992).

147. Gao, B. X., Stricker, C. & Ziskind-Conhaim, L. Transition from GABAergic to glycinergic synaptic transmission in newly formed spinal networks. *J. Neurophysiol.* 86, 492–502 (2001).

148. Rosato-Siri, M. D., Zoccolan, D., Furlan, F. & Ballerini, L. Interneurone bursts are spontaneously associated with muscle contractions only during early phases of mouse spinal network development: a study in organotypic cultures. *Eur. J. Neurosci.* 20, 2697–2710 (2004).

149. Ballerini, L. & Galante, M. Network bursting by organotypic spinal slice cultures in the presence of bicuculline and / or strychnine is developmentally regulated. 10, 2871–2879 (1998).

150. Ballerini, L., Galante, M., Grandolfo, M. & Nistri, A. Generation of rhythmic patterns of activity by ventral interneurones in rat organotypic spinal slice culture. 459–475 (1999).

151. Giacco, V. *et al.* Cytokine inflammatory threat, but not LPS one, shortens GABAergic synaptic currents in the mouse spinal cord organotypic cultures. *J. Neuroinflammation* **16**, (2019).

152. Fabbro, A. *et al.* Spinal Cord Explants Use Carbon Nanotube Interfaces To Enhance Neurite Outgrowth and To Fortify Synaptic Inputs. 2041–2055 (2012).

153. Medelin, M. *et al.* Altered development in GABA co-release shapes glycinergic synaptic currents in cultured spinal slices of the SOD1 G93A mouse model of amyotrophic lateral sclerosis. **13**, 3827–3840 (2016).

154. Pandamooz, S., Nabiuni, M., Miyan, J., Ahmadiani, A. & Dargahi, L. Organotypic Spinal Cord Culture: a Proper Platform for the Functional Screening. *Mol. Neurobiol.* **53**, 4659–4674 (2016).

155. Krassioukov, A. V. *et al.* An in vitro model of neurotrauma in organotypic spinal cord cultures from adult mice. *Brain Res. Protoc.* **10**, 60–68 (2002).

156. Liu, J. J., Ding, X. Y., Xiang, L., Zhao, F. & Huang, S. L. A novel method for oxygen glucose deprivation model in organotypic spinal cord slices. *Brain Res. Bull.* **135**, 163–169 (2017).

157. Li, B. *et al.* Effect of ALS IgG on motor neurons in organotypic spinal cord cultures. *Can. J. Neurol. Sci.* **35**, 220–225 (2008).

158. Kosuge, Y., Sekikawa-Nishida, K., Negi, H., Ishige, K. & Ito, Y. Characterization of chronic glutamate-mediated motor neuron toxicity in organotypic spinal cord culture prepared from ALS model mice. *Neurosci. Lett.* **454**, 165–169 (2009).

159. Gerardo-Nava, J. *et al.* Differential pattern of neuroprotection in lumbar, cervical and thoracic spinal cord segments in an organotypic rat model of glutamate-induced excitotoxicity. *J. Chem. Neuroanat.* **53**, 11–17 (2013).

160. Barish, M. E. Increases in intracellular calcium ion concentration during depolarization of cultured embryonic Xenopus spinal neurones. *J. Physiol.* **444**, 545–565 (1991).

161. Berridge, M. J., Lipp, P. & Bootman, M. D. THE VERSATILITY AND UNIVERSALITY OF CALCIUM SIGNALLING. **1**, 11–21 (2000).

162. Calvo-Rodriguez, M. *et al.* Increased mitochondrial calcium levels associated with neuronal death in a mouse model of Alzheimer's disease. *Nat. Commun.* **11**, 1–17 (2020).

163. Moody, W. J. & Bosma, M. M. Ion Channel Development , Spontaneous Activity , and Activity-Dependent Development in Nerve and Muscle Cells. *Physiol. Rev.* **85**, 883–941 (2005).

164. Momose-Sato, Y., Honda, Y., Sasaki, H. & Sato, K. Optical imaging of large-scale correlated wave activity in the developing rat CNS. *J. Neurophysiol.* **94**, 1606–1622 (2005).

165. Ben-Ari, Y., Gaiarsa, J. L., Tyzio, R. & Khazipov, R. GABA: a pioneer transmitter that excites immature neurons and generates primitive oscillations. *Physiol. Rev.* **87**, 1215 – 1284 (2007).

166. Holliday, J. & Spitzer, N. C. Spontaneous calcium influx and its roles in differentiation of spinal neurons in culture. *Dev. Biol.* **141**, 13–23 (1990).

167. Gomez, T. M., Snow, D. M. & Letourneau, P. C. Characterization of spontaneous calcium transients in nerve growth cones and their effect on growth cone migration. *Neuron* **14**, 1233–1246 (1995).

168. Spitzer, N. C. Activity-dependent neuronal differentiation prior to synapse formation: The functions of calcium transients. *J. Physiol. Paris* **96**, 73–80 (2002).

169. Ghosh, A. & Greenberg, M. E. Calcium signaling in neurons: molecular mechanisms and cellular consequences. *Science* **268**, 239–247 (1995).

170. Krasnow, A. M., Ford, M. C., Valdivia, L. E., Wilson, S. W. & Attwell, D. Regulation of developing myelin sheath elongation by oligodendrocyte calcium transients in vivo. *Nat. Neurosci.* **21**, (2018).

171. Hanson, M. G. & Landmesser, L. T. Normal patterns of spontaneous activity are required for correct motor axon guidance and the expression of specific guidance molecules. *Neuron* **43**, 687–701 (2004).

172. Holliday, J., Adams, R. J., Sejnowski, T. J. & Spitzer, N. C. Calcium-induced release of calcium regulates differentiation of cultured spinal neurons. *Neuron* **7**, 787–796 (1991).

173. Gu, X., Olson, E. C. & Spitzer, N. C. Spontaneous neuronal calcium spikes and waves during early differentiation. *J. Neurosci.* **4**, 6325–6335 (1994).

174. Feller, M. B. Spontaneous correlated activity in developing neural circuits. *Neuron* **22**, 653–656 (1999).

175. Wang, X. *et al.* Astrocytic Ca2+ signaling evoked by sensory stimulation in vivo. *Nat. Neurosci.* **9**, 816–823 (2006).

176. Petravicz, J., Fiacco, T. A. & McCarthy, K. D. Loss of IP3 receptor-dependent Ca2+ increases in hippocampal astrocytes does not affect baseline CA1 pyramidal neuron synaptic activity. *J. Neurosci.* **28**, 4967–4973 (2008).

177. Okubo, Y. & Iino, M. Visualization of astrocytic intracellular Ca 2+ mobilization . *J. Physiol.* **9**, 1671–1681 (2019).

178. Agarwal, A. *et al.* Transient Opening of the Mitochondrial Permeability Transition Pore Induces Microdomain Calcium Transients in Astrocyte Processes. *Neuron* **93**, 587-605.e7 (2017).

179. Volterra, A., Liaudet, N. & Savtchouk, I. Astrocyte Ca2+ signalling: An unexpected complexity. *Nat. Rev. Neurosci.* **15**, 327–335 (2014).

180. Bazargani, N. & Attwell, D. Astrocyte calcium signaling: The third wave. *Nat. Neurosci.* **19**, 182–189 (2016).

181. Heath, M. J. S., Womack, M. D. & MacDermott, A. B. Substance P elevates intracellular calcium in both neurons and glial cells from the dorsal horn of the spinal cord. *J. Neurophysiol.* **72**, 1192–1198 (1994).

182. Cirillo, G., Luca, D. De & Papa, M. Calcium Imaging of Living Astrocytes in the Mouse Spinal Cord following Sensory Stimulation. *Neural Plast.* **2012**, 1–7 (2012).

183. Salter, M. W. & Hicks, J. L. ATP-evoked increases in intracellular calcium in neurons and glia from the dorsal spinal cord. *J. Neurosci.* **14**, 1563–1575 (1994).

184. Ho, C., Hicks, J. & Salter, M. W. A novel P2-purinoceptor expressed by a subpopulation of astrocytes from the dorsal spinal cord of the rat. *Br. J. Pharmacol.* **116**, 2909–2918 (1995).

185. Serrano, A., Haddjeri, N., Lacaille, J.-C. & Robitaille, R. GABAergic network activation of glial cells underlies hippocampal heterosynaptic depression. *J. Neurosci.* **26**, 5370–5382 (2006).

186. Guerra-Gomes, S., Sousa, N., Pinto, L. & Oliveira, J. F. Functional roles of astrocyte calcium elevations: From synapses to behavior. *Front. Cell. Neurosci.* **11**, 1–7 (2018).

187. Nedergaard, M., Rodríguez, J. J. & Verkhratsky, A. Glial calcium and diseases of the nervous system. *Cell Calcium* **47**, 140–149 (2010).

188. Spitzer, N. C., Lautermilch, N. J., Smith, R. D. & Gomez, T. M. Coding of neuronal differentiation by calcium transients. *BioEssays* **22**, 811–817 (2000).

189. Fabbro, A., Pastore, B., Nistri, A. & Ballerini, L. Activity-independent intracellular Ca2+ oscillations are spontaneously generated by ventral spinal neurons during development in vitro. *Cell Calcium* **41**, 317–329 (2007).

190. Sibilla, S. *et al.* The patterns of spontaneous Ca2+ signals generated by ventral spinal neurons in vitro show time-dependent refinement. *Eur. J. Neurosci.* **29**, 1543–1559 (2009).

191. Brunet, N., Tarabal, O., Esquerda, J. E. & Calderó, J. Excitotoxic motoneuron degeneration induced by glutamate receptor agonists and mitochondrial toxins in organotypic cultures of chick embryo spinal cord. *J. Comp. Neurol.* **516**, 277–290 (2009).

192. Beyer, E. C., Paul, D. L. & Goodenough, D. A. Connexin family of gap junction proteins. *J. Membr. Biol.* 187–194 (1990).

193. Koulakoff, A., Ezan, P. & Giaume, C. Neurons control the expression of connexin 30 and connexin 43 in mouse cortical astrocytes. *Glia* 1299–1311 (2008).

194. Cheung, G., Chever, O. & Rouach, N. Connexons and pannexons: newcomers in neurophysiology. *Front. Cell. Neurosci.* 1–19 (2014).

195. Theis, M. & Giaume, C. Connexin-based intercellular communication and astrocyte heterogeneity. *Brain Res.* **1487**, 88–98 (2012).

196. Leithe, E., Mesnil, M. & Aasen, T. The connexin 43 C-terminus: A tail of many tales. *Biochim. Biophys. Acta - Biomembr.* **1860**, 48–64 (2018).

197. Xie, H. Y., Cui, Y., Deng, F. & Feng, J. C. Connexin: A potential novel target for protecting the central nervous system? *Neural Regen. Res.* **10**, 659–666 (2015).

198. Kameritsch, P., Pogoda, K. & Pohl, U. Channel-independent influence of connexin 43 on cell migration. *Biochim. Biophys. Acta - Biomembr.* 1993–2001 (2012).

199. Matsuuchi, L. & Naus, C. C. Gap junction proteins on the move: connexins, the cytoskeleton and migration. *Biochim. Biophys. Acta - Biomembr.* 94–108 (2013).

200. Giaume, C. & Liu, X. From a glial syncytium to a more restricted and specific glial networking. *J. Physiol. Paris* **106**, 34–39 (2012).

201. Nagy, J. I., Li, W., Hertzberg, E. L. & Marotta, C. A. Elevated connexin43 immunoreactivity at sites of amyloid plaques in Alzheimer's disease. *Brain Res.* **717**, 173–178 (1996).

202. John, G. R. *et al.* IL-1beta differentially regulates calcium wave propagation between primary human fetal astrocytes via pathways involving P2 receptors and gap junction channels. *Proc. Natl. Acad. Sci.* **96**, 11613–11618 (1999).

203. Retamal, M. A. *et al.* Cx43 hemichannels and gap junction channels in astrocytes are regulated oppositely by proinflammatory cytokines released from activated microglia. *J. Neurosci.* **27**, 13781–13792 (2007).

204. Rouach, N. *et al.* Gap junctions and connexin expression in the normal and pathological central nervous system. Biol Cell. *Biol Cell* **94**, 457–475 (2002).

205. Nagy, J. I. & Li, W. E. A brain slice model for in vitro analyses of astrocytic gap junction and connexin43 regulation: actions of ischemia, glutamate and elevated potassium. *Eur. J. Neurosci.* **12**, 4567– 4572 (2000).

206. Liao, C. K., Jeng, C. J., Wang, H. S., Wang, S. H. & Wu, J. C. Lipopolysaccharide induces degradation of connexin43 in rat astrocytes via the ubiquitin-proteasome proteolytic pathway. *PLoS One* **8**, 1–11 (2013).

207. Brand-Schieber, E. *et al.* Connexin43, the Major Gap Junction Protein of Astrocytes, Is Down-Regulated in Inflamed White Matter in an Animal Model of Multiple Sclerosis. *J. Neurosci. Res.* **80**, 798–808 (2005).

208. Zhang, F. F., Morioka, N., Nakashima-Hisaoka, K. & Nakata, Y. Spinal astrocytes stimulated by tumor necrosis factor-α and/or interferon-γ attenuate connexin 43-gap junction via c-jun terminal kinase activity. *J. Neurosci. Res.* **91**, 745–756 (2013).

209. Almad, A. A. *et al.* Connexin 43 affects disease progression and motor neuron toxicity in Amyotrophic Lateral Sclerosis. *Glia* **64**, 1154–1169 (2016).

210. Sanderson, M. J. Intercellular Waves of Communication. *Physiology* **11**, 262–269 (1996).

211. De Bock, M. *et al.* Connexin 43 hemichannels contribute to cytoplasmic Ca 2+ oscillations by providing a bimodal Ca 2+-dependent Ca 2+ entry pathway. *J. Biol. Chem.* **287**, 12250–12266 (2012).

212. Cornell-Bell, A. H., Finkbeiner, S. M., Cooper, M. S. & Smith, S. J. Glutamate induces calcium waves in cultured astrocytes: Long-range glial signaling. *Science (80-.).* **247**, 470–473 (1990).

213. Nedergaard, M. Direct signaling from astrocytes to neurons in cultures of mammalian brain cells. *Science (80-.).* **263**, 1768–1771 (1994).

214. Leznik, E. & Llinás, R. Role of Gap Junctions in Synchronized Neuronal Oscillations in the Inferior Olive. *J. Neurophysiol.* **94**, 2447–2456 (2005).

215. Scemes, E. & Giaume, C. Astrocyte Calcium Waves : What They Are and What They Do. *Glia* **725**, 716–725 (2006).

216. Chever, O., Lee, C. Y. & Rouach, N. Astroglial connexin43 hemichannels tune basal excitatory synaptic transmission. *J. Neurosci.* **34**, 11228–11232 (2014).

217. Contreras, J. E. *et al.* Role of connexin-based gap junction channels and hemichannels in ischemia-induced cell death in nervous tissue. *Brain Res. Rev.* **47**, 290–303 (2004).

218. Wang, N. *et al.* Connexin targeting peptides as inhibitors of voltage- and intracellular Ca2+-triggered Cx43 hemichannel opening. *Neuropharmacology* **75**, 506–516 (2013).

219. Davidson JO, Green CR, Bennet L, et al. A key role for connexin hemichannels in spreading ischemic brain injury. *Curr Drug Target* **14**, 36–46 (2013).

220. O'Carroll, S. J., Alkadhi, M., Nicholson, L. F. B. & Green, C. R. Connexin43 mimetic peptides reduce swelling, astrogliosis, and neuronal cell death after spinal cord injury. *Cell Commun. Adhes.* **15**, 27–42 (2008).

221. O'Carroll, S. J., Gorrie, C. A., Velamoor, S., Green, C. R. & Nicholson, L. F. B. Connexin43 mimetic peptide is neuroprotective and improves function following spinal cord injury. *Neurosci. Res.* **75**, 256–267 (2013).

222. Cronin, M., Anderson, P. N., Cook, J. E., Green, C. R. & Becker, D. L. Blocking connexin43 expression reduces inflammation and improves functional recovery after spinal cord injury. *Mol cell neurosci* **39**, 152–160 (2008).

223. Huang, C. *et al.* Critical role of connexin 43 in secondary expansion of traumatic spinal cord injury. *J. Neurosci.* **32**, 3333–3338 (2012).

224. Zhou, J. J., Cheng, C., Qiu, Z., Zhou, W. H. & Cheng, G. Q. Decreased connexin 43 in astrocytes inhibits the neuroinflammatory reaction in an acute mouse model of neonatal sepsis. *Neurosci. Bull.* **31**, 763–8 (2015).

225. Umebayashi, D. *et al.* Blockade of gap junction hemichannel protects secondary spinal cord injury from activated microglia-mediated glutamate exitoneurotoxicity. *J. Neurotrauma* **31**, 1967–1974 (2014).

226. Yin, X. *et al.* Roles of astrocytic connexin-43, hemichannels, and gap junctions in oxygen-glucose deprivation/reperfusion injury induced neuroinflammation and the possible regulatory mechanisms of salvianolic acid B and carbenoxolone. *J. Neuroinflammation* **15**, 1–24 (2018).

227. Chen, G. *et al.* Connexin-43 induces chemokine release from spinal cord astrocytes to maintain late-phase neuropathic pain in mice. *Brain* **137**, 2193–2209 (2014).

228. Rossi, S. *et al.* Interleukin-1β causes synaptic hyperexcitability in multiple sclerosis. *Ann. Neurol.* **71**, 76–83 (2012).

229. Furlan, R. *et al.* Caspase-1 regulates the inflammatory process leading to autoimmune demyelination. *J. Immunol.* **163**, 2403–2409 (1999).

230. Letournel-Boulland, M. L., Fages, C., Rolland, B. & Tardy, M. Lipopolysaccharides (LPS), up-regulate the IL-1-mRNA and down-regulate the glial fibrillary acidic protein (GFAP) and glutamine synthetase (GS)-mRNAs in astroglial primary cultures. *Eur Cytokine* 51–6 (1994).

231. Pocock, J. M. & Kettenmann, H. Neurotransmitter receptors on microglia. *Trends Neurosci.* **30**, 527–35 (2007).

232. Funk, K. *et al.* Modulation of chloride homeostasis by inflammatory mediators in dorsal root ganglion neurons. *Mol. Pain* (2008).

233. Coull, J. A. M. Trans-synaptic shift in anion gradient in spinal lamina I neurons as a mechanism of neuropathic pain. *Nature* **424**, 938–42 (2003).

234. Dunning, D. D., Hoover, C. L., Soltesz, I., Smith, M. A. & O'Dowd, D. K. GABA(A) receptor-mediated miniature postsynaptic currents and alpha-subunit expression in developing cortical neurons. *J. Neurophysiol.* 3286–97 (1999).

235. Moroni, M., Meyer, J. O., Lahmann, C. & Sivilotti, L. G. In glycine and GABA(A) channels, different subunits contribute asymmetrically to channel conductance via residues in the extracellular domain. *J. Biol. Chem.* **286**, 13414–22 (2011).

236. Dixon, C., Sah, P., Lynch, J. W. & Keramidas, A. GABAA receptor α and γ subunits shape synaptic currents via different mechanisms. *J. Biol. Chem.* **289**, 5399–411 (2014).

237. Lewis, R. S. Calcium signalling mechanisms in T lymphocytes. *Annu. Rev. Immunol.* **19**, 497–521.

238. Quintana, A. *et al.* Calcium microdomains at the immunological synapse: how ORAI channels, mitochondria and calcium pumps generate local calcium signals for efficient T-cell activation. *EMBO J.* **30**, 3895–3912 (2011).

239. Schwarz, A. *et al.* Fine-tuning of regulatory T cell function: the role ofcalcium signals and naive regulatory T cells for regulatory T cell deficiency in multiple sclerosis. *J. Immunol.* **190**, 4965–4970 (2013).

240. Usmani, S. *et al.* 3D meshes of carbon nanotubes guide functional reconnection of segregated spinal explants. *Sci. Adv.* **2**, 1–10 (2016).

241. Streit, J. Regular Oscillations of Synap tic Activity in Spinal Networks In Vitro. **70**, (1993).

242. Rasmussen, R., Nedergaard, M. & Petersen, N. C. Sulforhodamine 101, a widely used astrocyte marker, can induce cortical seizure-like activity at concentrations commonly used. *Sci. Rep.* **6**, 1–9 (2016).

243. McDonald, J. W., Althomsons, S. P., Hyrc, K. L., Choi, D. W. & Goldberg, M. P. Oligodendrocytes from forebrain are highly vulnerable to AMPA/kainate receptor-mediated excitotoxicity. *Nat. Med.* **4**, 291– 297 (1998).

244. Ren, J., Momose-Sato, Y., Sato, K. & Greer, J. J. Rhythmic neuronal discharge in the medulla and spinal cord of fetal rats in the absence of synaptic transmission. *J. Neurophysiol.* **95**, 527–534 (2006).

245. Hjorth, J., Blackwell, K. T. & Kotaleski, J. H. Gap junctions between striatal fast-spiking interneurons regulate spiking activity and synchronization as a function of cortical activity. *J. Neurosci.* **16**, 5276–5286 (2009).

246. Wang, N. *et al.* Connexin mimetic peptides inhibit Cx43 hemichannel opening triggered by voltage and intracellular Ca2+ elevation. *Basic Res. Cardiol.* **107**, 17 (2012).

247. Bazzigaluppi, P., Weisspapir, I., Stefanovic, B., Leybaert, L. & Carlen, P. L. Astrocytic gap junction blockade markedly increases extracellular potassium without causing seizures in the mouse neocortex. *Neurobiol. Dis.* **101**, 1–7 (2017).

248. Contreras, J. E. *et al.* Metabolic inhibition induces opening of unapposed connexin 43 gap junction hemichannels and reduces gap junctional communication in cortical astrocytes in culture. *Proc. Natl. Acad. Sci. U. S. A.* **99**, 495–500 (2002).

Appendix

1. Microglial cells express TLR4 receptors

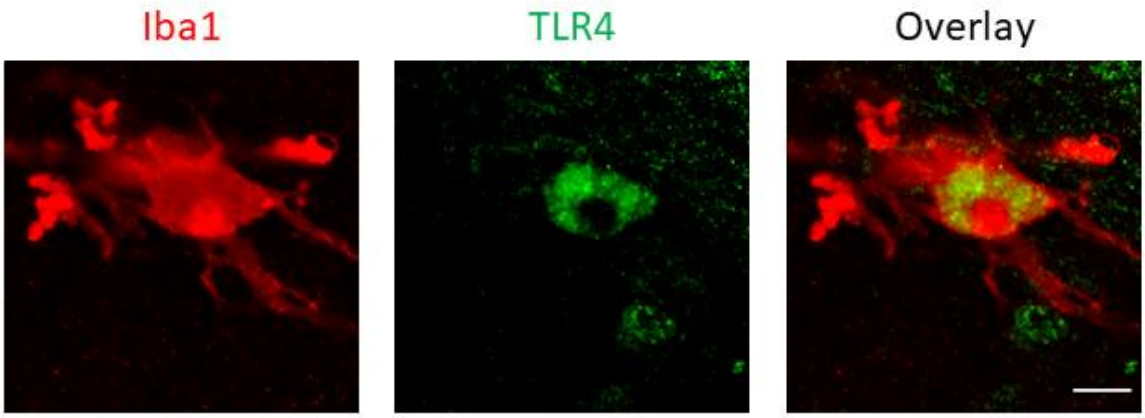

Representative confocal images of 2 WIV control slices immunolabeled for Iba1 in red and TLR4 in green, marker respectively for microglia and TRL4. For the staining, fixed samples (4% PFA, 1 h, RT) were quenched with 0.1 M of glycine solution for 10 min. Slices were blocked with PBS 1×, 10% FBS (Sigma), 1% BSA (Sigma) and 0.3% Triton X-100 (Sigma) at RT for 1 h and then incubated overnight at 4 °C with anti-Iba1 (rabbit polyclonal, 1:500, Wako) and anti-TLR4 (mouse monoclonal, 1:500, Invitrogen) primary antibodies. The third image shows the overlap between the two signals, which means that the microglial cells in our slices system express the TLR4 on their surfaces, necessary to trigger the inflammatory responses. Together with the supernatants essay, necessary to determine the portfolio of synthetized cytokines and chemokines during the induced inflammation (see Figure 3, Methods and Results section, paper 1[151]), this result confirms

that microglia have the toolkits to switch from a priming and surveillant stage to an active one, capable of producing active molecules to deal with the inflammation. Scale bar 5 µm.

2. Oligodendrocytes disruption after acute treatment with CKs and LPS

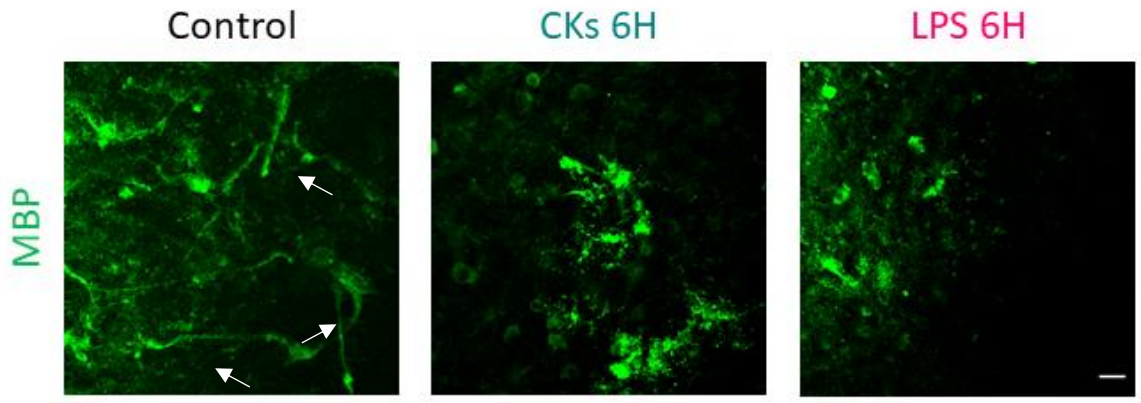

Representative immunostaining of the different experimental conditions, performed on 3 WIV slices with the MBP antibody. For the staining, fixed samples (4% PFA, 1 h, RT) were quenched with 0.1 M of glycine solution for 10 min. Slices were blocked with PBS 1×, 10% FBS (Sigma), 1% BSA (Sigma) and 0.3% Triton X-100 (Sigma) at RT for 1 h and then incubated overnight at 4 °C with anti-MBP primary antibody (rabbit polyclonal; 1:500, Abcam), able to recognize the myelin. We can observe that after the CKs and LPS 6 hours treatments, disruption of the myelin envelopes occurs, if compared to the Control, since it is not possible to see the typical filamentous myelin shape, underlined by the arrows in the control, suggesting us that probably there is a damage in the oligodendrocytes and the establish of the myelin is not occurring in the proper way. Scale bar 25 µm.

frontiers in Immunology

METHODS
published: 24 March 2020
doi: 10.3389/fimmu.2020.00471

Optimization of Organotypic Cultures of Mouse Spleen for Staining and Functional Assays

Francesca Finetti[1], Nagaja Capitani[1], Noemi Manganaro[1], Vanessa Tatangelo[1], Francesca Libonati[1], Giulia Panattoni[2], Ivo Calaresu[2], Laura Ballerini[2], Cosima T. Baldari[1] and Laura Patrussi[1]**

[1] Department of Life Sciences, University of Siena, Siena, Italy, [2] International School for Advanced Studies (SISSA/ISAS), Trieste, Italy

By preserving cell viability and three-dimensional localization, organotypic culture stands out among the newest frontiers of cell culture. It has been successfully employed for the study of diseases among which neoplasias, where tumoral cells take advantage of the surrounding stroma to promote their own proliferation and survival. Organotypic culture acquires major importance in the context of the immune system, whose cells cross-talk in a complex and dynamic fashion to elicit productive responses. However, organotypic culture has been as yet poorly developed for and applied to primary and secondary lymphoid organs. Here we describe in detail the development of a protocol suitable for the efficient cutting of mouse spleen, which overcomes technical difficulties related to the peculiar organ texture, and for optimized organotypic culture of spleen slices. Moreover, we used microscopy, immunofluorescence, flow cytometry, and qRT-PCR to demonstrate that the majority of cells residing in spleen slices remain alive and maintain their original location in the organ architecture for several days after cutting. The development of this protocol represents a significant technical improvement in the study of the lymphoid microenvironment in both physiological and pathological conditions involving the immune system.

Keywords: organotypic culture, spleen, vibratome, precision-cut, white pulp, red pulp, lymphoma

OPEN ACCESS

Edited by:
Fabrizio Mattei,
Higher Institute of Health (ISS), Italy

Reviewed by:
Alessandro Poggi,
San Martino Hospital (IRCCS), Italy
Guilan Shi,
University of South Florida, United States

****Correspondence:***
Cosima T. Baldari
cosima.baldari@unisi.it
Laura Patrussi
patrussi2@unisi.it

Specialty section:
This article was submitted to Cancer Immunity and Immunotherapy, a section of the journal Frontiers in Immunology

Received: *26 November 2019*
Accepted: *28 February 2020*
Published: *24 March 2020*

Citation:
Finetti F, Capitani N, Manganaro N, Tatangelo V, Libonati F, Panattoni G, Calaresu I, Ballerini L, Baldari CT and Patrussi L (2020) Optimization of Organotypic Cultures of Mouse Spleen for Staining and Functional Assays. Front. Immunol. 11:471. doi: 10.3389/fimmu.2020.00471

INTRODUCTION

Organotypic culture has emerged as a powerful technique which allows the analysis of tissue behavior in a variety of conditions. Initially developed as an alternative to classical 2-D *in vitro* culture of neurons, slices obtained by sectioning the brain region of interest with tissue choppers allowed to maintain neurons alive outside of the body and were found to be suitable for electrophysiological studies (1). Preparation and *in vitro* growth of these slices were progressively optimized to be maintained in culture for several days thanks to the introduction of modern tissue choppers such as vibrating microtomes, that produce thinner and less damaged slices, and tissue support systems, such as agarose, to preserve the 3-D organization of the tissue (1, 2).

Organotypic culture has been extended to several other organs of the neuroendocrine system (1) and, more recently, to tumor-derived tissues (3). Of note, only one report describes the application of this technique to lymphoid tissues of human origin (4), notwithstanding the wealth of information generated over the last decade on the complex interactions that

occur among immune, stromal, and cancer cells (5, 6). Cancer immunotherapies, now applied to a variety of cancers, often result in heterogeneous responses, to which the specific features of the individual tumor microenvironment may contribute (7). Hence, the optimization of organotypic culture of lymphoid organs is critically important to understand the immune cell microenvironment in a variety of tumors.

Efficient preparation of spleen slices faces the challenge posed by the complex structure and texture of this lymphoid organ. The spleen is indeed organized as a "tree" of branching arterial vessels, in which the smaller arterioles end in a venous sinusoidal system. The organ is surrounded by a fibrous capsule of connective tissue, from which the connective trabeculae protrude into the splenic tissue to support vessels (8). Due to this peculiar organ texture, preparation of spleen slices with a chopper is precluded. Spleen is crushed by the blade and slices are not useful for further analyses (unpublished observations).

We developed a new protocol that allowed us to efficiently cut mouse spleens in intact slices and to maintain these alive and responsive for at least 48 h, making them suitable for functional assays. The protocol, that is a modification of protocols developed to obtain precision-cut slices of mouse brain, liver and lung (9–11), is based on the sequential following steps: (1) spleen inclusion into agarose blocks; (2) precision-cut using a vibrating microtome; and (3) 48-h culture of spleen slices. The protocol developed for the preparation of organotypic cultures of mouse spleens has turned out to be a valuable tool to (i) prepare spleen slices with a sufficient degree of tissue integrity; and (ii) maintain this complex tissue in culture for days, in order to be used for functional assays.

MATERIALS AND EQUIPMENT

Spleen Harvesting

Scissors, micro-dissecting forceps, 2-ml polypropylene microtubes (Sarstedt), ice box, ice. Culture medium: high glucose Dulbecco Modified Eagle's Medium (DMEM) (Sigma-Aldrich) with 2 U/ml penicillin G (Sigma-Aldrich) and 7.5% bovine calf serum (BCS, Hyclone).

Precision-Cut of Mouse Spleen

Scissors, curved micro-dissecting forceps, scalpel, small spatula, plastic film, tweezers, agarose, thermometer, microwave, 50 ml beaker, milliQ water, phosphate-buffered saline (PBS), 3.5 ml transfer-pipette (Sarstedt), Compresstome® VF-300-0Z Vibrating Microtome with Specimen tube and Syringe chilling block (Precisionary instruments, Greenville, NC, USA), diagnostic microscope slides (Menzel Glaser- Thermo Scientific), pipettes, pipette tips.

Culture of Spleen Slices

Laminar airflow chamber, sterile 48-well plates with flat bottom (Sarstedt), cell culture incubator with 5% CO_2. Culture medium: high glucose Dulbecco Modified Eagle's Medium (DMEM) (Sigma-Aldrich) with 2 U/ml penicillin G (Sigma-Aldrich) and 7.5% BCS (Hyclone).

METHODS

Animals

C57BL/6J mice were housed in a pathogen-free and climate-controlled (20 ± 2°C, relative humidity 55 ± 10%) animal facility at the University of Siena. Mice were provided with water and pelleted diet *ad libitum*. All cages are provided with environmental enrichment in the form of nesting material and mouse houses. Procedures and experimentation were carried out in accordance with the 2010/63/EU Directive and approved by the Italian Ministry of Health. Animals were euthanized and spleens were harvested, immediately transferred to ice-cold culture medium (see "Materials" section) and stored on ice.

Slice Stimulation, RNA Purification, and RT-PCR

RNA extractions were carried out on samples composed of 1, 3, or 5 spleen slices. Samples were homogenized in 1.5 ml microtubes using polypropylene double-ended pestle (Sigma-Aldrich) in 350 µl RLT lysis buffer of the RNeasy Mini Kit (Qiagen) until completely homogenized. RNA was then extracted and retrotranscribed as described (12). RNA amount and quality were assessed using QIAxpert System (Qiagen). Real-time PCR was performed in triplicate on 96-well optical PCR plates (Sarstedt AG, Nümbrecht, Germany) using SSo FastTM EvaGreenR SuperMix (Biorad Laboratories, Hercules, CA) and a CFX96 Real-Time system (Bio-Rad Laboratories, Waltham, MA). Results were processed and analyzed as described (12). Transcript levels were normalized to GAPDH. Spleen slices (3 slices per sample) either freshly cut or cultured for 48 h at 37°C in culture medium were stimulated with A23187 (Merck, cat. C7522, 500 ng/ml) and phorbol 12-myristate 13-acetate (PMA, Merck, cat. 524400, 100 ng/ml) in culture medium for 6 h at 37°C, homogenized in 350 µl RLT lysis buffer and RNA was extracted as described above. Primers used for amplification were: mouse CCL19 Forward 5′-3′, CAA GAA CAA AGG CAA CAG C; mouse CCL19 Reverse 5′-3′, CGG CTT TAT TGG AAG CTC TG; mouse CXCL13 Forward 5′-3′, CAT CAT GAG GTG GTG CAA AG; mouse CXCL13 Reverse 5′-3′, GGG TCA CAG TGC CAA AGG AAT; mouse GAPDH Forward 5′-3′, AAC GAC CCC TTC ATT GAC; mouse GAPDH Reverse 5′-3′, TCC ACG ACA TAC TCA GCA C; mouse IL-2 Forward 5′-3′, CCC TTG CTA ATC ACT CCT CA; mouse IL-2 Reverse 5′-3′, GAA GTG GAG CTT GAA GTG GG; mouse IL-10 Forward 5′-3′, CCG GAC AGC ACA CTT CAC AG; mouse IL-10 Reverse 5′-3′, TCC ACC ATT TCC CAG ACA AC; mouse IFN-γ Forward 5′-3′, ACT GGC AAA AGG ATG GTG AC; mouse IFN-γ Reverse 5′-3′, AAA CTT GGC AAT CTC ATG AAT G.

Optical and Immunofluorescence Microscopy

Spleen slices were carefully placed on diagnostic microscope slides (Menzel Glaser-Thermo Scientific), left either unlabeled or stained for 8 min with Trypan blue solution 0.4% (Sigma-Aldrich) diluted 1:2 in PBS, washed with PBS until complete removal of the exceeding dye, covered with 24 × 60 mm coverslips (VWR) and observed with SZX12 stereo light

microscope (Olympus) and DMRB microscope (Leica microsystems) equipped with Zeiss AxioCam MRc5 digital camera. Images were processed using the AxioVision Rel. 4.6.3. software.

Immunofluorescence microscopy was performed following a modification of the protocol previously described (13). Briefly, spleen slices were transferred with a small spatula to 10-well diagnostic microscope slides (Thermo Scientific), one slice/well, and incubated for 30 min at RT with 30 µl fixation buffer (4% paraformaldehyde in PBS) in the dark, washed with PBS and incubated for 30 min at RT with 30 µl permeabilization solution (PBS 0.1% BSA plus 0.01% Triton X-100). Slices were then stained with 30 µl/well of either unconjugated primary Ab or fluorescently labeled Ab in Hanks' salts at RT in the dark for 2 h, washed with PBS and incubated with 30 µl/well of fluorochrome-conjugated secondary antibodies at RT in the dark for 2 h. Slides were washed with Hanks' salts; mounting medium (PBS 90% glycerol) was added and slides covered with 24 × 60 mm coverslips (VWR) and sealed with conventional nail polish. Images were acquired on Zeiss LSM700 confocal microscope using 63 ×, 40 × and 10 × objectives. Primary antibodies: FITC Rat anti-mouse CD19 (BD Pharmingen, cat. 553758) 1:30 in Hanks' salts; Alexa Fluor 488 anti-mouse CD3ε (eBiosciences, cat. 53-0031-82) 1:30 in Hanks' salts; Rat anti-mouse ER-TR7 (ABD Serotec, cat. MCA2402) 1:50 in Hanks' salts; mouse monoclonal anti-Follicular DC Marker (Santa Cruz, cat. sc-58529, Ki-M9R clone) 1:50 in Hanks' salts. Secondary antibodies: DyLight® goat anti-rat 488 (Bethyl, cat. A110-105-D2) and 550 (Bethyl, cat. A110-105-D3) 1:100 in Hanks' salts; Alexa Fluor goat anti-mouse 488 (Thermo-Fisher scientific, cat. A-11001) 1:100 in Hanks' salts; isotype control: FITC Rat IgG2a (BD Pharmingen, cat. 553924).

Flow Cytometry, Chemotaxis Assays, and Trypan Blue Exclusion

Spleen slices were disgregated using 70-µm Cell strainer filter (BD Falcon™) and 1 ml syringe (BioSigma). Cell death was measured by flow cytometry on slice-derived splenocytes by quantifying the % of either Annexin V^+/Propidium Iodide $(PI)^-$ or PI^+ cells as described (12). Briefly, 2×10^5 cells were resuspended in 200 µl PBS and stained with Annexin V FITC (eBiosciences) for 15 min at RT. When required, PI was added to the samples at the final concentration of 10 ng/ml immediately before the flow cytometric analysis using Guava Easy Cyte (Millipore, Billerica, MA) cytometer. Alternatively, cells were stained with Annexin V PE (eBiosciences), fixed (fixation buffer, 4% paraformaldehyde in PBS) and permeabilized (permeabilization solution, PBS 0.1% BSA plus 0.01% Triton X-100), and T lymphocytes, B lymphocytes, follicular dendritic cells (FDC) or reticular fibroblasts were stained with anti-mouse CD3ε (eBiosciences) 1:30 in PBS, Rat anti-mouse CD19 (BD Pharmingen) 1:30 in PBS, anti-Follicular DC Marker 1:50 in PBS, and Rat anti-mouse ER-TR7, respectively. Surface CXCR4 and CCR7 were stained with either Rabbit anti-CXCR4 antibody (Abcam, cat. AB124824), 1:50 in PBS, or Rabbit monoclonal anti-CCR7 antibody (Novus Biologicals, cat. NB110-55680, Y59 clone), 1:50 in PBS, and Alexa Fluor goat anti-rabbit 488 secondary antibodies (Thermo-Fisher scientific, cat. A-11002) 1:400 in PBS, in combination with PE Rat anti-mouse CD3ε (eBiosciences, cat. 145-2C11, 2C11 clone) 1:30 in PBS or PE Mouse anti-mouse CD22.2 (BD Pharmingen, cat. 553384, Cy34.1 clone) 1:30 in PBS, and analyzed by flow cytometry. Chemotaxis assays were modified from the protocol reported in (14). Briefly, spleen slices were placed on the upper well of Boyden chamber, and allowed to position over the porous membrane of the insert. CXCL12 (Merck, cat. SRP4388, 100 ng/ml) or MIP-3β (Merck, cat. SRP4495, 100 ng/ml) were diluted in culture medium and placed in the lower well of the chamber. Cells were allowed to migrate for 3 h at 37°C, then the migrated cells were recovered from the lower chamber and stained with PE Rat anti-mouse CD3ε (eBiosciences) 1:30 in PBS and FITC Rat anti-mouse CD19 (BD Pharmingen) 1:30 in PBS, and analyzed by flow cytometry. Slice-derived splenocytes were stained for 8 min with Trypan blue solution 0.4% (Sigma-Aldrich) diluted 1:2 in PBS and Trypan $blue^+$ cells were counted using an optical microscope. The percentage of dead cells was assessed by calculating the percentage of Trypan $blue^+$ cells over the total cell count.

Statistical Analyses

Mean values, standard deviations and Student's *t*-test were calculated using GraphPad (Prism 7). A level of $p<0.05$ was considered statistically significant.

Stepwise Procedure for Preparation and *in vitro* Culture of Spleen Slice

Spleen Preparation for Sectioning

- Lay down spleen on clean plastic film using tweezers or curved micro-dissecting forceps;
- Carefully remove fat, fur and debris using scissors and/or scalpel;
- Immediately transfer spleen into ice-cold culture medium until next step.

Spleen Inclusion into the Agarose Block

- Set up Compresstome® VF-300-0Z Vibrating Microtome (Precisionary Instruments, Greenville, NC, USA) following the manufacturers' instructions;
- Pre-chill syringe chilling block (Precisionary Instruments, Greenville, NC, USA) in ice for at least 10 min;
- Wash diagnostic microscope slides (Thermo Scientific) with MilliQ, then wash with absolute ethanol and allow them to air-dry;
- In a 50 ml beaker prepare 3% agarose solution in MilliQ, melt it by microwave and allow it to cool down to 45°C at room temperature, repeatedly checking the temperature with thermometer and shaking the solution to avoid agarose clumps;
- Open the provided specimen tube (Precisionary Instruments, # VF-SPS-VM-12.5) and fill it with 3–4 ml of 45°C agarose solution (**Figure 1A**). Check the temperature with thermometer until it reaches 38°C (**Figure 1B**).

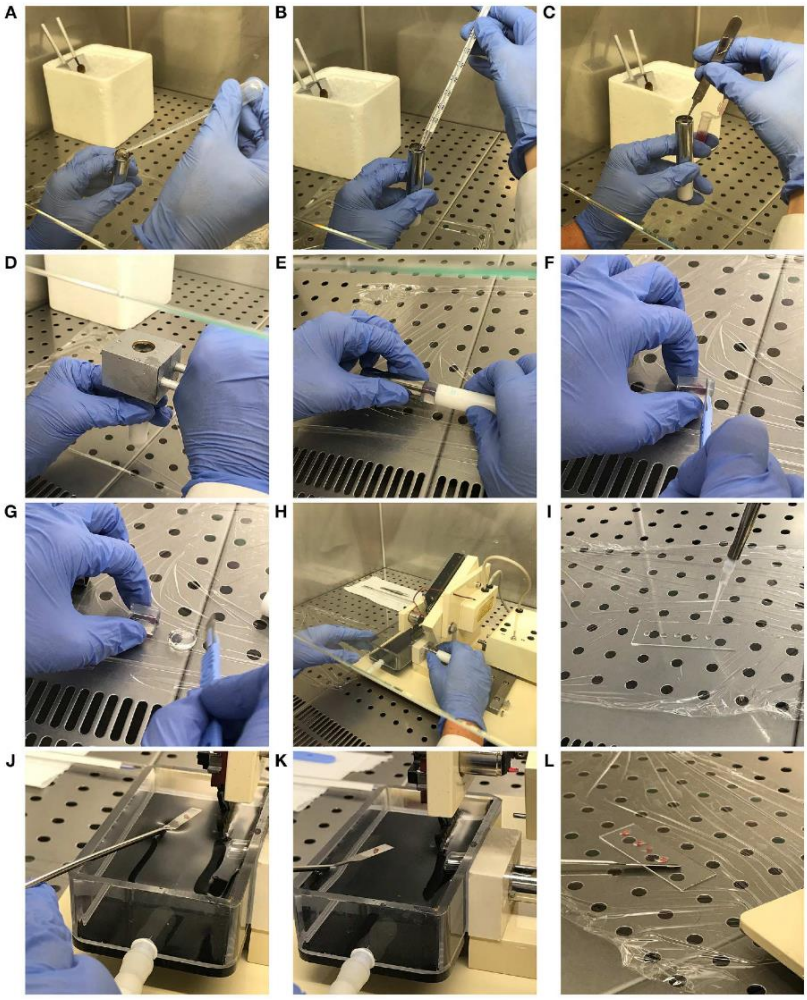

FIGURE 1 | Mouse spleen inclusion in agarose and precision-cut: step-by-step description of the protocol. **(A)** Syringe chilling block pre-cooling and specimen tube filling. **(B)** Agarose temperature checking. **(C)** Spleen inclusion into the agarose block. **(D)** Chilling of the spleen-containing agarose block. **(E)** Extraction of the agarose block containing the embedded sample. **(F,G)** Exceeding agarose removal from the agarose block. **(H)** Specimen tube insertion into the sample housing. **(I)** Preparation of the microscope slide with PBS drops. **(J,K)** Spleen slice preparation and recovery from the buffer tank with a spatula. **(L)** Spleen slice transfer in the PBS drops of the microscope slide.

- Carefully pick up the spleen from ice-cold culture medium using tweezers and rapidly insert it vertically into the agarose-containing specimen tube. Pay attention to maintain the spleen in a vertical position during this step (**Figure 1C**).
- Immediately place the pre-chilled syringe chilling block (see step 3.6.2.2) over the specimen tube and leave immobile for at least 2 min (**Figure 1D**). This process accelerates agarose solidification and chills the whole sample.

Preparation of Spleen Slices

- Extract the agarose block containing the embedded sample from the specimen tube and place it on clean plastic film (**Figure 1E**). Proceed to remove the portions of agarose which do not contain organ portions with the scalpel, carefully placing the blade perpendicular to the agarose block (**Figures 1F,G**). Place the carved agarose block back in the specimen tube. This step allows the specimen tube containing

agarose-embedded full-length spleen to fit with the Motor Box plunger of the Compresstome.
- Insert the specimen tube in the housing and fill the buffer tray with sterile PBS (**Figure 1H**).
- In order to obtain non-damaged spleen slices, set the cut speed to the minimum and the blade oscillation to the maximum in the instrument control box. Importantly, set the slice thickness to ∼ 230 μm. This is absolutely required to obtain good quality spleen slices. Lower thickness results in profound damage of the spleen structure, while higher thickness does not allow microscope observation and analyses.
- Proceed to spleen slice preparation following the technical instructions provided by the manufacturer.
- While proceeding with tissue cut, place 4–5 drops of PBS in each washed microscope slide with a 200 μl pipette (**Figure 1I**).
- Recover spleen slices using a spatula (**Figures 1J,K**) and transfer them in the PBS drops (**Figure 1L**), carefully removing any trace of agarose.

Culture of Spleen Slices

- Transfer slices from the microscope slide to a sterile 48-well plate with flat bottom (Sarstedt) containing 100 μl culture medium in a laminar airflow chamber under sterile conditions (one or more slides per well).
- Maintain in cell culture incubator at 37°C and with 5% CO_2.
- Check the volume of culture medium every day and be careful not to exceed 100 μl to avoid oxygen deprivation. In case of evaporation, add just the culture medium amount required to cover the slice.

Critical Parameters and Trouble Shooting

The efficiency of the whole process primarily depends on step 3.6.2., which describes the building of the agarose block containing the spleen (**Figures 1A–D**). The temperature of the agarose solution must not exceed 40°C and should ideally be maintained around 38°C to avoid organ damage. Moreover, this temperature allows optimal insertion of the spleen into the agarose, which then quickly polymerizes thereby maintaining the organ in the exact position and vertical orientation where it was placed. This is particularly important since this bean-like organ tends to rotate and lie down over the specimen tube when the agarose solution is too fluid, thereby precluding well-oriented spleen cut.

Non-intact slides, such as slides with breaks in the spleen capsule, must not be used for further analyses since they do not maintain the original organ architecture and they rapidly crinkle. In order to preserve slice integrity, fat and other debris must be removed from the spleen before cut, and air bubble formation in the agarose during the inclusion step must be avoided. Small bubbles are nevertheless quite common since tweezers, sometimes immersed for a few seconds into agarose to maintain the spleen vertical, generate bubbles when extracted from the solidifying agarose.

Although some slices are still included in the polymerized agarose when transferred to the PBS-containing buffer tray, the majority detach from the agarose disk during cut and float in the PBS, making it extremely hard to retrieve them without inflicting severe damages to the organ structure. We adjusted this step of the protocol using a small spatula to get close to and capture even the smaller PBS-floating slices.

RESULTS

Spleen Slices Cultured for 48 h *in vitro* Preserve Organ Integrity

Slices obtained applying the protocol described in the "Methods" section were transferred to diagnostic microscope slides and either left unstained or stained with Trypan blue. Optical microscopy was used to evaluate organ architecture. As shown in **Figure 2**, fresh slices were intact and the splenic structure was unaffected by the cut, with red pulp spacing out wide white pulp areas (**Figure 2A**).

Slices were cultured for 24, 48, 72, and 96 h in 48-well plates at 37°C with culture medium, one slice per well. To evaluate whether the *in vitro* culturing procedure affects organ architecture, cultured slices were transferred to diagnostic microscope slides and subjected to optical microscopy. As shown in **Figure 2**, slices cultured for 24 and 48 h were intact and both the splenic structure and the red-white pulp ratio remained almost unchanged when compared to fresh tissues (**Figures 2B,C**). Beginning from 72 h we observed a high degree of disruption of the slice architecture with wide necrotic zones affecting both the red and the white pulp (**Figure 2D**) and small ruptures lacerating both the organ texture and the surrounding capsule (see dashed rectangles in **Figure 2D**), possibly due to extreme slice fragility. We were unable to perform optical microscopy of 96 h-cultured slices, which were extremely damaged during their transfer to the microscope slides (data not shown). Our data suggest that 48 h is the longest time point of *in vitro* culture which maintains unaffected the architecture of spleen slices.

48 H-Culture Does Not Significantly Affect Cell Viability of Spleen Slice Cells

In an attempt to understand whether 48 h-cultured slices also maintain a reasonable degree of cell viability, we analyzed cell death in spleen slices either freshly prepared or cultured for 24, 48, 72, or 96 h at 37°C. Slices were transferred to diagnostic microscope slides, either left unstained, or stained with Trypan blue and then analyzed by optical microscopy. Trypan blue staining of spleen slices showed substantial non-specific staining of the trabecular outer capsule, which occurred independently of the culture time (**Figures 3A–D**). Trypan blue-positive cells could be observed in both red and white pulp of fresh slices (**Figure 3A**) and in samples cultured for 24 and 48 h, where staining was not significantly different from staining performed on fresh samples (**Figures 3A–C**). In contrast, spleen slices cultured for 72 h showed stronger Trypan blue positivity (**Figure 3D**), which suggests a high degree of cell death. As reported above, we were unable to perform Trypan blue staining

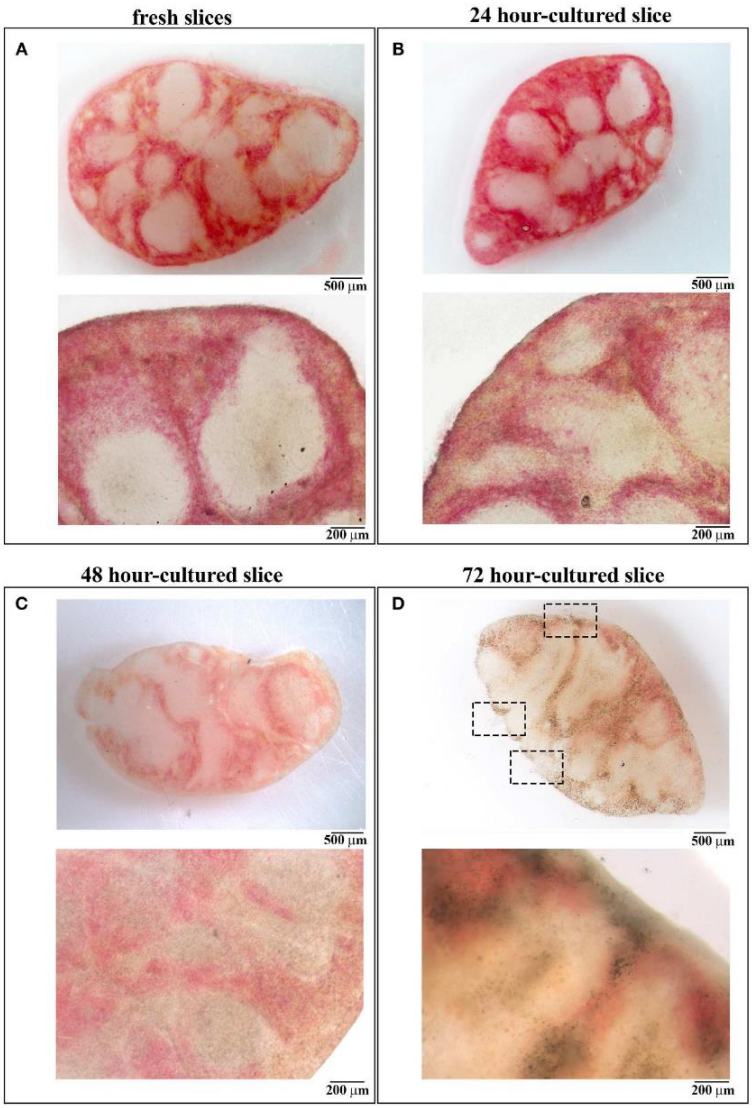

FIGURE 2 | 48 h-cultured spleen slices maintain unaltered their architecture. **(A–D)** Images obtained by stereomicroscopy (upper panels) and optical microscopy (lower panels) of spleen slices either immediately after cutting **(A)** or after *in vitro* culture for 24 **(B)**, 48 **(C)**, and 72 **(D)** hours. Representative images are shown ($n = 3$). Size bars are indicated.

in 96 h-cultured slices, since they broke down during their transfer to the microscope slides.

To quantify the extent of cell death, freshly prepared or cultured spleen slices were disgregated and Trypan blue exclusion assays were performed. In line with the results obtained by optical microscopy, the percentages of Trypan blue$^+$ cells in 24- and 48 h-cultured slices were comparable to fresh tissues, while longer culture times elicited significantly higher positivity, with a very high percentage of Trypan blue$^+$ cells in 96 h-cultured slices, indicating a high degree of cell death in slices cultured for over 48 h (**Figure 3E**). The extent of cell death was also quantified by flow cytometry in spleen slices either

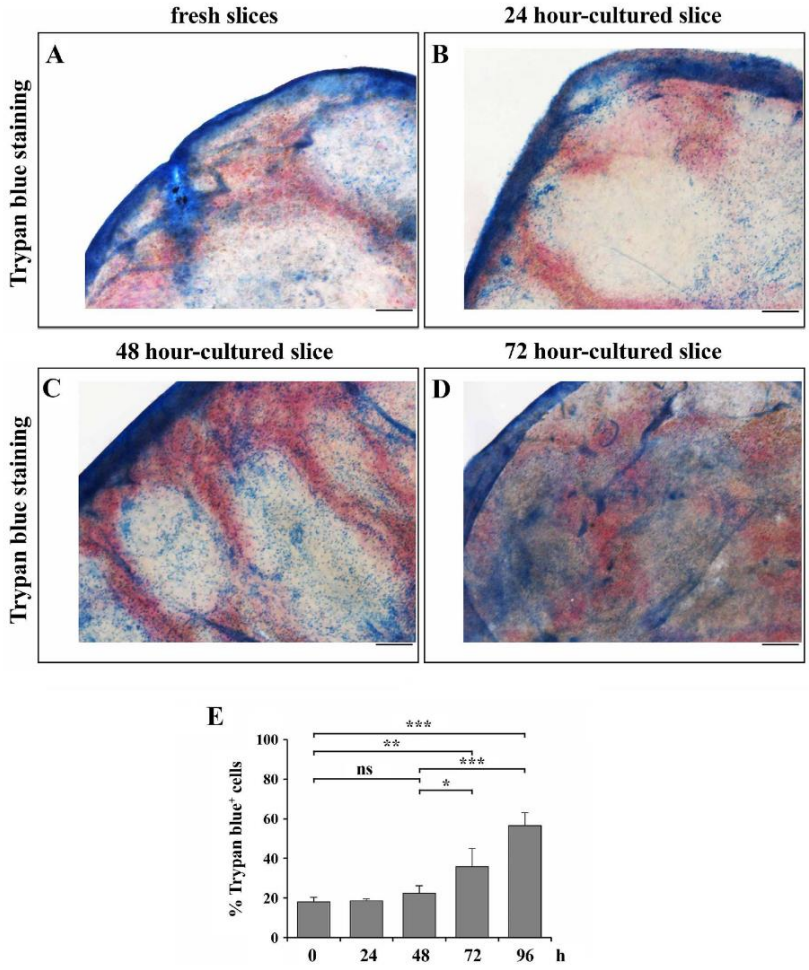

FIGURE 3 | 48 h-culture does not significantly increase cell death of spleen slices. **(A–D)** Optical microscopy pictures of spleen slices either immediately after cutting **(A)** or cultured *in vitro* for 24 **(B)**, 48 **(C)**, and 72 **(D)** h and stained with Trypan blue. Representative images are shown ($n = 3$). Size bar, 200 μm. **(E)** Trypan blue exclusion assay performed on spleen slices disgregated either immediately after cutting (0) or after *in vitro* culturing for 24, 48, 72, and 96 h, stained with Trypan blue and counted by optical microscopy. The data are presented as the percentage of Trypan blue$^+$ cells over total cells ($n = 3$). Mean ± SD. Student's *t*-test; $^{***}p \leq 0.001$; $^{**}p \leq 0.01$; $^{*}p \leq 0.05$.

freshly prepared or cultured for 24, 48, 72, or 96 h at 37°C, disgregated and stained with Annexin V and PI. As shown in **Figure 4**, slices cultured for 24 and 48 h showed percentages of PI$^+$ dead cells, as well as of Annexin V$^+$/PI$^-$ early apoptotic cells, comparable to freshly cut slices (**Figures 4A–C**). By contrast, the percentage of Annexin V$^+$/PI$^-$ early apoptotic cells and, to a higher extent, of PI$^+$ dead cells increased in slices cultured at 37°C for longer times (**Figures 4A–C**). These results indicate the beginning of the deterioration process in slices subjected to prolonged *in vitro* culture. To investigate whether the viability of the different cell types present in the slices was differentially affected during slice culture, we carried out a flow cytometric analysis of spleen slices either freshly prepared or cultured for 48 or 96 h at 37°C, disgregated and stained with PI in combination with antibodies against CD3, CD19, and FDC, which specifically stain the spleen-resident T cells, B cells and FDCs, respectively. As shown in **Figure 4D**, the deterioration process equally affects all cell types analyzed. Staining of spleen-resident reticular fibroblasts was carried out using an antibody against the specific cytoplasmic marker ER-TR7. This requires

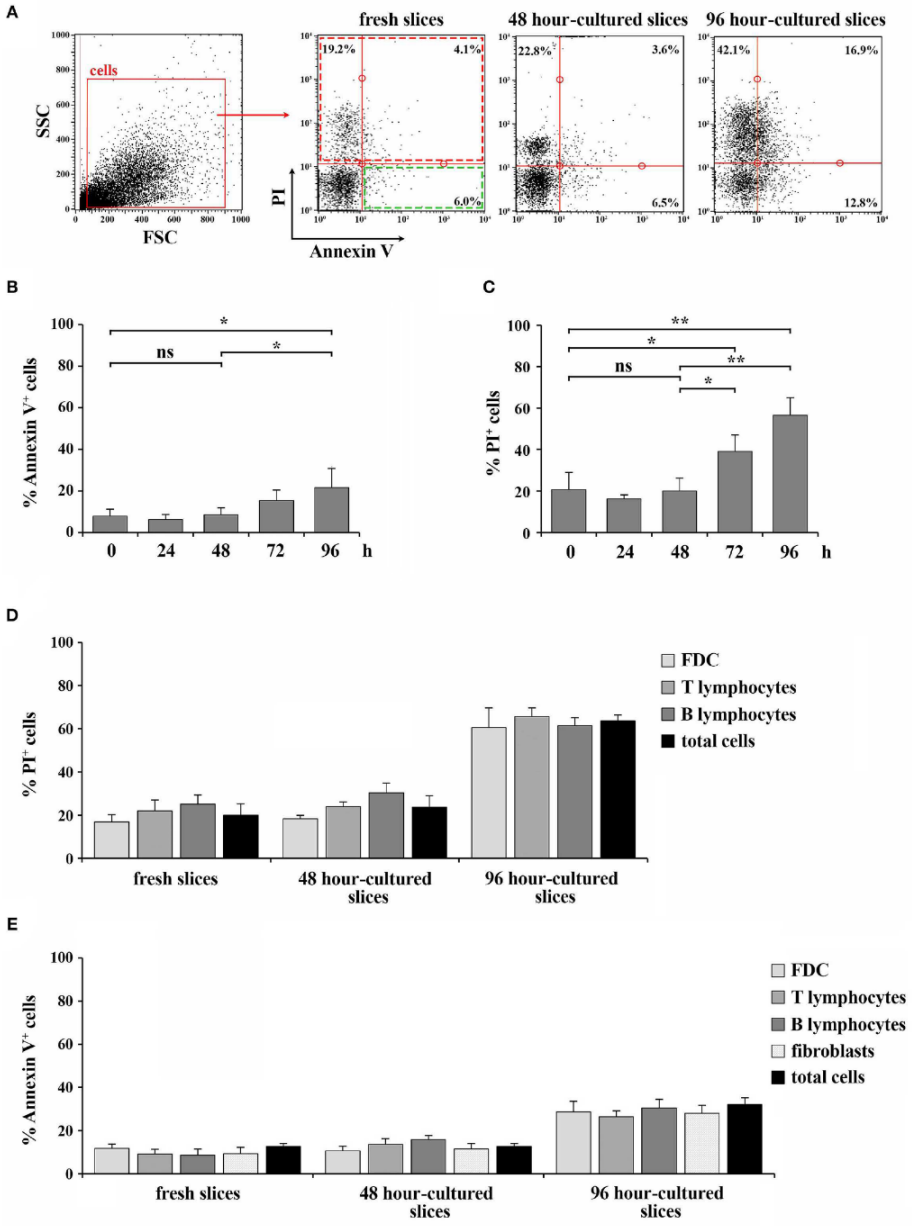

FIGURE 4 | 48 h-culture does not selectively affect the viability of cell types within spleen slices. **(A–C)** Flow cytometric analysis of the percentage of Annexin V^+ cells **(B)** or PI^+ cells **(C)** in spleen slices disgregated either immediately after cutting (fresh slices, 0) or after *in vitro* culturing for 24, 48, 72, and 96 h, and stained with Annexin V FITC and with 10 ng/ml PI. The data are presented as the percentage of either Annexin V^+ or PI^+ cells over total cells ($n = 3$). Representative flow cytometric plots are shown in **(A)**. **(D)** Flow cytometric analysis of spleen slices either immediately after cutting (fresh slices) or cultured *in vitro* for 48 h (48 h-cultured), disgregated, labeled for CD3, CD19, or FDC marker and with 10 ng/ml PI. **(E)** Flow cytometric analysis of spleen slices either immediately after cutting (fresh slices) or cultured *in vitro* for 48 h (48 h-cultured), disgregated, labeled for CD3, CD19, FDC, or ER-TR7 and Annexin V PE. The data are presented as the percentage of either PI^+ **(D)** or Annexin V^+ **(E)** cells over $CD3^+$, $CD19^+$, FDC^+, or ER-$TR7^+$ cells ($n = 4$). Mean ± SD. Student's *t*-test; $^{**}p \leq 0.01$; $^{*}p \leq 0.05$.

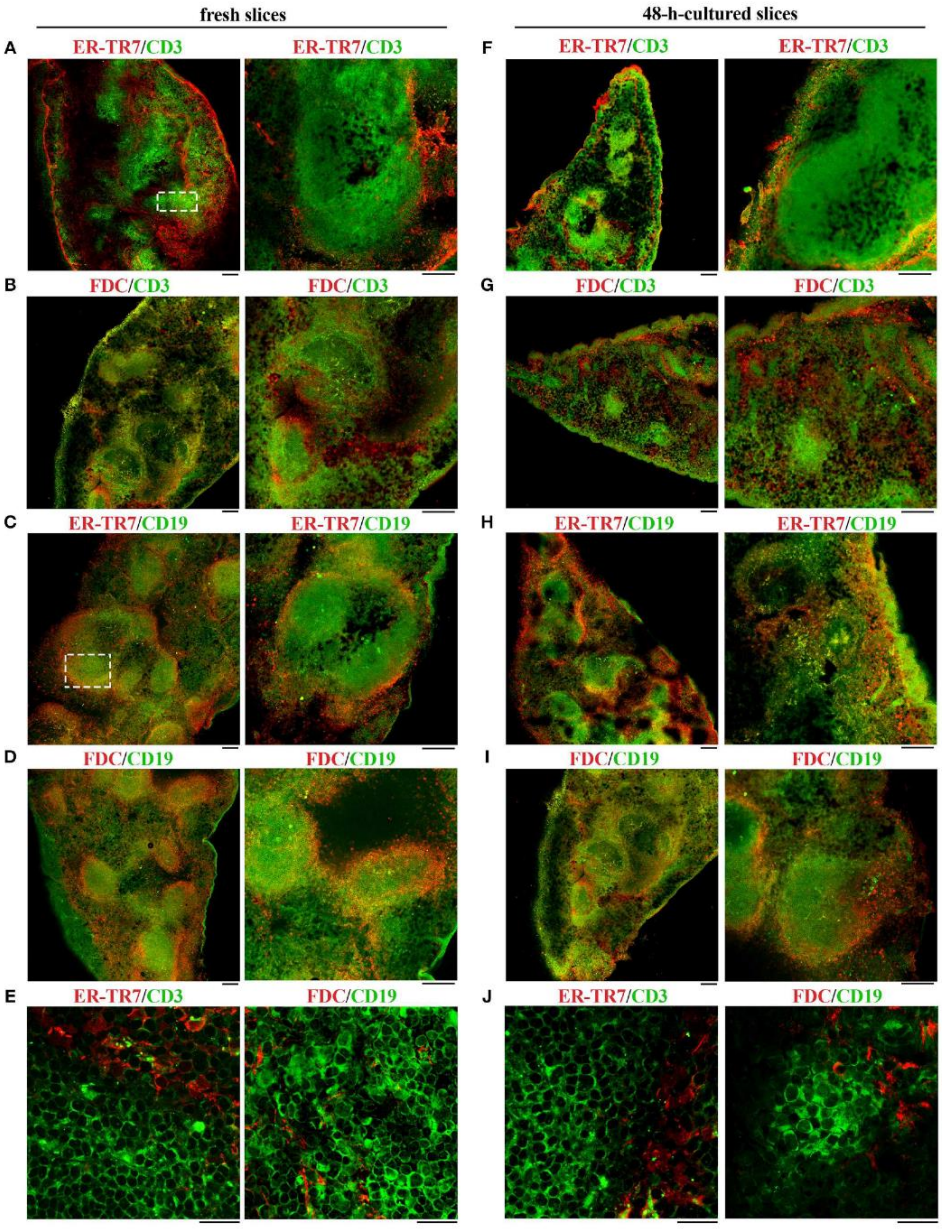

FIGURE 5 | 48 h-culture does not alter the distribution of cell populations in spleen slices. Immunofluorescence analysis of spleen slices either immediately after cutting (fresh slices, **A–E**) or cultured *in vitro* for 48 h (48-h-cultured, **F–J**), permeabilized and labeled for ER-TR7 (red)/CD3 (green) **(A,E,F,J)**, ER-TR7 (red)/CD19 (green) **(C,H)**, FDC marker (red)/CD3 (green), **(B,G)** or FDC marker (red)/CD19 (green) **(D,E,I,J)**. The pictures refer to non-contiguous spleen slices. Median optical sections are shown. Size bar, 100 μm **(A–D,F–I)**, and 20 μm **(E,J)**.

plasma-membrane permeabilization, which prevents labeling of dead cells with PI. To overcome this limitation the relative levels of death in spleen-resident cell populations was also evaluated by staining slice-derived cells with the surface apoptotic marker Annexin V in combination with antibodies against CD3, CD19, FDC, and ER-TR7. As shown in **Figure 4E**, the percentage of Annexin V^+ cells was similar among cell types and did not significantly change compared to total cells. Collectively, our data demonstrate that while 48 h-cultured slices maintain the correct tissue organization and do not display an enhanced degree of cell death compared to freshly cut slices, 72 h-cultured slices appear significantly damaged, indicating that spleen slices can be maintained in culture for no more than 48 h, at least in the culture conditions used.

Spleen Slices Cultured for 48 h *in vitro* Maintain the Tissue Localization of Cell Populations

The lymphoid tissue that constitutes the white pulp is organized around the arterial vessels in T- and B-cell compartments, whose maintenance is controlled by specific chemokines that attract T and B cells to their respective localization (8, 15). To evaluate the localization of immune cells and to assess the extent of organ texture degeneration in spleen slices subjected to prolonged *in vitro* culturing, cell distribution was assessed by immunofluorescence in spleen slices either immediately after cutting (fresh slices) or cultured for 48 h at 37°C in culture medium (**Figures 5A–J** and **Supplementary Figure 1**). In fresh slices immune cells were mainly distributed in lymphoid compartments, with T cells localized in T cell areas (**Figure 5A**, dashed rectangle), B cells mainly confined to germinal centers (**Figure 5C**, dashed rectangle), with a framework of ER-TR7-secreting reticular fibroblasts and FDC surrounding the marginal zones (**Figures 5A–E**). This structure was maintained almost unchanged in slices cultured for 48 h (**Figures 5F–J**), although we observed a partial decrease in the size (panel G) and/or cellularity (panels G-I) of white pulp areas, which might be accounted for by a partial loss of non-adherent lymphocytes in the culture medium. These results, together with the fact that we were unable to perform the immunofluorescence analysis of 96 h-cultured slices due to their high degree of degeneration, suggest that 48 h-cultured spleen slices are suitable for functional assays.

RNA Extracted From 48 H-Cultured Spleen Slices Is Suitable for qRT-PCR Analysis

RNA was extracted from homogenates obtained from 1, 3, and 5 spleen slices either immediately after cutting (0 h) or maintained in culture for 48 and 96 h. RNA was quantified and its quality checked using QIAxpert System (Qiagen). As shown in **Figure 6A** and in **Table 1**, the amount of RNA was very low when extracted from 1 slice immediately after cut. Conversely, both the yield and the quality of RNA extracted from 3 and 5 slices were sufficient to allow for retrotranscription (**Figure 6A** and **Table 1**). Similar results were obtained when we analyzed samples cultured for 48 h, where we observed a limited decrease in both yield and quality of RNA (**Figure 6A** and **Table 1**). As expected, RNA recovery in 96 h-cultured slices was very low (**Figure 6A** and **Table 1**). Based on these results, the quality of

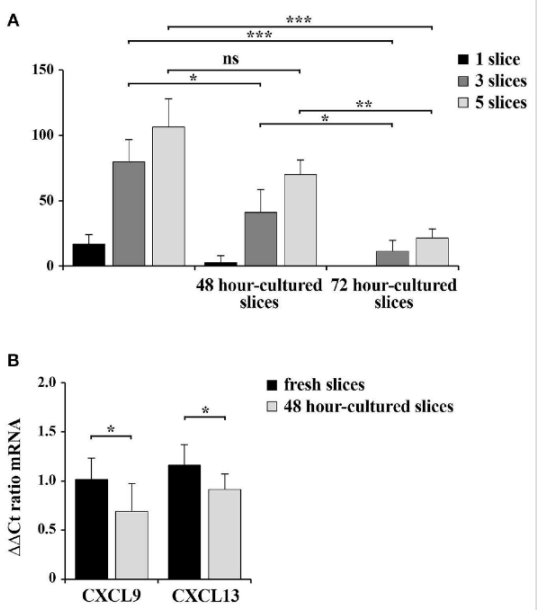

FIGURE 6 | 48 h-cultured spleen slices show a slight decrease in RNA yield and quality. **(A)** RNA concentration in samples from 1, 3, or 5 spleen slices homogenized in RNA extraction buffer either immediately after cutting or after *in vitro* culturing for 48 and 72 h. The measurement of RNA concentration was performed using QIAxpert System (Qiagen). **(B)** Quantitative RT-PCR analysis of CCL19 and CXCL13 mRNA in samples from 5 spleen slices homogenized either immediately after cutting or after *in vitro* culturing for 48 h. The relative gene transcript abundance was determined on triplicate samples using the ddCt method. *Gapdh* was used as housekeeping gene. Mean ± SD. Student's *t*-test; $^{***}p \leq 0.001$; $^{**}p \leq 0.01$; $^{*}p \leq 0.05$.

TABLE 1 | Yield and quality of RNA isolated from spleen slices (1, 3, or 5 slices/sample) immediately after cutting or cultured for either 48 or 96 h.

Slice number	Culture time (hours)	RNA (ng/μl)	Impurities (A260)	Residue (%)	A260	A260/A280
1	0	11.2	0.43	1.1	0.71	1.83
3	0	83.2	0.00	0.4	2.08	2.06
5	0	121.2	0.01	0.3	4.28	2.08
1	48	N/A	0.11	21.7	0	0
3	48	51.4	0.02	0.9	1.32	2.13
5	48	91.0	0.00	0.5	2.27	2.10
1	96	N/A	0.00	2.6	0.00	0
3	96	11.3	0.01	0.8	0.81	2.17
5	96	32.3	0.02	0.7	0.90	2.11

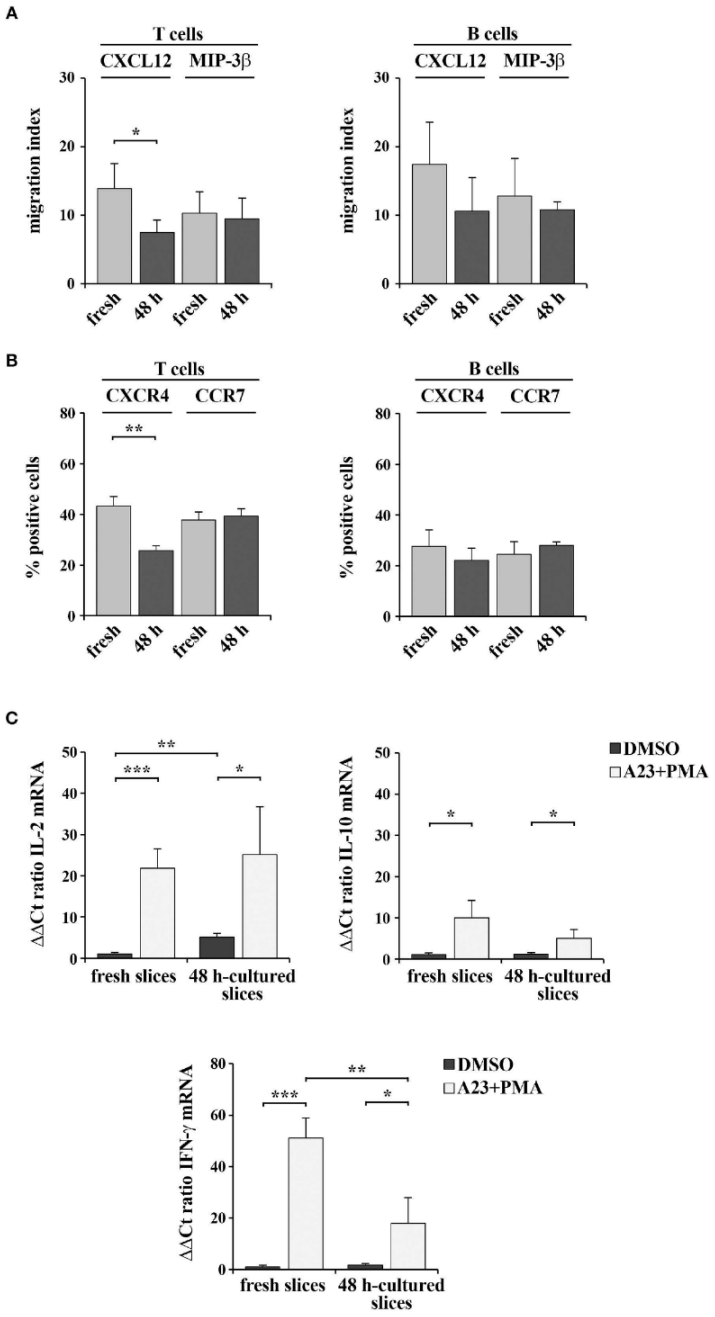

FIGURE 7 | 48 h-culture does not significantly alter spleen slice responsiveness to exogenous stimuli. **(A)** Migration of T and B cells from intact spleen slices, either freshly prepared or cultured *in vitro* for 48 h and placed on the upper wells of Boyden chambers. Slice-resident T and B cells were allowed to migrate for 3 h toward

(Continued)

FIGURE 7 | the lower wells containing 100 ng/ml CXCL12 or MIP3-β. Cells recovered from the lower wells were stained with PE anti-CD3 and FITC anti-CD19 antibodies and counted by flow cytometry. The data, obtained on duplicate samples from each spleen slice, are presented as mean migration index (ratio migrated cells in chemokine-treated vs. untreated samples) ± SD. **(B)** Flow cytometric analysis of the percentages of $CXCR4^+$ or $CCR7^+$ T lymphocytes (stained with anti-CD3 antibodies) and $CXCR4^+$ or $CCR7^+$ B lymphocytes (stained with anti-CD22 antibodies) in spleen slices disgregated either immediately after cutting (fresh) or after *in vitro* culturing for 48 h. The data are presented as the percentage of either $CXCR4^+$ or $CCR7^+$ cells over total $CD3^+$ or $CD22^+$ cells ($n = 3$). **(C)** Quantitative RT-PCR analysis of IL-2, IL-10, and IFN-γ mRNA in samples from 3 spleen slices stimulated for 6 h with 500 ng/ml A23187 (A23) and 100 ng/ml PMA (A23+PMA) or with carrier (DMSO) either immediately after cutting or after *in vitro* culturing for 48 h and then homogenized for RNA extraction. The relative gene transcript abundance was determined on triplicate samples using the ddCt method. *Gapdh* was used as housekeeping gene. Mean ± SD. Student's *t* test; $^{***}p \leq 0.001$; $^{**}p \leq 0.01$; $^{*}p \leq 0.05$.

the RNA was assessed by qRT-PCR analysis on RNA obtained from 5 slices either fresh or cultured for 48 h. In order to define the sensitivity of the assay, the transcripts encoding for the chemokines CCL19 (CC–chemokine ligand) and CXCL13 (CXC–chemokine ligand) were selected, due to their very low expression levels in lymphoid tissues under physiologic conditions (16). GAPDH was used as the housekeeping gene. The transcripts for both CCL19 and CXCL13 were easily detectable in fresh slices and were still clearly detectable in slices cultured for 48 h, although slightly decreased (**Figure 6B**) despite the lower RNA yield of these cultured samples (**Figure 6A**). Collectively, our data highlight the advantages of the new method described here to obtain live spleen sections which preserve both structure and cell viability and that can be used for functional assays.

Spleen Slices Cultured for 48 h *in vitro* Are Responsive to Exogenous Stimuli

We assessed whether 48-h *in vitro* culturing preserves the responsiveness of spleen slices to exogenous stimulation. The chemotactic ability of cells within spleen slices either immediately after cutting or cultured for 48 h at 37°C was analyzed by Transwell assays. Intact slices were placed on the upper wells of Boyden chambers and cells were allowed to migrate to the lower wells toward the chemokines CXCL12 or MIP-3β, which bind the respective lymphocyte-specific receptors CXCR4 and CCR7 (17). Migrated T and B cells were then stained with anti-mouse CD3 PE and anti-mouse CD19 FITC antibodies and quantified by flow cytometry. As shown in **Figure 7A**, chemotaxis of both T and B cells toward MIP-3β (**Figure 7A**) was barely affected by *in vitro* culturing, as was surface CCR7 (**Figure 7B**). CXCL12-dependent chemotaxis, although still clearly detectable in 48 h-cultured slices, was slightly decreased (**Figure 7A**), however this was likely the consequence of a loss of surface CXCR4 rather than a loss of responsiveness (**Figure 7B**). Hence, cells residing in slices cultured *in vitro* for 48 h maintain their responsiveness to chemotactic stimuli.

Freshly cut and 48 h-cultured spleen slices were also analyzed for their ability to respond to the non-specific mitogenic combination of the Ca^{2+} ionophore A23187 and PMA. As a read-out of cell stimulation, we quantified by qRT-PCR the mRNA levels of the cytokines IL-2, IL-10, and IFN-γ, which are expressed in lymphocytes and stromal cells following mitogenic stimulation (18, 19). As shown in **Figure 7C**, both freshly cut slices and slices cultured *in vitro* for 48 expressed enhanced amounts of the analyzed cytokines following stimulation. Interestingly, while IFN-γ expression was lower in the 48-h *in vitro* cultured slices compared to the freshly cut ones, the expression of both IL-2 and IL-10 was unaffected by *in vitro* culturing (**Figure 7C**). Collectively, these results demonstrate that spleen slices cultured *in vitro* for 48 h are suitable for functional assays and retain the sensitivity to exogenous stimuli similar to freshly prepared spleen slices.

DISCUSSION

Here we set up a method that allows for the efficient precision-cut of mouse spleens to obtain non-damaged, live slices for organotypic spleen culture. We furthermore optimized the *in vitro* culture of these slices. We show that spleen slices can be maintained in culture for 48 h without marked loss of organ architecture and with a minimal loss of cell viability, which allows to perform functional assays on slices treated *in vitro*. Moreover, the quality of the RNA isolated from cell homogenates of 48 h-cultured slices is sufficient to allow for the amplification of low-abundance chemokine transcripts.

Organotypic culture technology is routinely used to perform organotypic culture of central nervous system sections (20, 21). However, its application to lymphoid organs has lagged behind. We found only one paper describing this technique on human spleen and lymph node biopsies, where the authors obtain slices not <400 μm-thick which survive in culture for up to 1 week (4). The method we propose, which produces 230 μm-thick spleen slices or lower, represents a new application of this technique that meets the need to provide an easy-to-handle way to simulate the 3-D context of the immune system where all cellular components are represented in the respective physiological locations. The limited thickness of the slices that we obtain will be useful for treatments *in vitro*, which can easily reach the whole depth of the slices. However, the standard conditions that we apply for the *in vitro* culture of spleen slices do not allow us to maintain tissue slices viable for longer than 48 h, as instead reported by Hoffmann and colleagues for human lymphoid biopsies (4), possibly due to insufficient oxygen perfusion. Organotypic culture often requires dedicated culture media supplemented with specific nutrients or growth factors (22, 23). Optimizing the *in vitro* culture protocol may help prolonging the viability of vibratome-generated, thin spleen slices for longer-term functional assays *in vitro*.

Studying the response of immune cells within their microenvironment has become a central requirement for the development of personalized immunotherapy-based treatments

against cancer (24). It is noteworthy that, among recent technical advances, new miniaturized "organ-on-a-chip" cultures were introduced in an attempt to recapitulate *in vitro* the organ environment by mimicking blood flow through microfluidic systems (25, 26). However, the high costs of this technique preclude its generalized exploitation. By comparison, the organotypic culture represents a cheap, easy-to-handle method to study *in vitro* the interplay among the cellular components of the stromal microenvironment in both physiological and pathological settings and to test the immune cell response to drugs.

DATA AVAILABILITY STATEMENT

All datasets generated for this study are included in the article/**Supplementary Material**.

ETHICS STATEMENT

The animal study was reviewed and approved by the Italian Ministry of Health (197/2015-PR) and OPBA, University of Siena.

AUTHOR CONTRIBUTIONS

LP, FF, NM, NC, VT, and FL performed the work. LP and CB wrote the manuscript. LB, GP, and IC contributed to set up the spleen slice culture conditions.

FUNDING

The research leading to these results has received funding from AIRC under IG 2017—ID. 20148 project—P.I. Baldari Cosima.

ACKNOWLEDGMENTS

The authors wish to thank David Mercati and Sonia Grassini for technical assistance.

SUPPLEMENTARY MATERIAL

The Supplementary Material for this article can be found online at: https://www.frontiersin.org/articles/10.3389/fimmu.2020.00471/full#supplementary-material

REFERENCES

1. Schwerdtfeger LA, Tobet SA. From organotypic culture to body-on-a-chip: a neuroendocrine perspective. *J Neuroendocrinol*. (2019) 31:e12650. doi: 10.1111/jne.12650
2. Cyrus Arman A, Sampath AP. Patch clamp recordings from mouse retinal neurons in a dark-adapted slice preparation. *J Vis Exp*. (2010) 12:2107. doi: 10.3791/2107
3. Misra S, Moro CF, Del Chiaro M, Pouso S, Sebestyén A, Löhr M, et al. *Ex vivo* organotypic culture system of precision-cut slices of human pancreatic ductal adenocarcinoma. *Sci Rep*. (2019) 9:2133. doi: 10.1038/s41598-019-38603-w
4. Hoffmann P, Skibinski G, James K. Organ culture of human lymphoid tissue I. Characteristics of the system. *J Immunol Methods*. (1995) 179:37–49. doi: 10.1016/0022-1759(94)00268-2
5. Nagarsheth N, Wicha MS, Zou W. Chemokines in the cancer microenvironment and their relevance in cancer immunotherapy. *Nat Rev Immunol*. (2017) 17:559–72. doi: 10.1038/nri.2017.49
6. Lu LC, Chang CJ, Hsu CH. Targeting myeloid-derived suppressor cells in the treatment of hepatocellular carcinoma: current state and future perspectives. *J Hepatocell Carcinoma*. (2019) 6:71–84. doi: 10.2147/jhc.s159693
7. Osipov A, Saung MT, Zheng L, Murphy AG. Small molecule immunomodulation: the tumor microenvironment and overcoming immune escape. *J Immunother Cancer*. (2019) 7:224. doi: 10.1186/s40425-019-0667-0
8. Mebius RE, Kraal G. Structure and function of the spleen. *Nat Rev Immunol*. (2005) 5:606–16. doi: 10.1038/nri1669
9. Mattei G, Cristiani I, Magliaro C, Ahluwalia A. Profile analysis of hepatic porcine and murine brain tissue slices obtained with a vibratome. *PeerJ*. (2015) 3:e932. doi: 10.7717/peerj.932
10. Lev-Cohain N, Sapir G, Harris T, Azar A, Gamliel A, Nardi-Schreiber A, et al. Real-time ALT and LDH activities determined in viable precision-cut mouse liver slices using hyperpolarized [1-13C]pyruvate—implications for studies on biopsied liver tissues. *NMR Biomed*. (2019) 32:e4043. doi: 10.1002/nbm.4043
11. Rieg AD, Bünting NA, Cranen C, Suleiman S, Spillner JW, Schnöring H, et al. Tyrosine kinase inhibitors relax pulmonary arteries in human and murine precision-cut lung slices. *Respir Res*. (2019) 20:111. doi: 10.1186/s12931-019-1074-2
12. Patrussi L, Capitani N, Ulivieri C, Manganaro N, Granai M, Cattaneo F, et al. p66Shc deficiency in the Eμ-TCL1 mouse model of chronic lymphocytic leukemia enhances leukemogenesis by altering the chemokine receptor landscape. *Haematologica*. (2019) 104:2040–52. doi: 10.3324/haematol.2018.209981
13. Patrussi L, Capitani N, Martini V, Pizzi M, Trimarco V, Frezzato F, et al. Enhanced chemokine receptor recycling and impaired S1P1 expression promote leukemic cell infiltration of lymph nodes in chronic lymphocytic leukemia. *Cancer Res*. (2015) 75:4153–63. doi: 10.1158/0008-5472.CAN-15-0986
14. Patrussi L, Capitani N, Cannizzaro E, Finetti F, Lucherini OM, Pelicci PG, et al. Negative regulation of chemokine receptor signaling and B-cell chemotaxis by p66Shc. *Cell Death Dis*. (2014) 5:e1068. doi: 10.1038/cddis.2014.44
15. Schulz O, Hammerschmidt SI, Moschovakis GL, Förster R. Chemokines and chemokine receptors in lymphoid tissue dynamics. *Annu Rev Immunol*. (2016) 34:203–42. doi: 10.1146/annurev-immunol-041015-055649
16. Eberlein J, Nguyen TT, Victorino F, Golden-Mason L, Rosen HR, Homann D. Comprehensive assessment of chemokine expression profiles by flow cytometry. *J Clin Invest*. (2010) 120:907–23. doi: 10.1172/JCI40645
17. Patrussi L, Capitani N, Baldari CT. Abnormalities in chemokine receptor recycling in chronic lymphocytic leukemia. *Cell Mol Life Sci*. (2019) 76:3249–61. doi: 10.1007/s00018-019-03058-9
18. Chopra RK, Holbrook NJ, Powers DC, McCoy MT, Adler WH, Nagel JE. Interleukin 2, interleukin 2 receptor, and interferon-γ synthesis and mRNA expression in phorbol myristate acetate and calcium lonophore A23187-stimulated T cells from elderly humans. *Clin Immunol Immunopathol*. (1989) 53:297–308. doi: 10.1016/0090-1229(89)90058-5
19. Rachon D, Rimoldi G, Wuttke W. *In vitro* effects of benzophenone-2 and octyl-methoxycinnamate on the production of interferon-γ and interleukin-10 by murine splenocytes. *Immunopharmacol Immunotoxicol*. (2006) 28:501–10. doi: 10.1080/08923970600927751
20. Pampaloni NP, Rago I, Calaresu I, Cozzarini L, Casalis L, Goldoni A, et al. Transparent carbon nanotubes promote the outgrowth of enthorino-dentate projections in lesioned organ slice cultures. *Dev Neurobiol*. (2019). doi: 10.1002/dneu.22711. [Epub ahead of print].
21. Musto M, Rauti R, Rodrigues AF, Bonechi E, Ballerini C, Kostarelos K, et al. 3D organotypic spinal cultures: exploring neuron and neuroglia responses upon prolonged exposure to graphene oxide. *Front Syst Neurosci*. (2019) 13:1. doi: 10.3389/fnsys.2019.00001
22. Brandenburger M, Wenzel J, Bogdan R, Richardt D, Nguemo F, Reppel M, et al. Organotypic slice culture from human adult ventricular myocardium. *Cardiovasc Res*. (2012) 93:50–9. doi: 10.1093/cvr/cvr259
23. Raju ENS, Kuechler J, Behling S, Sridhar S, Hirseland E, Tronnier V, et al. Maintenance of stemlike glioma cells and microglia in an

organotypic glioma slice model. *Neurosurgery*. (2015) 77:629–43. doi: 10.1227/NEU.0000000000000891
24. Flemming A. Tumour heterogeneity determines immune response. *Nat Rev Immunol*. (2019) 19:662–3. doi: 10.1038/s41577-019-0230-8
25. Sun W, Luo Z, Lee J, Kim HJ, Lee KJ, Tebon P, et al. Organ-on-a-chip for cancer and immune organs modeling. *Adv Healthc Mater*. (2019) 8:e1900754. doi: 10.1002/adhm.201801363
26. Lee SH, Sung JH. Organ-on-a-chip technology for reproducing multiorgan physiology. *Adv Healthc Mater*. (2018) 7:1700419. doi: 10.1002/adhm.201700419

Conflict of Interest: The authors declare that the research was conducted in the absence of any commercial or financial relationships that could be construed as a potential conflict of interest.